Thesis for the degree of
Doctor of Philosophy
in the Faculty of Science
University of London

Hypersonic Planar Flow through a Nozzle, with Upstream Influence; a Composite Approach

by Takeshi Shimizu

Department of Mathematics
University College London

1998

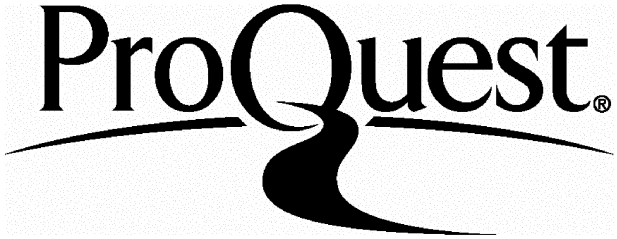

Abstract

This thesis consists of a theoretical computational study of flows at high Reynolds number and high Mach number, where upstream influence or non-uniqueness is of concern. Hypersonic flow has the special and important feature of prolonged upstream influence, in the presence of viscous forces, as upstream influence in a compressible boundary layer increases with increasing Mach number. Non-uniqueness is associated with eigenvalues and corresponding eigenfuctions in an expansion in powers of the distance from a reference point. One of the objectives in this thesis is to allow for the presence of upstream influence in an internal flow system, which is accompanied by local non-uniqueness of the solutions. The eigenfunction above is due essentially to the interaction of viscous and inviscid layers, and is analogous to an eigenfunction in hypersonic external flow. This non-uniqueness of the solution is a particular focus in the analysis.

The present study is concerned mostly with upstream influence in hypersonic planar flow through a nozzle and the eigenvalue problem is discussed in the context of a composite approach. A single composite system of equations is derived to cover the four separate regions of the nozzle flow identified by asymptotic analysis, the composite system being still a subset of the Navier-Stokes system. Non-uniqueness in the flow, due to upstream influence within the composite partial-differential system, is examined both by numerical treatment of certain similarity solutions and by means of eigenvalue analysis in the flow solution. The presence of upstream influence is also shown by analysis of a limiting pressure equation. Finally, in a preliminary attempt at solving the composite partial-differential system in full, a semi-implicit computational method is introduced to compute the flow solution, incorporating the strong upstream influence present. Further discussion is also presented in brief at the end.

Acknowlegdements

I cannot adequately express my deepest gratitude to my supervisor, Professor Frank T. Smith, FRS, for his constant encouragement and attention, unequivocal support and concern throughout my research and subsequent preparation of this thesis. My thanks go wholeheartedly to him.

> Mirabilis nimis facta est scientia tua super me,
> sublimis, et non attingam eam.
> Si sumpsero pennas aurorae et habitavero in extremis maris,
> etiam illuc manus tua deducet me, et tenebit me dextera tua.

I am grateful to Dr Peter Smith at the Defence Evaluation and Research Agency, Farnborough, for his positive suggestions and advice early on in this work. I would like to thank my colleagues at University College London for their assistance and friendship.

Thanks go also to the Overseas Research Scholarship Scheme who partially funded the first three years of my research.

Finally, I wish to dedicate this thesis to my parents. Without their encouragement and support, my academic career would be only a distant dream.

Context

Chapter 1

Introduction

There have been various upsurges of activity and development in hypersonic flow theory, computation and experiment, during the 1950s and in the mid 80s to mid 90s, with the advent of hypersonic atmospheric entry vehicles. Reviews on different features of hypersonic flows are in Stewartson (1964), Neiland (1970), Werle, Dwoyer and Hankey (1973), Brown, Stewartson and Williams (1975), Smith and Gajjar (1983), Lysenko and Maslov (1984), Mack (1984), Holden (1985), Brotherton-Ratcliffe (1986), Malik (1987), Seddougui, Bowles, and Smith (1989), Smith (1989), Bowles (1990), Brown, Cheng and Lee (1990), Blackaby (1991) and Brown, Khorrami, Neish and Smith (1991) and references therein. Hypersonic aerodynamics is different from the more conventional and more explored regime of supersonic aerodynamics, for a number of reasons some of which are given later in this chapter.

The present thesis attempts to analyse and compute the solution for certain hypersonic planar flows through nozzles, under the assumption of laminar steady flow. One of the objectives is to allow for the presence of upstream influence in the internal flow system, which is accompanied by local non-uniqueness of the solutions. The current study actually arose from contacts and jointly supported projects, between University College London and the Defence Evaluation and Research Agency, Farnborough, with regard to theoretical and computational understanding of wind-tunnel or duct flows under hypersonic conditions, conducted with the aim of improving experimental and/or industrial hypersonic wind-tunnel testing and design. There is special concern with improving on classical inviscid estimates of the downstream flow in ducts. The background for the work is discussed in section 1.1 below, followed by comments on hypersonic theory and upstream influence in section 1.2 and a description of the scope of the current thesis in section 1.3.

There are a number of other aspects of hypersonic flow research which are of much interest, such as hypersonic transition (which is still far from understood, see e.g. references in section 1.2 and also Stetson 1987) and the hypersonic blunt-body

problem (see e.g. Moretti and Abbett 1966). These other aspects are not of direct concern to the present work, however, and their details are not discussed below.

1.1 General Background

1.1.1 Internal Flows - Subsonic, Supersonic, Hypersonic

The flow regimes of supersonic and hypersonic motion are defined in terms of the Mach number M, which is the local ratio of the flow speed to the speed of sound. The definition is reviewed by, e.g., Anderson (1982).

Subsonic flow is a flow where the local Mach number $M < 1$ everywhere, and hence the flow velocity is everywhere less than the speed of sound. This type of flow is characterised by smooth streamlines and continuously varying properties, provided that no large-scale separation takes place to produce concentrated thin shear layers (due to viscous effects, as in section 1.1.3 below).

A flowfield where $M > 1$ everywhere is defined as supersonic. Shock waves occur frequently as part of most supersonic fields. Across such a shock wave there is a discontinuous and sometimes rather severe change in flow properties. The flow behind a shock wave can be supersonic or subsonic. This is in addition to the possible existence of shear layers mentioned in the previous paragraph.

In internal flow, for completely shock-free isentropic supersonic flow to exist in a nozzle, the pressure ratio (the ratio of the downstream pressure to the upstream, reservoir, pressure) must be precisely the value

$$\left(1 + \frac{\gamma - 1}{2} M^2\right)^{\frac{-\gamma}{\gamma - 1}} \tag{1.1}$$

according to inviscid theory (section 1.1.2 below), where γ is the ratio of specific heat. See Anderson (1989), Brown *et al.* (1991) and chapter 2. Otherwise, lateral shocks are to be expected within the nozzle motion. The practical interest is often in finding such shock-free flows inside the nozzle and that is our interest also in the present work.

In external flow past an airfoil or other vehicle, if the free-stream Mach number M_∞ remains subsonic but is sufficiently near 1, typically $0.8 < M_\infty < 1.2$, the occurrence of flow expansion may result in locally supersonic regions appearing. This mixed regime of subsonic and supersonic flow fields is defined as transonic flow. See e.g. Liepman and Roshko's (1957) book and, concerning interactions, Bowles and Smith's (1993) review.

As M_∞ is increased to higher supersonic speeds, however, certain flow properties increase almost explosively across a shock wave, and the representative flow angles

according to classical inviscid theory become ever smaller (for example see Liepman and Roshko's (1957) book), subject again to viscous effects and substantial separations taking place. Hypersonic flow is defined conventionally (or often, in engineering terms) as a flow regime for $M_\infty > 5$, although in reality the special characteristics associated with hypersonic flow can appear rather gradually as M_∞ is increased.

1.1.2 Inviscid Theory

The typical ratio of inviscid (inertial) to viscous forces is given by the Reynolds number Re, which is defined as a characteristic flow speed multiplied by a characteristic length scale and divided by the kinematic viscosity of the fluid. In flows at high Reynolds number the viscous effects can sometimes be confined to thin boundary layers near solid surfaces, although often followed by separated flow downstream and thickened wake regions which particularly occur in adverse pressure gradients. The flow outside the boundary layer however is essentially inviscid, or can be taken to be so as a first, classical, guess (see for example Van Dyke 1964; Smith 1982), and its properties depend on whether the flow range is incompressible, subsonic, supersonic or hypersonic as noted previously.

The assumption of inviscid flow (or, more strictly, the flow of an effectively inviscid fluid), in which viscosity, thermal conduction and diffusion are taken as negligible, may be restrictive as indicated above. However, the large regions of extended flow over bodies, outside the thin boundary layer on the surface, and the flows through wind tunnels and rocket engine nozzles, which often do not involve motions with large gradients, can often be assumed to be inviscid to a good approximation (see Anderson 1989). For the internal flow case between solid fixed walls the wall boundary layers grow and meet sufficiently far downstream, and the inviscid core then vanishes, but inviscid theory applies in a short duct such as the nozzle of a wind tunnel. Even in a long internal flow (with ratio of length to diameter typically greater than 10) inviscid theory as a crude approximation may be used, although such calculations are only a rough approximation of the real internal flow, especially in the hypersonic regime as the boundary layers then tend to grow rapidly in thickness with increasing Mach number (see section 1.1.3 below).

Hypersonic aerodynamics is highly nonlinear; even the assumption of small perturbations, which in subsonic and supersonic flows leads to simple linear theories, does not necessarily yield a system of linear equations for hypersonic flow. See for example Van Dyke (1954). In spite of this, various approximate methods have been successfully developed for the analysis of inviscid hypersonic flows. Anderson (1989) discusses several of these methods, some of them based upon the predictions of the

hypersonic small-disturbance equations.

In a large part of the applications of aerodynamics in general, the Reynolds number is very high and therefore the influence of viscosity might be taken to be negligible in the theoretical analysis, for much of the farfield, as mentioned previously. The Navier-Stokes equations (which are written down at the end of this chapter) can then be reduced by neglect of the viscous terms to the Eulerian form, viz.

$$\frac{\partial \varrho}{\partial t} + \mathrm{div}\,(\varrho \mathbf{v}) = 0, \tag{1.2}$$

$$\varrho \frac{D\mathbf{v}}{Dt} = -\mathrm{grad} p + \varrho \mathbf{X}, \tag{1.3}$$

$$p = R\varrho T, \tag{1.4}$$

$$c_p \varrho \frac{DT}{Dt} = \frac{Dp}{Dt}, \tag{1.5}$$

where the operator

$$\frac{D}{Dt} = \frac{\partial}{\partial t} + u\frac{\partial}{\partial x} + v\frac{\partial}{\partial y}$$

for two-dimensional motions. Here $\mathbf{v}$ is the velocity in Cartesian coordinates Oxy, ϱ is the density, t is time, p is the thermo-dynamic pressure, $\mathbf{X}$ are the components of any external force per unit mass of fluid, R is the gas constant, T is the temperature, and c_p is the specific heat at constant pressure. Strictly the formulation behind (1.2) - (1.5) assumes that the flow variables u, v, p, ϱ, T, μ and the coordinates x, y are typically of $O(1)$, in nondimensional form.

The analysis and solution of the Eulerian equations for a slender nozzle flow will be considered in chapter 2.

1.1.3 Viscous Effects

The classical theory of the boundary layer which was first introduced by Ludwig Prandtl in 1904 divides the flowfield into inviscid and viscous parts (see for example reviews by Van Dyke 1964 and Smith 1982).

The viscous boundary layer then appears in a narrow region attached to the solid surface. The Navier-Stokes equations reduce to the governing equations of the compressible boundary layer,

$$\frac{\partial(\varrho_0 u_0)}{\partial x} + \frac{\partial(\varrho_0 v_0)}{\partial y} = 0, \tag{1.6}$$

$$\varrho_0 \left(u_0 \frac{\partial u_0}{\partial x} + v_0 \frac{\partial u_0}{\partial y} \right) = -\frac{dp_0}{dx} + \frac{\partial}{\partial y}\left(\mu_0 \frac{\partial u_0}{\partial y} \right), \tag{1.7}$$

$$\varrho_0 c_p \left(u_0 \frac{\partial T_0}{\partial x} + v_0 \frac{\partial T_0}{\partial y} \right) = u_0 \frac{dp_0}{dx} + \frac{\partial}{\partial y} \left(k \frac{\partial T_0}{\partial y} \right) + \mu_0 \left(\frac{\partial u_0}{\partial y} \right)^2, \tag{1.8}$$

$$p_0 = R \varrho_0 T_0, \tag{1.9}$$

$$\mu_0 = \gamma C T_0, \tag{1.10}$$

where μ is the viscosity, and k is the coefficient of thermal diffusivity. Here all the variables with subscript zero are of order unity, owing to the boundary-layer scalings, and y represents the scaled boundary-layer normal cordinate. The boundary conditions here are, typically,

$$u_0 = 0, \quad T_0 = T_w(x) \qquad \text{at} \quad y = 0, \tag{1.11}$$

$$(u_0, T_0) \longrightarrow (u_\infty, T_\infty) \qquad \text{as} \quad y \longrightarrow \infty, \tag{1.12}$$

where $T_w(x)$ is the wall temperature distribution and u_∞, T_∞ are respectively the slip velocity and temperature just outside the boundary layer (from the outer inviscid solution).

The characteristics of hypersonic boundary layers are dominated by temperature increases caused by viscous dissipation. The viscosity coefficient increases with temperature, from (1.10), and this by itself makes the boundary layer much thicker (see e.g. Stewartson 1964). In addition, because the pressure p is constant in the normal direction through the boundary layer, the increase in temperature T results in a decrease in density ϱ through the equation of state (1.9). In order to pass the required mass flow through the boundary layer at reduced density, the boundary-layer thickness must be larger. Both of these phenomena combine to make hypersonic boundary layers grow more rapidly than at slower speeds. Indeed, the flat plate compressible laminar boundary layer thickness δ grows essentially as

$$\delta \propto \frac{M_\infty^2}{\sqrt{Re_x}} \tag{1.13}$$

where Re_x is the local Reynolds number (Stewartson 1964; Anderson 1989). Clearly, since δ varies as the square of M_∞, it can become inordinately large at hypersonic speed.

The thick boundary layer in hypersonic flow can exert a major displacement effect on the inviscid flow outside the boundary layer, causing a given body shape to appear much thicker than it really is. Due to the extreme thickness of the boundary-layer flow, the outer inviscid flow in section 1.1.2 is greatly changed; the changes in the inviscid flow in turn feed back to affect the growth of the boundary layer itself. The major interaction, or complete coupling, between the boundary layer and the outer inviscid flow is called viscous interaction (Neiland 1969, 1970; Werle *et al.* 1973; Khorrami 1991). It soon becomes important as the Mach number increases in internal duct flow and it then renders the inviscid estimates of section 1.1.2 inaccurate.

1.1.4 Experiments

Hypersonic wind tunnel testing is required in many stages during the development of a flying vehicle. In order to reproduce the physical phenomena in a scaled experiment similarity parameters must be considered. The simultaneous duplication of all the similarity parameters is not possible in ground based facilities. Such facilities can be grouped as follows: the classical hypersonic wind tunnel, the high enthalpy facilities and the low density wind tunnels. The current hypersonic flows are also of interest in the context of flow in the engine intakes and exhausts of hypersonic vehicles as described by Dusa and Younghans (1998) in a recent handbook and by Townend (1999) in a forthcoming review issue.

Earlier developments and extensive accounts on hypersonic wind tunnel testing are reviewed by Pope and Goin (1965), Lukasiewicz (1973) and Van Driest and Blume (1962). Kendall (1975) describes the wind tunnel experiments on the origin and growth of transition in zero pressure-gradient boundary layers for several Mach numbers between 1.6 and 8.5 at the Jet Propulsion Laboratory.

More recently, Muylaert *et al.* (1991) give a review of all the facilities used within the Hermes project of the European Space Agency. Their simulation capabilities, flow quality and measurement techniques are outlined; and in order to improve the level of understanding in hypersonic testing a standard model has been recommended.

Also, Giordano, Marraffa and Russo (1991) present results on the flow fields in the Simoun and Scirocco wind tunnel nozzles. The geometrical conflgurations analysed are conical with a circular section for Scirocco and contoured with a semicircular section for Simoun. Two-dimensional and three-dimensional results have been produced by a computer program which solves the parabolised Navier-Stokes equations. Isoline contours and transversal profiles of flow field parameters are shown to give an understanding of the predicted flow patterns which settle in the nozzles under different operating conditions.

Literature on experimental references can be found in journals such as Experiments in Fluids and AIAA Journal. Many other experiments, even some of a more fundamental, less applied nature, appear to be classified and/or are not available in the open literature.

1.1.5 Computational Fluid Dymanics

As hypersonic flowfield analysis is highly nonlinear, numerical computations or simulations giving the approximate numerical solution with the effect of various parameters on the physical results are of interest. Computational fluid dynamics in principle ap-

proximates numerical solutions to the exact nonlinear governing equations (whether full Navier-Stokes, parabolised Navier-Stokes, interactive boundary layer, composite, or other reduced systems) without linearisation, i.e. the equations without simplifying assumptions such as small perturbations, granted that there always exist numerical roundoff and truncation errors. Most of the computations tend to become very difficult or inaccurate as the Reynolds number and/or Mach number increases, due to the subtle scales and interactions involved (this providing a motivation for the present work). An exception is the interactive boundary layer approach as in Khorrami and Smith (1994) and references therein. Khorrami and Smith in their fig.4 make an interesting comparison with direct numerical simulations by Dr. J.J. Korte (see also Korte *et al.* 1992, Korte 1992), finding close agreement between the two planar-flow approaches at a Reynolds number of 8^6 ($\approx 2.62 \times 10^5$) and Mach number of 16, in external flow. Moreover, the interactive boundary layer approach tends to become ever more accurate as the Reynolds and Mach numbers continue to increase (unlike with most other computational methods), owing to its being founded on knowledge of the main flow scales and viscous-inviscid interactions present. That is the basis essentially behind the present study for internal nozzle flows.

We should add here that, in earlier numerical work, and indeed in some current treatments, the method of characteristics is used for supersonic nozzle design. The contour of a supersonic nozzle can be obtained by applying this method of characteristics downstream of the limiting characteristic. Application of the method in an actual nozzle design is given by Owczarek (1964), among others. The use of the method of characteristics for nozzle design is confined to inviscid flow.

Our concern is more with finite-difference approaches. Finite-difference methods are used to replace the partial derivatives in the governing flow equations with finite-difference quotients. For supersonic steady flows, for example, this allows the calculation to march downstream, starting from known initial conditions upstream, provided that viscous effects are excluded. The intensive work in this area since 1960 has produced a multitude of different algorithms. Roache (1976) gives extensive discussion of some of these methods, although there is also further progress more recently.

Other current literature in the area can be found in journals such as Computers and Fluids, the Journal of Computational Physics and the International Journal for Numerical Methods in Fluids, as well as the Journal of Fluid Mechanics, the AIAA Journal, Physics of Fluids, the Annual Reviews of Fluid Mechanics, the Philosophical Transactions of the Royal Society of London and the Proceedings of the Royal Society of London.

1.2 Hypersonic Theory and Upstream Influence

Hypersonic flow has the special and important feature of prolonged upstream influence, in the presence of viscous forces. The non-uniqueness of the solution near the leading edge of an insulated sharp flat plate in hypersonic planar flow, due to upstream influence, was discovered and analysed by Neiland (1969, 1970), Stewartson and Williams (1969) and Brown and Stewartson (1975), where the tangent-wedge method was used to describe the inviscid layer. It was partly anticipated in Lighthill's (1953a,b) work on upstream influence in a supersonic boundary layer, the characteristic length of the upstream influence increasing with increasing Mach number, and there are some signs of it in retrospect in Stewartson's (1964) chapter on hypersonic interactions. Later M.J. Werle, D.L. Dwoyer and W.L. Hankey (1973) considered the non-insulated wall also. This non-uniqueness is associated with a single eigenvalue and corresponding eigenfunction in an expansion in powers of the (small) distance from the leading edge. Brown and Stewartson (1975) concluded that the tangent-wedge method is extremely accurate, using a comparison with the equations of motion describing the inviscid layer, and this is confirmed by the studies of Khorrami (1991) and Khorrami and Smith (1994).

The eigenfunction is due to the interaction of the viscous and inviscid layers, and is analogous to the eigenfunction in supersonic flow discussed by M.J. Lighthill. See also the hypersonic free-interaction study by Smith and Gajjar (1983), and other more recent aspects of hypersonic flow such as in Ruban and Timoshin (1986, on interactions), Smith (1989, on viscous instabilities), Cassel *et al.* (1995, on interactions) (also Rizzetta *et al.* 1978), Brown, Cheng and Lee (1990, on mixed interactions), Brown and Smith (1990, on inviscid instabilities) (followed by Cowley and Hall (1990) among others), Timoshin and Smith (1995, on three-dimensional hypersonic boundary layers), as well as work on Görtler and longitudinal vortices (Hall and Fu 1992; Hall and Smith 1991; Malik and Hall 1989) and on sub-characteristics in the hypersonic range. The behaviour and effect of the eigenvalue in the hypersonic viscous and inviscid layers are analysed in detail by Khorrami (1991) and Khorrami and Smith (1994); see also the review of Brown *et al.* (1991). The value of the coefficient multiplying the (leading-edge) eigenfunction is governed by the downstream conditions (among other boundary conditions), for example at the trailing edge or in the far-wake. Thus there is upstream influence along the entire plate (and wake, if present). We find the same feature holding in the current internal flows.

1.3 The Present Thesis

We now discuss in brief the contents and reasoning of the following chapters in the present thesis.

Chapter 2 describes the basic flow model for high-Reynolds-number planar flow through a planar nozzle in the hypersonic range. The flow structure consists of four differently scaled regions which are governed either by inviscid theory or by boundary layer theory, or by a combination thereof, the entire area being subject to upstream influence. Shock-free flow is assumed through the nozzle. The four regions consist of the thick inviscid core and the accompanying, thin, classical compressible boundary layer, in the near-throat stage, and further downstream (in the farfield) two interacting regions of comparable but unknown thickness spanning the nozzle. See Brown *et al.* (1991). The flow quantities are non-dimensionalised and examined in terms of their scales to generalise the problem. The same ideas apply in axisymmetric nozzle flows.

Chapter 3 sets up the governing equations which are used throughout the rest of the thesis. In particular, in this thesis, a single composite system of governing equations is introduced, which is chosen to cover the four original regions of the flow structure (chapter 2) and remains a subset of the compressible Navier-Stokes system. At the farfield stage for instance the width of the nozzle expands significantly and self-similar exact solutions can be deduced to analyse the conditions there. Also in this chapter are examined exact solutions for compressible boundary layer flow and the Illingworth-Stewartson transformation.

Chapter 4 derives and examines exact similarity solutions analytically and numerically in which the flow geometry is assumed to take a power-law form (proportional to a power of the downstream distance). The partial differential equations in chapter 3 reduce to a set of ordinary differential equations here. The effects of variations in the coefficients, the viscosity, the wall temperature and the flow geometry in particular are observed.

Chapter 5 then focuses on upstream influence. Non-uniqueness in the local solutions is proved analytically and through a numerical method, by means of eigenvalues in the flow solution. A small perturbation term associated with upstream influence is shown to be possible in the stream function. Then the special cases of large and small effective viscosity are analysed to distinguish the effective perturbation terms in each case.

Chapter 6 explores the interesting limit of compressible lubrication results for the entire flow solution, a limit which seems peculiar to the present internal motions. The Reynolds number can still be significantly large since the typical width of the throat of a nozzle is very narrow compared with the typical length. A pressure equation is derived here, in the special case of large viscosity, and solved mainly analytically

to confirm the presence of prolonged upstream influence, in view of the boundary conditions which need to be imposed downstream.

Chapter 7 extends the limit results obtained in the previous chapter to more general cases. A semi-implicit computational method based on the above flow properties is introduced as a first attempt to solve the partial differential equations for the flow solution numerically, incorporating the strong upstream influence present (cf. Blottner 1962; Carter 1979; Davis 1984). Various conditions are applied to the nozzle parameters, and computational results are derived, convergent or divergent, to evaluate the method.

Finally, Chapter 8 summarises the findings of the thesis and provides further comments.

1.4 Navier-Stokes Equations

The complete equations of motion of a compressible viscous fluid are the continuity and the Navier-Stokes equations, which are derived for example in Stewartson (1964). They read

$$\frac{\partial \varrho}{\partial t} + \operatorname{div}(\varrho \mathbf{v}) = 0, \tag{1.14}$$

$$\varrho\left\{\frac{\partial v_\alpha}{\partial t} + (\mathbf{v}.\operatorname{grad}) v_\alpha\right\} = -\frac{\partial p}{\partial x_\alpha} + \varrho X_\alpha$$

$$+\frac{\partial}{\partial x_\alpha}\left\{\left(\mu' - \frac{2}{3}\mu\right)\operatorname{div}\mathbf{v}\right\} + \frac{\partial}{\partial x_\beta}\left(\mu\frac{\partial v_\beta}{\partial x_\alpha}\right) + \frac{\partial}{\partial x_\beta}\left(\mu\frac{\partial v_\alpha}{\partial x_\beta}\right), \tag{1.15}$$

$$p = R\varrho T, \tag{1.16}$$

$$\varrho\frac{\partial}{\partial t}(c_p T) + \varrho v_\alpha\frac{\partial}{\partial x_\alpha}(c_p T) = \Phi + \frac{Dp}{Dt} + \frac{\partial}{\partial x_\alpha}\left(k\frac{\partial T}{\partial x_\alpha}\right) \tag{1.17}$$

where as noted before $\mathbf{v}$ is the velocity in Cartesian coordinates Oxy, ϱ is the density, t is time, p is the thermo-dynamic pressure, X are the components of any external force per unit mass of fluid, μ is the viscosity, R is the gas constant, T is the temperature, c_p is the specific heat at constant pressure, Φ is the dissipation function, and k is the coefficient of thermal diffusivity.

Exact analytical solutions of the complete Navier-Stokes equations exist for only a few very specialised cases. Instead, the equations are frequently simplified by making appropriate approximations about the flow, as is done in this thesis. Approximate solutions of the complete Navier-Stokes equations for many practical problems can also be obtained numerically, as described earlier.

Chapter 2

High-Reynolds Number Flow Structure through Nozzle

2.1 Basic Flow Model

The analysis and hence the computation of compressible viscous fluid flow differs in the two environments of external and internal flow, as described fairly recently by Brown *et al.* (1991) and also Anderson (1993). External flow generally refers to flow past an airfoil and internal flow is exemplified by the flow in nozzles and wind tunnels (see references in chapter 1). This thesis relates to a symmetric nozzle flow which starts from a reservoir upstream, passes through a narrow throat and then expands gradually downstream where it becomes hypersonic. The motion is taken to be two-dimensional.

Non-dimensionalised variables are used throughout this thesis, namely the velocity components u, v, pressure p, density ϱ, temperature T, viscosity μ and cartesian coordinates x, y, as defined below. The x-axis is aligned along the centre-line of the nozzle. The y-ordinate is set at right angles to x. The corresponding velocity components are denoted by u and v, respectively.

From thermodynamics the pressure p, density ϱ and temperature T are linked by the equation of state for a perfect gas,

$$p = R\varrho T, \tag{2.1}$$

with R denoting the gas constant and T denoting the absolute temperature.

The function μ is the coefficient of viscosity or the dynamic coefficient of viscosity, to distinguish it from the ratio $\nu = \mu/\varrho$, which is the kinematic coefficient of viscosity or, simply the kinematic viscosity. The variable μ is assumed here to be subject to the Chapman viscosity law

$$\mu = \gamma CT. \tag{2.2}$$

Therefore it is a temperature-dependent variable. Laws other than (2.2) can be accommodated also throughout the following study.

The velocity components are nondimensionalised with respect to u_∞, lengths to l_∞, pressure to p_∞ and so on as follows

$$u = \frac{u_D}{u_\infty}, \quad v = \frac{v_D}{u_\infty}, \quad p = \frac{p_D}{p_\infty}, \quad \varrho = \frac{\varrho_D}{\varrho_\infty},$$

$$T = \frac{T_D}{T_\infty}, \quad \mu = \frac{\mu_D}{\mu_\infty}, \quad x = \frac{x_D}{l_\infty}, \quad y = \frac{y_D}{l_\infty},$$

where the suffix ∞ refers to representative dimensional flow conditions in the nozzle. In particular l_∞ is the minimum throat width and therefore the normalised nozzle width, $S(x)$, has a minimum value of 1 at the throat. The time t is nondimensional in similar fashion. The suffix D denotes the original dimensional variables.

The nondimensional parameter which measures the relative magnitude of the viscous effects is the Reynolds number Re, defined by

$$Re = \frac{u_\infty l_\infty \varrho_\infty}{\mu_\infty} = \frac{u_\infty l_\infty}{\nu_\infty}. \tag{2.3}$$

This is proportional to the ratio of a typical dynamic pressure to a typical viscous stress.

The relative magnitudes of viscosity and heat conductivity are measured by the Prandtl number σ, which is defined by

$$\sigma = \frac{c_p \mu}{k}. \tag{2.4}$$

Here the constant c_p is the specific heat at constant pressure and the function k is the coefficient of heat conductivity.

Therefore the continuity equation in non-dimensional form becomes

$$\frac{\partial \varrho}{\partial t} + \frac{\partial}{\partial x}(\varrho u) + \frac{\partial}{\partial y}(\varrho v) = 0, \tag{2.5}$$

while the equations of momentum in x and y components are, respectively,

$$\varrho \frac{\partial u}{\partial t} + \varrho u \frac{\partial u}{\partial x} + \varrho v \frac{\partial u}{\partial y} = -\frac{dp}{dx} + \mathrm{X}_x + Re^{-1}\left\{ \frac{\partial}{\partial x}\left(\mu \frac{\partial u}{\partial x}\right) + \frac{\partial}{\partial y}\left(\mu \frac{\partial u}{\partial y}\right) \right\}, \tag{2.6}$$

$$\varrho \frac{\partial v}{\partial t} + \varrho u \frac{\partial v}{\partial x} + \varrho v \frac{\partial v}{\partial y} = -\frac{dp}{dy} + \mathrm{X}_y + Re^{-1}\left\{ \frac{\partial}{\partial x}\left(\mu \frac{\partial v}{\partial x}\right) + \frac{\partial}{\partial y}\left(\mu \frac{\partial v}{\partial y}\right) \right\}, \tag{2.7}$$

where X are the components of any external force per unit mass of the fluid, as in Newton's laws of motion. The energy equation is

$$\varrho c_p \left(\frac{\partial T}{\partial t} + u\frac{\partial T}{\partial x} + v\frac{\partial T}{\partial y} \right) - \left(\frac{\partial p}{\partial t} + u\frac{\partial p}{\partial x} \right) = Re^{-1}\frac{\partial}{\partial y}\left(k\frac{\partial T}{\partial y} \right) + Re^{-1}\mu \left(\frac{\partial u}{\partial y} \right)^2 . \quad (2.8)$$

In fact the whole of this thesis will be concerned with steady flows, so that $\partial/\partial t$ is taken to be identically zero.

2.2 Inviscid Theory

In a real fluid the viscosity is never strictly zero. However, in a large part of the applications of aerodynamics in general, the Reynolds number is very high and therefore the influence of viscosity might be taken to be negligible in the theoretical analysis, for much of the farfield. This idealised concept of a perfect fluid gives the inviscid theory as below.

The Navier-Stokes equations can then be reduced by neglect of the viscous terms to the Eulerian form, as mentioned in chapter 1, viz.

$$\varrho \frac{D\mathbf{v}}{Dt} = -\text{grad}p + \varrho \mathrm{X}, \quad (2.9)$$

$$\frac{\partial \varrho}{\partial t} + \text{div}\,(\varrho \mathbf{v}) = 0, \quad (2.10)$$

$$p = R\varrho T, \quad (2.11)$$

$$c_p \varrho \frac{DT}{Dt} = \frac{Dp}{Dt}, \quad (2.12)$$

where (2.9) - (2.12) assume that the flow variables u, v, p, ϱ, T, μ and the coordinates x, y are typically of $O(1)$.

A viscous boundary layer must appear in a narrow region attached to the solid surface, where $|y - S|$ is small, as considered in section 2.3. The analysis and solution of the Eulerian equations for slender nozzles will be shown in section 2.4 below and provides, for part of the nozzle flow at least, an outer solution to which the inner boundary-layer solution must match.

2.3 Boundary-Layer Theory

A comprehensive review of the boundary-layer equations has been given by Schlichting (1951) and more recently, for compressible boundary layers, by Stewartson (1964), Anderson(1991), Khorrami (1991), Brown *et al.* (1991), among others.

The Navier-Stokes equations can be reduced to the classical boundary-layer equations as follows. All dependent variables are expanded, near the nozzle walls, in the form

$$\begin{aligned} u &= u_0 + Re^{-1/2}u_1 + \cdots, \\ v &= Re^{-1/2}v_0 + \cdots, \\ \varrho &= \varrho_0 + Re^{-1/2}\varrho + \cdots, \\ p &= Re^{-1}p_0 + \cdots, \\ T &= Re^{-1}T_0 + \cdots, \\ \mu &= Re^{-1}\mu_0 + \cdots. \end{aligned}$$

Also, x remains typically of order unity but y is scaled with $Re^{-1/2}$ which is small. Hence from substitution into the Navier-Stokes equations the governing equations are

$$\frac{\partial(\varrho_0 u_0)}{\partial x} + \frac{\partial(\varrho_0 v_0)}{\partial y} = 0, \tag{2.13}$$

$$\varrho_0\left(u_0\frac{\partial u_0}{\partial x} + v_0\frac{\partial u_0}{\partial y}\right) = -\frac{dp_0}{dx} + \frac{\partial}{\partial y}\left(\mu_0\frac{\partial u_0}{\partial y}\right), \tag{2.14}$$

$$\varrho_0 c_p\left(u_0\frac{\partial T_0}{\partial x} + v_0\frac{\partial T_0}{\partial y}\right) = u_0\frac{dp_0}{dx} + \frac{\partial}{\partial y}\left(k\frac{\partial T_0}{\partial y}\right) + \mu_0\left(\frac{\partial u_0}{\partial y}\right)^2, \tag{2.15}$$

$$p_0 = R\varrho_0 T_0, \tag{2.16}$$

$$\mu_0 = \gamma C T_0. \tag{2.17}$$

Again, the lack of influence of displacing y to $y + S(x)$, near the wall, is taken into account by means of Prandtl's transposition theorem in effect. The subscripts zero are omitted for convenience above. The boundary conditions here are

$$u = 0, \quad T = T_w(x) \qquad \text{at} \quad y = 0, \tag{2.18}$$

$$(u, T) \longrightarrow (u_\infty, T_\infty) \qquad \text{as} \quad y \longrightarrow \infty, \tag{2.19}$$

where u_∞ and T_∞ are respectively the slip velocity and temperature just outside the boundary layer (from the outer inviscid solution).

The boundary layer equations are parabolic in x, provided $u \geq 0$, and therefore the flow profile may be calculated by marching downstream in the x direction, for prescribed T_w, u_∞, T_∞ in (2.18), (2.19).

2.4 Four Regions

Internal steady flow through a slender hypersonic nozzle will be analysed in this thesis, first with regard to the four regions as discussed by Brown *et al.* (1991). The configuration produces a two-stage flow structure downstream of the nozzle throat; a first stage near the throat and a second, hypersonic, stage further downstream. This is accompanied by a two layer structure, in the normal y direction, consisting of the core inviscid layer and the viscous boundary layer between the core and the nozzle wall.

2.4.1 Near-Throat Stage

In the near-throat stage, the compressible boundary layer can remain thin and attached as assumed above. So here we address first the Euler form corresponding to the core of the motion. For a slender nozzle with typical small slope β the new coordinate $\hat{x}$ is introduced by means of the definition $\hat{x} = \beta x$, so that

$$[x, y] \longrightarrow \left[\beta^{-1}\hat{x}, y\right],$$

and then the solution of the core takes the form where ψ is the stream function.

$$[u, v, p, \varrho, \psi] \longrightarrow [u, \beta\hat{v}, p, \varrho, \psi]. \tag{2.20}$$

Therefore the governing equations form the classical thin-layer version

$$\frac{\partial(\varrho u)}{\partial\hat{x}} + \frac{\partial(\varrho\hat{v})}{\partial y} = 0, \tag{2.21}$$

$$\varrho\left(u\frac{\partial u}{\partial\hat{x}} + \hat{v}\frac{\partial u}{\partial y}\right) = -\frac{\partial p}{\partial\hat{x}}, \tag{2.22}$$

$$\frac{\partial p}{\partial y} = 0. \tag{2.23}$$

The inviscid flow is isentropic and therefore the energy equation is

$$p/\varrho^{\gamma} = F(\psi) = \text{const.} \tag{2.24}$$

This is subject typically to the mass-flow constraints $\psi = 0, 1$ at $y = -S, 0$ respectively, where S gives the normalised nozzle shape.

From the continuity equation above

$$\psi = \varrho u y + B(\hat{x}) \tag{2.25}$$

and, since the mass-flow constraint holds,

$$\varrho u S = 1. \tag{2.26}$$

Since u is a function of x only, the momentum equation becomes

$$\varrho u u' = -p', \tag{2.27}$$

with the prime denoting d/dx here, and therefore

$$\varrho u u' = -c_1 \gamma \varrho^{\gamma-1} \varrho',$$

giving on integration

$$\frac{1}{2}u^2 = -\frac{c_1 \gamma \varrho^{\gamma-1} + c_2}{\gamma - 1},$$

where the constant $c_1 = \varrho_{res}{}^{\gamma}/p_{res}$ and $c_2 = \gamma \varrho_{res}{}^{2\gamma-1}/p_{res}$. Here ϱ_{res}, p_{res} are the density and the pressure in the reservoir. Since $u = 1/\varrho S$ from (2.26)

$$\frac{1}{2\varrho^2 S^2} = \frac{c_2 - c_1 \gamma \varrho^{\gamma-1}}{\gamma - 1},$$

or

$$S(x)^2 = \frac{\gamma - 1}{2\varrho^2 \left(c_2 - \gamma c_1 \varrho^{\gamma-1}\right)}. \tag{2.28}$$

This determines the distribution $\varrho(x)$ in terms of the given nozzle shape $S(x)$, with the $u(x)$, $p(x)$ solutions following from (2.26), (2.27). At the reservoir $x \longrightarrow -\infty$, while in the far field stage downstream as $x \longrightarrow \infty$, $S \longrightarrow \infty$ for the nozzle. Therefore $S^2 \longrightarrow \infty$ as $\varrho \longrightarrow 0$ (downstream) or $\varrho \longrightarrow (c_2/c_1\gamma)^{\frac{1}{\gamma-1}}$ (reservoir) from (2.24).

2.4.2 The Farfield Stage

In the farfield stage, strong hypersonic viscous-inviscid interaction occurs, as follows. The streamwise scale is $Re\Delta^{2-\gamma}$ which is significantly smaller than that of Brown *et al.* (1991), $\Delta^{\frac{1}{2}(\gamma+1)}$.

The coordinates take the form where Δ is typical nozzle width S downstream.

$$[x, y, S] \longrightarrow \left[Re\Delta^{2-\gamma}x, \Delta\bar{y}, \Delta\bar{S}\right] \tag{2.29}$$

and the solution in the inviscid core yields the form

$$[u - u_c, v, p, \varrho, \psi] \approx \left[\Delta^{1-\gamma}, \Delta^{\gamma-1}, \Delta^{-\gamma}, \Delta^{-1}, 1\right], \tag{2.30}$$

whereas in the boundary layer where u_c is the velocity u along the centre line.

$$[u, v, p, \varrho] \approx \left[1, \Delta^{\gamma-1}, \Delta^{-\gamma}, \Delta^{-\gamma}\right]. \tag{2.31}$$

In the core or inviscid layer flow where no shock is present (see Brown *et al.* 1991) the velocity u in the continuity equation becomes replaced by unity and so

$$\frac{\partial \varrho}{\partial x} + \frac{\partial (\varrho v)}{\partial y} = 0. \tag{2.32}$$

In such inviscid fluid flow the viscous terms vanish and the momentum equation in the y direction is

$$\varrho \left(\frac{\partial v}{\partial x} + v \frac{\partial v}{\partial y} \right) = -\frac{\partial p}{\partial y}, \tag{2.33}$$

while the energy equation is expressed as the isentropic relation

$$p = K \varrho^{\gamma}, \tag{2.34}$$

where K is a positive constant. In the inviscid core flow the energy equation is similarly expressed (Brown *et al.*) as

$$\gamma p \left(u \frac{\partial \varrho}{\partial x} + v \frac{\partial \varrho}{\partial y} \right) = \varrho \left(u \frac{\partial p}{\partial x} + v \frac{\partial p}{\partial y} \right), \tag{2.35}$$

which is derived from the Eulerian form of the Navier-Stokes equation

$$c_p \varrho \frac{DT}{Dt} = \frac{Dp}{Dt}.$$

The boundary-layer equations can be simplified by the Howarth-Dorodnitsyn transformation. The purpose of this transformation is to remove the density ϱ from the equations, by introducing the new variable

$$y^* = \int_0^y \frac{\varrho dy}{\varrho_\infty}, \qquad \varrho = \varrho_\infty \left(\frac{\partial y^*}{\partial y} \right)$$

instead of y, leaving x unchanged. The velocity components are given in terms of the stream function ψ by

$$u = \frac{\partial \psi}{\partial y^*}, \tag{2.36}$$

$$v = -\frac{\partial \psi}{\partial x} = -\frac{\varrho}{\varrho_\infty} \left[\frac{\partial \psi}{\partial x} + \left(\frac{\partial y^*}{\partial x} \right)_y \frac{\partial \psi}{\partial y^*} \right] = -\frac{\varrho}{\varrho_\infty} \frac{\partial \psi}{\partial x}. \tag{2.37}$$

Substituting into the momentum equation yields

$$\varrho \left[u \frac{\partial u}{\partial x} + \left(-\frac{\varrho_\infty}{\varrho} \frac{\partial \psi}{\partial x} \right) \frac{\varrho}{\varrho_\infty} \frac{\partial u}{\partial y^*} \right] = -\frac{dp}{dx} + \frac{\varrho}{\varrho_\infty} \frac{\partial}{\partial y^*} \left(\mu \frac{\varrho}{\varrho_\infty} \frac{\partial u}{\partial y^*} \right),$$

or

$$\varrho \left(u \frac{\partial u}{\partial x} - \frac{\partial \psi}{\partial x} \frac{\partial u}{\partial y^*} \right) = -\frac{dp}{dx} + \frac{\varrho}{\varrho_\infty} \frac{\partial}{\partial y^*} \left(\frac{\gamma c_p}{\varrho_\infty} \frac{\partial u}{\partial y^*} \right)$$

or

$$u\frac{\partial u}{\partial x} - \frac{\partial \psi}{\partial x}\frac{\partial u}{\partial y^*} = -\frac{1}{\varrho}\frac{dp}{dx} + \frac{\gamma\, c_p}{{\varrho_\infty}^2}\frac{\partial^2 u}{\partial y^{*2}}$$

Since the enthalpy equation reads

$$\frac{1}{\varrho} = -\frac{(\gamma-1)}{2\gamma p}\left(2H - u^2\right),$$

and therefore the x-momentum equation becomes

$$u\frac{\partial u}{\partial x} - \frac{\partial \psi}{\partial x}\frac{\partial u}{\partial y^*} = -\frac{(\gamma-1)}{2\gamma p}\left(2H - u^2\right)p' + \gamma\, c_p\frac{\partial^2 u}{\partial y^{*2}}. \tag{2.38}$$

Similarly substitution into the energy equation yields

$$\varrho\left[u\frac{\partial H}{\partial x} + \left(-\frac{\varrho_\infty}{\varrho}\frac{\partial \psi}{\partial x}\right)\frac{\varrho}{\varrho_\infty}\frac{\partial H}{\partial y^*}\right] = \frac{\varrho}{\varrho_\infty}\frac{\partial}{\partial y^*}\left(\mu\frac{\varrho}{\varrho_\infty}\frac{\partial H}{\partial y^*}\right),$$

or

$$u\frac{\partial H}{\partial x} - \frac{\partial \psi}{\partial x}\frac{\partial H}{\partial y^*} = \gamma\, c_p\frac{\partial^2 H}{\partial y^{*2}}, \tag{2.39}$$

when the Prandtl number σ is taken as unity.

The boundary-layer thickness grows to the scale of Δ, the typical nozzle width S downstream, where x is of order $Re\Delta^{2-\gamma}$. By comparison, the pressure gradient in the y direction becomes significant at a distance $x \sim S^{\gamma+1/2}$, because of the inviscid core behaviour. These scalings are given in Brown *et al.* (1991)

Therefore as $S \longrightarrow O(\Delta)$ downstream, we assume that the viscous length scale $Re\Delta^{2-\gamma} \ll \Delta^{\frac{1}{2}\gamma+1}$ and then $\partial p/\partial y$ remains zero.

Hence we assume that

$$Re\Delta^{2-\gamma} \ll \Delta^{\frac{\gamma+1}{2}},$$

i.e.

$$\Delta^{\frac{3\gamma}{2}-\frac{3}{2}} \gg Re.$$

Consequently

$$\Delta \gg Re^{\frac{2}{3(\gamma-1)}} \tag{2.40}$$

holds for the present ones. Therefore, if Δ is greater than $O(Re^{\frac{2}{3(\gamma-1)}})$ then the y-momentum $\partial P/\partial y$ is negligible. In this thesis the case $\Delta \gg Re^{\frac{2}{3(\gamma-1)}}$ is analysed.

2.5 Upstream Influence

The non-uniqueness of the solution in viscous-inviscid compressible fluid flow due to upstream influence was discovered by Stewartson and Williams (1969) and Neiland (1970), especially the latter in the hypersonic case, in the solution near the leading edge of a flat plate. A change in the boundary conditions downstream has effect on the solution in the upstream region, as perturbations move upstream in hypersonic flow, not only for the boundary layer but also for the external inviscid layer.

The analysis of such upstream influence will be shown in Chapter 5.

Chapter 3

Governing Equations

3.1 Composite Governing Equations

In section 2.4 the separate governing equations were derived under certain assumptions in each of the main four distinct flow regions. These equations are of course reduced forms of the Navier-Stokes equations, the number of terms present being reduced in each region and some of the terms being interpreted in different form under transformation. A single, composite system of equations exists, however, which covers (includes) the separate regional equations above and yet is still a subset of the Navier-Stokes system. In this thesis the boundary layer equations (2.13) - (2.15), which still fulfill the above role, are taken as the composite governing equations for the entire region of the nozzle.

The order of magnitude of each term in the composite governing equations may be considered in each of the four regions described in the previous chapter, as follows.

In the inviscid layer in the near-throat stage, the continuity equation (2.21) is identical with the equation (2.13). Since in effect $\mu = 0$ in the inviscid layer, the momentum equation (2.22) has no viscous term and the equation (2.14) consists of all the terms of the equation (2.22) without the viscous term. The isentropic relation (2.24) is intrinsically contained in the energy equation (2.15).

In the inviscid layer in the farfield stage, since the typical value of the velocity u becomes nearly 1, the continuity equation (2.32) is identical with the equation (2.13) but with $u = 1$. Likewise the y-momentum equation (2.33) reduces simply to $\partial p/\partial y = 0$, because of the assumption made at the end of section 2.4, and then the x-momentum equation is incorporated in (2.14) without the viscous term and with $u = 1$. Again, the isentropic relation is contained in the energy equation (2.15).

In the viscous layer, the governing equations (2.36) - (2.39) are derived from the

boundary layer equations (2.13) - (2.15) by the Howard-Dorodnitsyn transformation, and all the terms of both sets of equations correspond to each other. The same applies to either viscous layer, whether in the near-throat or the farfield stage.

Therefore the boundary layer equations as a composite system are consistent with all the governing equations throughout the entire region of the nozzle. The composite problem to be solved now thus takes the form

$$\frac{\partial(\varrho_0 u_0)}{\partial x} + \frac{\partial(\varrho_0 v_0)}{\partial y} = 0, \tag{3.1}$$

$$\varrho_0 \left(u_0 \frac{\partial u_0}{\partial x} + v_0 \frac{\partial u_0}{\partial y} \right) = -\frac{dp_0}{dx} + Re^{-1} \frac{\partial}{\partial y} \left(\mu_0 \frac{\partial u_0}{\partial y} \right), \tag{3.2}$$

$$\varrho_0 c_p \left(u_0 \frac{\partial T_0}{\partial x} + v_0 \frac{\partial T_0}{\partial y} \right) = u_0 \frac{dp_0}{dx} + Re^{-1} \frac{\partial}{\partial y} \left(k \frac{\partial T_0}{\partial y} \right) + Re^{-1} \mu_0 \left(\frac{\partial u_0}{\partial y} \right)^2, \tag{3.3}$$

$$p_0 = R \varrho_0 T_0, \tag{3.4}$$

$$\mu_0 = \gamma C T_0, \tag{3.5}$$

with the boundary conditions for the nozzle.

$$u_0 = v_0 = 0 \quad \text{and} \quad T_0 = T_w \qquad \text{at} \qquad y = 0, \tag{3.6}$$

$$u_0' = T_0' = 0 \qquad \text{at} \qquad y = y_0 \quad (\text{centre} - \text{line}). \tag{3.7}$$

These boundary conditions (in y) are as explained in section 2 except that now the matching or interfacial conditions are absent because of the present composite approach. Boundary or starting conditions in x are also assumed together with a total flux constraint (on ψ), which prevents trivial zero flow solutions.

To eliminate the Re factor, we set $C = \hat{C}Re$, along with $\mu_0 = \hat{\mu}_0 Re$ and $k = \hat{k}Re$. Then the equations (3.1) - (3.7) hold with Re replaced by 1, and C, μ_0, k replaced by $\hat{C}$, $\hat{\mu}_0$, $\hat{k}$ respectively. Henceforth in this thesis we then use C, μ_0, k to represent $\hat{C}$, $\hat{\mu}_0$, $\hat{k}$ in turn, with Re effectively unity in (3.1) - (3.7).

3.2 Illingworth-Stewartson Transformation

The compressible boundary layer flow, or nozzle flow as in (3.1) - (3.7), involves a rather large number of independent variables. The calculations required become complicated particularly when a non-zero pressure gradients present. Illingworth (1949) and Stewartson (1950) presented transformation which correlates incompressible and compressible boundary layers. The method is slightly modified by Schlichting

(1951) as follows. The compressible boundary layer equations are reduced to almost the same form as that valid for incompressible fluid flow. This reduction is achieved by the assumptions that the boundary is thermally insulating, i.e. adiabatic, the viscosity μ varies as the absolute temperature T, and the Prandtl number σ has an arbitrary constant value. Then the various results in the incompressible theory can be taken over into the compressible case. The reason for our interest in this aspect of external compressible boundary layers is that it provides a motivation for the subsequent search for similarity solutions of the present composite system (3.1) - (3.7) above for nozzle flows.

The Illingworth-Stewartson transformation introduces two new coordinates by means of the definitions

$$\tilde{x} = \int_0^x b\frac{p_1 c_1}{p_0 c_0}dx \quad \text{and} \quad \tilde{y} = \frac{c_1}{c_0}\int_0^y \frac{\varrho}{\varrho_0}dy. \tag{3.8}$$

Here the constant b is provided as

$$b = \left(\frac{T_w}{T_0}\right)^{\frac{1}{2}} \frac{T_0 + S_1}{T_w + S_1},$$

which is derived from the Sutherland's law of viscosity, for convenience, where T_0 denotes the the reference temperature and T_w the wall temperature, and S_1 is a temperature constant. Also, c denotes the velocity of sound, the subscript 1 refers to conditions at the outer edge of the boundary layer, and

$$c_1{}^2 = (\gamma - 1)\, c_p T_1 \quad \text{and} \quad c_0{}^2 = (\gamma - 1)\, c_p T_0.$$

We note that the reasoning applies for both external and internal (nozzle) flows, as we will see later, but we work here in terms of the external boundary layer context, for convenience. The continuity equation is satisfied through the derivatives of the stream function $\psi(x, y)$ as

$$\frac{\partial \psi}{\partial y} = \frac{\varrho}{\varrho_0}u \quad \text{and} \quad \frac{\partial \psi}{\partial x} = -\frac{\varrho}{\varrho_0}v.$$

After the transformation ψ is regarded as a function of $\tilde{x}$ and $\tilde{y}$, so that

$$\frac{\partial \psi}{\partial x} = \frac{d\tilde{x}}{dx}\frac{\partial \psi}{\partial \tilde{x}} + \frac{\partial \tilde{y}}{\partial x}\frac{\partial \psi}{\partial \tilde{y}} = \frac{b p_1 c_1}{p_0 c_0}\frac{\partial \psi}{\partial \tilde{x}} + \frac{\partial \tilde{y}}{\partial x}\frac{\partial \psi}{\partial \tilde{y}}$$

and

$$\frac{\partial \psi}{\partial y} = \frac{\partial \tilde{y}}{\partial y}\frac{\partial \psi}{\partial \tilde{y}} = \frac{c_1 \varrho}{c_0 \varrho_0}\frac{\partial \psi}{\partial \tilde{y}},$$

since $\partial \tilde{x}/\partial y = 0$. Therefore the momentum equation after the Illingworth-Stewartson transformation becom

$$u\frac{\partial u}{\partial x} + v\frac{\partial u}{\partial y} = \left(\frac{c_1}{c_0}\right)^3 \frac{p_1 b}{p_0}\left[\frac{\partial \psi}{\partial \tilde{y}}\frac{\partial^2 \psi}{\partial \tilde{y}\partial \tilde{x}} - \frac{\partial \psi}{\partial \tilde{x}}\frac{\partial^2 \psi}{\partial \tilde{y}^2} + \frac{1}{c_1}\frac{dc_1}{d\tilde{x}}\left(\frac{d\psi}{d\tilde{y}}\right)^2\right].$$

Along the flow at the outer edge of the boundary layer the enthalpy remains constant as the isentropic relations hold,

$$h_1 = c_p T_1 + \frac{1}{2}{u_1}^2 = c_p T_0,$$

or, in terms of the velocity of sound, we have

$${c_1}^2 + \frac{1}{2}(\gamma - 1){u_1}^2 = {c_0}^2,$$

yielding

$$\frac{1}{c_1}\frac{dc_1}{dx} = -\frac{1}{2}(\gamma - 1)\frac{u_1}{{c_1}^2}\frac{du_1}{dx}.$$

Therefore

$$u\frac{\partial u}{\partial x} + v\frac{\partial u}{\partial y} = \left(\frac{c_1}{c_0}\right)^3 \frac{p_1 b}{p_0}\left(\frac{\partial \psi}{\partial \tilde{y}}\frac{\partial^2 \psi}{\partial \tilde{y}\partial \tilde{x}} - \frac{\partial \psi}{\partial \tilde{x}}\frac{\partial^2 \psi}{\partial \tilde{y}^2}\right) - \frac{1}{2}(\gamma - 1)\frac{u^2}{{c_1}^2}u_1\frac{du_1}{dx}$$

since

$$\frac{d\tilde{x}}{dx} = b\frac{p_1 c_1}{p_0 c_0}.$$

The viscous term in the equation can be written as

$$\frac{1}{\varrho}\frac{\partial}{\partial y}\left(\mu\frac{\partial u}{\partial y}\right) = \frac{\nu_0 b p_1}{p_0}\left(\frac{c_1}{c_0}\right)^3 \frac{\partial^3 \psi}{\partial \tilde{y}^3},$$

and the pressure gradient term as

$$-\frac{1}{\varrho}\frac{dp}{dx} = -\frac{T}{\varrho_1 T_1}\frac{dp_1}{dx} = \frac{T}{T_1}u_1\frac{du_1}{dx}.$$

The relative stagnation-enthalpy difference which is the dimensionless temperature function is introduced by the definition

$$\vartheta = \frac{c_p T + \frac{1}{2}u^2}{c_p T_0} - 1 = \frac{\hat{h} + \frac{1}{2}u^2}{h_0} - 1,$$

where $\hat{h}$ denotes the local, as distinct from the stagnation, enthalpy. This is written in terms of the velocity of sound as

$$-\frac{1}{\varrho}\frac{dp}{dx} = \left[(1+\vartheta)\left(\frac{c_0}{c_1}\right)^2 - \frac{\gamma - 1}{2}\frac{u^2}{{c_1}^2}\right]u_1\frac{du_1}{dx}.$$

Finally the momentum equation becomes

$$\frac{\partial \psi}{\partial \tilde{y}}\frac{\partial^2 \psi}{\partial \tilde{y}\partial \tilde{x}} - \frac{\partial \psi}{\partial \tilde{x}}\frac{\partial^2 \psi}{\partial \tilde{y}^2} = (1+\vartheta)\left(\frac{c_0}{c_1}\right)^5 \frac{p_0}{p_1 b}u_1\frac{du_1}{dx} + \nu_0\frac{\partial^3 \psi}{\partial \tilde{y}^3}.$$

Further

$$\frac{du_1}{dx} = \frac{1}{c_0}\left(\tilde{u}_1\frac{dc_1}{dx} + c_1\frac{d\tilde{u}_1}{d\tilde{x}}\right),$$

which becomes

$$u_1\frac{du_1}{dx} = \left(\frac{c_1}{c_0}\right)^5 \frac{bp_1}{p_0}\tilde{u}_1\frac{d\tilde{u}_1}{d\tilde{x}}.$$

Therefore, after the Illingworth-Stewartson transformation, the momentum equation takes the form

$$\tilde{u}\frac{\partial\tilde{u}}{\partial\tilde{x}} + \tilde{v}\frac{\partial\tilde{u}}{\partial\tilde{y}} = \tilde{u}_1\frac{d\tilde{u}_1}{d\tilde{x}}(1+\vartheta) + \nu_0\frac{\partial^2\tilde{u}}{\partial\tilde{y}^2}. \tag{3.9}$$

In order to transform the energy equation, the momentum equation is multiplied by u and added to the energy equation, giving

$$\varrho u\frac{\partial}{\partial x}\left(c_pT + \frac{1}{2}u^2\right) + \varrho v\frac{\partial}{\partial y}\left(c_pT + \frac{1}{2}u^2\right) = \frac{\partial}{\partial y}\left[\mu\frac{\partial}{\partial y}\left(\frac{c_pT}{\sigma} + \frac{1}{2}u^2\right)\right].$$

The temperature function ϑ is then substituted to transform the equation into

$$\varrho u\frac{\partial\vartheta}{\partial x} + \varrho v\frac{\partial\vartheta}{\partial y} = \frac{\partial}{\partial y}\left\{\mu\left[\frac{1}{\sigma}\frac{\partial\vartheta}{\partial y} + \frac{\sigma-1}{\sigma}\frac{\partial}{\partial y}\left(\frac{u^2}{2c_pT_0}\right)\right]\right\}.$$

The partial derivatives with respect to x and y are replaced now by those with respect to $\tilde{x}$ and $\tilde{y}$, so that

$$\tilde{u}\frac{\partial\vartheta}{\partial\tilde{x}} + \tilde{v}\frac{\partial\vartheta}{\partial\tilde{y}} = \nu_0\left\{\frac{1}{\sigma}\frac{\partial^2\vartheta}{\partial\tilde{y}^2} + \frac{\sigma-1}{\sigma}\frac{\partial^2}{\partial\tilde{y}^2}\left(\frac{u^2}{2c_pT_0}\right)\right\}.$$

Since the Mach number at the outer edge of boundary layer is $M_1 = u_1/c_1$, and as the stagnation enthalpy remains constant,

$$\frac{u^2}{2c_pT_0} = \frac{\frac{1}{2}(\gamma-1)\,{M_1}^2}{1+\frac{1}{2}(\gamma-1)\,{M_1}^2}\left(\frac{\tilde{u}}{\tilde{u}_1}\right)^2.$$

Hence the energy equation after the Illingworth-Stewartson transformation acquires the form

$$\tilde{u}\frac{\partial\vartheta}{\partial\tilde{x}} + \tilde{v}\frac{\partial\vartheta}{\partial\tilde{y}} = \nu_0\left\{\frac{1}{\sigma}\frac{\partial^2\vartheta}{\partial\tilde{y}^2} + \frac{\sigma-1}{\sigma}\frac{\frac{1}{2}(\gamma-1)\,{M_1}^2}{1+\frac{1}{2}(\gamma-1)\,{M_1}^2}\frac{\partial^2}{\partial\tilde{y}^2}\left[\left(\frac{\tilde{u}}{\tilde{u}_1}\right)^2\right]\right\}. \tag{3.10}$$

The continuity equation is transformed to

$$\frac{\partial\tilde{u}}{\partial\tilde{x}} + \frac{\partial\tilde{v}}{\partial\tilde{y}} = 0, \tag{3.11}$$

in similar fashion. The boundary conditions are originally

$$u = v = 0 \quad \text{and} \quad T = T_w \quad \text{at} \quad y = 0,$$

$$u \longrightarrow u_1(x) \quad \text{and} \quad T \longrightarrow T_1(x) \quad \text{as} \quad y \longrightarrow \infty.$$

These boundary conditions are transformed as follows:

$$\tilde{u} = \tilde{v} = 0 \quad \text{and} \quad \vartheta = \vartheta_w \quad \text{at} \quad \tilde{y} = 0, \tag{3.12}$$

$$\tilde{u} \longrightarrow \tilde{u}_1(\tilde{x}) \quad \text{and} \quad \vartheta \longrightarrow 0 \quad \text{as} \quad \tilde{y} \longrightarrow \infty. \tag{3.13}$$

For later use, we observe that (3.13), which holds for the external boundary layer case, is replaced in the internal nozzle case by

$$u' = \vartheta' = 0 \quad \text{at} \quad y = y_0 \quad \text{(the centre line)}$$

from (3.7), the corresponding $u_1(x)$, $T_1(x)$ values at $y = y_0$ being unknown then.

In a limiting case, if the Prandtl number σ is unity, the energy equation (3.10) is reduced to the incompressible form,

$$\tilde{u}\frac{\partial \vartheta}{\partial \tilde{x}} + \tilde{v}\frac{\partial \vartheta}{\partial \tilde{y}} = \frac{\nu_0}{\sigma}\frac{\partial^2 \vartheta}{\partial \tilde{y}^2}. \tag{3.14}$$

Therefore, after the Illingworth-Stewartson transformation, the boundary layer equations for a compressible flow are transformed into those for an incompressible flow, from (3.9), (3.11) - (3.14), assuming that the boundary is thermally insulating, the viscosity is proportional to the temperature, and the Prandtl number σ is unity.

3.3 Self-Similar Exact Solutions

Similarity solutions constitute a simple class of solutions which enable the system of partial differential equations to be reduced to ordinary differential equations. Such similarity solutions were first deduced by Falkner and Skan (1931) and Hartree (1937) for incompressible fluid flow, and by Illingworth (1949), Stewartson (1949) and Li and Nagamatsu (1953) for compressible fluid flow.

From the definition of the stream function $\psi(x, y)$ the function can be defined by

$$\tilde{u} = \frac{\partial \psi}{\partial \tilde{y}} \quad \text{and} \quad \tilde{v} = -\frac{\partial \psi}{\partial \tilde{x}}, \tag{3.15}$$

with $\psi = 0$ at the wall say. Along with this continuity equation, the momentum equation and the energy equation after the Illingworth-Stewartson transformation, (3.9) and (3.14), can be written in terms of the stream function as

$$\frac{\partial\psi}{\partial\tilde{y}}\frac{\partial^2\psi}{\partial\tilde{x}\partial\tilde{y}} - \frac{\partial\psi}{\partial\tilde{x}}\frac{\partial^2\psi}{\partial\tilde{y}^2} = \tilde{u_1}\frac{d\tilde{u_1}}{d\tilde{x}}(1+\vartheta) + \nu_0\frac{\partial^3\psi}{\partial\tilde{y}^3}, \tag{3.16}$$

and

$$\frac{\partial\psi}{\partial\tilde{y}}\frac{\partial\vartheta}{\partial\tilde{x}} - \frac{\partial\psi}{\partial\tilde{x}}\frac{\partial\vartheta}{\partial\tilde{y}} = \frac{\nu_0}{\sigma}\frac{\partial^2\vartheta}{\partial\tilde{y}^2}. \tag{3.17}$$

A similarity form is introduced (or tried) now with the following assumptions :

$$\begin{aligned}\psi &= A\tilde{x}^a\tilde{u}_1^p f(\eta),\\ \tilde{y} &= B\tilde{x}^b\tilde{u}_1^q\eta,\\ \vartheta &= \vartheta(\eta),\end{aligned}$$

where A, B, a, b, p, q are undetermined constants, $f(\eta)$ is an unknown effective stream function of η only, and $\vartheta(\eta)$ is the effective temperature function.
In the downstream motion for instance, such a similar solution is suggested when the main stream velocity is taken to be of the form

$$u_1 = \kappa\tilde{x}^m. \tag{3.18}$$

In order to transform the equations (3.8) and (3.9) to the coordinates $\tilde{x}$ and η, and to eliminate $\tilde{x}$ in the resulting expression, the transformation is assumed to be in the particular form

$$\begin{aligned}\psi &= \left(\frac{2\nu_0}{m+1}\right)^{\frac{1}{2}}\tilde{x}^{\frac{1}{2}}\tilde{u}_1^{\frac{1}{2}}f,\\ \tilde{y} &= \left(\frac{2\nu_0}{m+1}\right)^{\frac{1}{2}}\tilde{x}^{\frac{1}{2}}\tilde{u}_1^{-\frac{1}{2}}\eta,\end{aligned}$$

$A = \left(\frac{2\nu_0}{m+1}\right)$, $a = \frac{1}{2}$, $p = \frac{1}{2}$,

and the operators are

$$\begin{aligned}\partial_{\tilde{y}} &= \left(\frac{m+1}{2\nu_0}\right)^{\frac{1}{2}}\kappa^{\frac{1}{2}}\tilde{x}^{\frac{m-1}{2}}\partial_\eta,\\ \partial_{\tilde{x}} &= \partial_{\tilde{x}} + \frac{m-1}{2}\frac{\eta}{\tilde{x}}\partial_\eta.\end{aligned}$$

The derivatives of the stream function are

$$\begin{aligned}\frac{\partial\psi}{\partial\tilde{y}} &= \kappa\tilde{x}^m f' \quad (= u_1 f'),\\ \frac{\partial^2\psi}{\partial\tilde{y}^2} &= \left(\frac{m+1}{2\nu_0}\right)^{\frac{1}{2}}\kappa^{\frac{3}{2}}\tilde{x}^{\frac{3m-1}{2}}f'',\end{aligned}$$

$$\begin{aligned}
\frac{\partial^3\psi}{\partial\tilde{y}^3} &= \frac{m+1}{2\nu_0}\kappa^2\tilde{x}^{2m-1}f''', \\
\frac{\partial\psi}{\partial\tilde{x}} &= \left(\frac{2\nu_0}{m+1}\right)^{\frac{1}{2}}\frac{m+1}{2}\kappa^{\frac{1}{2}}\tilde{x}^{\frac{m-1}{2}}f + \left(\frac{2\nu_0}{m+1}\right)^{\frac{1}{2}}\frac{m-1}{2}\kappa^{\frac{1}{2}}\tilde{x}^{\frac{m-1}{2}}\eta f', \\
\frac{\partial^2\psi}{\partial\tilde{x}\partial\tilde{y}} &= m\kappa\tilde{x}^{m-1}f' + \kappa\frac{m-1}{2}\tilde{x}^{m-1}\eta f'',
\end{aligned}$$

where the primes denote differentiation with respect to η. These are substituted into the momentum equation (3.8) and that yields

$$\nu_0\frac{m+1}{2\nu_0}\kappa^2\tilde{x}^{2m-1}f''' + \frac{m+1}{2}\kappa^2\tilde{x}^{2m-1}ff'' + \frac{m-1}{2}\kappa^2\tilde{x}^{2m-1}f'f''$$

$$= \kappa^2 m\tilde{x}^{2m-1}f'f' + \frac{m-1}{2}\kappa^2\tilde{x}^{2m-1}f'f'' - \kappa\tilde{x}^m\cdot m\kappa\tilde{x}^{m-1}(1+\vartheta),$$

or

$$f''' + ff'' = \frac{2m}{m+1}\left(f'^2 - 1 - \vartheta\right) \tag{3.19}$$

Here the parameter β is introduced by the definition

$$\beta = \frac{2m}{m+1}. \tag{3.20}$$

This characterises the pressure gradient of the external stream. Then the equation (3.11) becomes

$$f''' + ff'' = \beta\left(f'^2 - 1 - \vartheta\right). \tag{3.21}$$

Similarly for the energy equation, the derivatives of the relative stagnation-enthalpy differences are as follows:

$$\begin{aligned}
\frac{\partial\vartheta}{\partial\tilde{y}} &= \left(\frac{m+1}{2\nu_0}\right)^{\frac{1}{2}}\kappa^{\frac{1}{2}}\tilde{x}^{\frac{m-1}{2}}\vartheta', \\
\frac{\partial^2\vartheta}{\partial\tilde{y}^2} &= \frac{m+1}{2\nu_0}\kappa\tilde{x}^{m-1}\vartheta'', \\
\frac{\partial\vartheta}{\partial\tilde{x}} &= \frac{m-1}{2}\frac{\eta}{\tilde{x}}\vartheta'.
\end{aligned}$$

Then the equation (3.9) becomes

$$\nu_0\frac{m+1}{2\nu_0}\kappa\tilde{x}^{m-1}\vartheta'' + \frac{m+1}{2}\kappa\tilde{x}^{m-1}f\vartheta' + \frac{m-1}{2}\kappa\tilde{x}^{m-1}\eta f'\vartheta' - \frac{m-1}{2}\kappa\tilde{x}^{m-1}\eta f'\vartheta' = 0,$$

or

$$\vartheta'' + f\vartheta' = 0. \tag{3.22}$$

Therefore two ordinary differential equations are obtained for the functions $f(\eta)$ and $\vartheta(\eta)$

$$f''' + ff'' = \beta\left(f'^2 - 1 - \vartheta\right), \tag{3.13}$$

$$\vartheta'' + f\vartheta' = 0. \tag{3.14}$$

with the boundary conditions

$$f = f' = 0, \quad \vartheta = \vartheta_w \qquad \text{at} \qquad \eta = 0, \tag{3.15}$$

$$f' = 1, \quad \vartheta = 0 \qquad \text{at} \qquad \eta = \eta_0 \quad (\text{centre} - \text{line}). \tag{3.16}$$

In the case of an adiabatic wall, the equation (3.11) is identical with the Falkner-Skan equation for a similarity solution in incompressible flow, and the system of partial differential equations (3.8) and (3.9) are now reduced to one ordinary differential equation

$$f''' + ff'' = \beta\left(f'^2 - 1\right). \tag{3.17}$$

In the upstream flow region, this result has to be checked to find out whether it is valid before the throat, where x has a negative value. In the reservoir or upstream farfield stage where $x \longrightarrow -\infty$, in the core region, the width of the nozzle $S \longrightarrow +\infty$ since $S \propto |x|^m$. The density ϱ and the pressure p tend to constant values. And the velocity $u \sim 0$ since

$$u = \frac{1}{\varrho S} \sim |x|^{-m}.$$

In the reservoir, the variables are expanded with respect to η,

$$y = |\tilde{x}|^{\frac{m+1}{2}}\eta, \quad u = |\tilde{x}|^{-m}\bar{u}(\eta), \quad v = |\tilde{x}|^{-\frac{m+1}{2}}\bar{v}(\eta),$$

$$T = \bar{T}(\eta), \quad \varrho = \bar{\varrho}(\eta), \quad \mu = \bar{\mu}(\eta), \quad p = p_{res} + \bar{p}_1,$$

where p_1 is given by the core solution. From the continuity equation the stream function ψ is of the order of

$$\psi = |\tilde{x}|^{\frac{1-m}{2}} f$$

in the reservoir. Then a transformation is assumed, analogous with the downstream case, to be in the form

$$\begin{aligned} \psi &= \left(\frac{2\nu_0}{m-1}\right)^{\frac{1}{2}} |\tilde{x}|^{\frac{-m+1}{2}} f, \\ \tilde{y} &= \left(\frac{2\nu_0}{m-1}\right)^{\frac{1}{2}} |\tilde{x}|^{\frac{m+1}{2}} \eta \end{aligned}$$

and the operators are

$$\begin{aligned} \partial_{\tilde{y}} &= \left(\frac{m-1}{2\nu_0}\right)^{\frac{1}{2}} |\tilde{x}|^{\frac{-m-1}{2}} \partial_\eta, \\ \partial_{|\tilde{x}|} &\longrightarrow -\partial_{|\tilde{x}|} + \frac{m+1}{2}\frac{\eta}{|\tilde{x}|}\partial_\eta. \end{aligned}$$

The derivatives of the stream function are therefore

$$\begin{aligned}
\frac{\partial\psi}{\partial\tilde{y}} &= |\tilde{x}|^{-m}f', \\
\frac{\partial^2\psi}{\partial\tilde{y}^2} &= \left(\frac{m-1}{2\nu_0}\right)^{\frac{1}{2}}|\tilde{x}|^{\frac{-3m-1}{2}}f'', \\
\frac{\partial^3\psi}{\partial\tilde{y}^3} &= \frac{m-1}{2\nu_0}|\tilde{x}|^{-2m-1}f''', \\
\frac{\partial\psi}{\partial\tilde{x}} &= -\frac{\partial\psi}{\partial|\tilde{x}|} = -\left(\frac{2\nu_0}{m-1}\right)^{\frac{1}{2}}\frac{-m+1}{2}|\tilde{x}|^{\frac{-m-1}{2}}f + \left(\frac{2\nu_0}{m-1}\right)^{\frac{1}{2}}\frac{m+1}{2}|\tilde{x}|^{\frac{-m-1}{2}}\eta f', \\
\frac{\partial^2\psi}{\partial\tilde{x}\partial\tilde{y}} &= -\frac{\partial^2\psi}{\partial|\tilde{x}|\partial\tilde{y}} = m|\tilde{x}|^{-m-1}f' + \frac{m+1}{2}|\tilde{x}|^{-m-1}\eta f'',
\end{aligned}$$

where the primes denote differentiation with respect to η. These are substituted into the momentum equations (3.8) and that yields

$$\nu_0\frac{m-1}{2\nu_0}|\tilde{x}|^{-2m-1}f''' + \frac{m-1}{2}|\tilde{x}|^{-2m-1}ff'' + \frac{m+1}{2}|\tilde{x}|^{-2m-1}f'f''$$

$$= m|\tilde{x}|^{-2m-1}f'f' + \frac{m+1}{2}|\tilde{x}|^{-2m-1}f'f'' - m|\tilde{x}|^{-2m-1}(1+\vartheta).$$

Hence

$$f''' + ff'' = \frac{2m}{m-1}\left(f'^2 - 1 - \vartheta\right) \tag{3.18}$$

if the parameter $\bar{\beta}$

$$\bar{\beta} = \frac{2m}{m-1}. \tag{3.19}$$

Similarly the energy equation (3.9) becomes

$$\nu_0\frac{m-1}{2\nu_0}|\tilde{x}|^{-m-1}\vartheta'' + \frac{m-1}{2}|\tilde{x}|^{-m-1}f\vartheta' + \frac{m+1}{2}|\tilde{x}|^{-m-1}\eta f'\vartheta' - \frac{m+1}{2}|\tilde{x}|^{-m-1}\eta f'\vartheta' = 0,$$

or

$$\vartheta'' + f\vartheta' = 0. \tag{3.20}$$

In order to seek a resemblance with the Illingworth-Stewartson transformation, the ordinary boundary layer equations have to be expressed in terms of $\tilde{\eta}$. Since $\psi = |\tilde{x}|^{\frac{1-m}{2}}\bar{\psi}(\tilde{\eta}) + \cdots$, the continuity equations

$$\varrho u = \psi_y, \quad \varrho v = -\psi_x$$

can be written in terms of $\tilde{\eta}$

$$\begin{aligned}
\bar{\varrho}\bar{u}|\tilde{x}|^{-m} &= |\tilde{x}|^{\frac{1-m}{2}}\bar{\psi}'|x|^{-\frac{m+1}{2}}, \\
\bar{\varrho}\bar{v}|\tilde{x}|^{-\frac{m+1}{2}} &= +\frac{1-m}{2}|\tilde{x}|^{\frac{-1-m}{2}}\bar{\psi} - \frac{m+1}{2}\tilde{\eta}\bar{\psi}'|\tilde{x}|^{\frac{-1-m}{2}}.
\end{aligned}$$

When $|x|$ terms have been cancelled out

$$\begin{aligned}\bar{\varrho}\bar{u} &= \bar{\psi}_{\tilde{\eta}}\bar{\varrho},\\ \bar{\varrho}\bar{v} &= \frac{1-m}{2}\bar{\psi} - \frac{m+1}{2}\tilde{\eta}\bar{\psi}_{\tilde{\eta}}\bar{\varrho},\end{aligned}$$

and so the continuity equations can be written simply as

$$\bar{u} = \bar{\psi}_{\tilde{\eta}}, \tag{3.21}$$

$$\bar{\varrho}\bar{v} = \frac{1-m}{2}\bar{\psi} - \frac{m+1}{2}\tilde{\eta}\bar{u}\bar{\varrho}. \tag{3.22}$$

Since $u' = \bar{u}_{\tilde{\eta}}\bar{\varrho}$ the x-momentum equation can be expressed as

$$\varrho\left(m\bar{u}^2 + \frac{m+1}{2}\tilde{\eta}\bar{u}\bar{u}' + \bar{v}\bar{u}'\right) = -2m\bar{p} + (\bar{\mu}\bar{u}')',$$

or in terms of $\tilde{\eta}$

$$\varrho\left(m\bar{u}^2 + \frac{m+1}{2}\eta\bar{u}\bar{\varrho}\bar{u}_{\tilde{\eta}} + \bar{v}\bar{\varrho}\bar{u}_{\tilde{\eta}}\right) = -2m\bar{p} + \left(\bar{\mu}\bar{\varrho}\bar{u}_{\tilde{\eta}}\right)_{\tilde{\eta}}\bar{\varrho}.$$

The velocity u can be written as the derivative of the stream function, $\psi_{\tilde{\eta}}$, and then

$$\varrho\left[m\bar{\psi}_{\tilde{\eta}}^2 + \left(\frac{1-m}{2}\bar{\psi} - \bar{\varrho}\bar{v}\right)\bar{\psi}_{\tilde{\eta}\tilde{\eta}} + \bar{v}\bar{\varrho}\bar{\psi}_{\tilde{\eta}\tilde{\eta}}\right] = -2m\bar{p} + \left(\bar{\mu}\bar{\varrho}\bar{\psi}_{\tilde{\eta}\tilde{\eta}}\right)_{\tilde{\eta}}\bar{\varrho}.$$

It follows that

$$\begin{aligned}m\bar{\psi}_{\tilde{\eta}}^2 + \frac{1-m}{2}\bar{\psi}\bar{\psi}_{\tilde{\eta}\tilde{\eta}} &= -\frac{2m\bar{p}}{\bar{\varrho}} + \left(\bar{\mu}\bar{\varrho}\bar{\psi}_{\tilde{\eta}\tilde{\eta}}\right)_{\tilde{\eta}}\\ &= -\frac{2m\bar{p}}{\bar{\varrho}} + (\bar{\mu}\bar{\varrho})_{\tilde{\eta}}\bar{\psi}_{\tilde{\eta}\tilde{\eta}} + (\bar{\mu}\bar{\varrho})\bar{\psi}_{\tilde{\eta}\tilde{\eta}\tilde{\eta}}.\end{aligned} \tag{3.23}$$

Similarly the energy equation becomes

$$\bar{\varrho}c_p\left(\frac{m+1}{2}\bar{u}\eta\bar{T}' + \bar{v}\bar{T}'\right) = m'\bar{T}' + m\bar{T}''.$$

Since the equation (3.22) holds, we then have

$$c_p\left(\frac{1-m}{2}\bar{\psi}\bar{T}' - \bar{\varrho}\bar{v}\bar{T}' + \bar{\varrho}\bar{v}\bar{T}'\right) = m'\bar{T}' + m\bar{T}'',$$

or

$$c_p\frac{1-m}{2}\bar{\psi}\bar{T}' = m'\bar{T}' + m\bar{T}''.$$

So in terms of $\tilde{\eta}$

$$c_p\frac{1-m}{2}\bar{\psi}\bar{\varrho}\bar{T}_{\tilde{\eta}} = \bar{\varrho}\left(m\bar{\varrho}\bar{T}_{\tilde{\eta}}\right)_{\tilde{\eta}}. \tag{3.24}$$

Therefore the boundary-layer equations can be written as

$$\left(\gamma C\frac{p_{res}}{R}\right)\bar{\psi}_{\tilde{\eta}\tilde{\eta}\tilde{\eta}}-\left(\frac{1-m}{2}\right)\bar{\psi}\bar{\psi}_{\tilde{\eta}\tilde{\eta}}=m\bar{\psi}_{\tilde{\eta}}^{2}+2m\bar{p}\frac{R}{p_{res}}\bar{T}, \tag{3.25}$$

$$\frac{\gamma C}{\sigma}\frac{R}{p_{res}}\bar{T}_{\tilde{\eta}\tilde{\eta}}-\frac{1-m}{2}\bar{\psi}\bar{T}_{\tilde{\eta}}=0. \tag{3.26}$$

Next, new variables are introduced to simplify the coefficients:

$$\begin{aligned}\bar{T} &= \lambda_4\vartheta_T,\\ \bar{\psi} &= \lambda_5 f_T,\\ \tilde{\eta} &= \lambda_6\eta_T \qquad \text{or} \qquad \frac{d}{d\tilde{\eta}}=\frac{1}{\lambda_6}\frac{d}{d\eta_T},\end{aligned}$$

with λ_4, λ_5, λ_6 to be found. Then the equation (3.25) becomes

$$\begin{aligned}\left(\gamma C\frac{p_{res}}{R}\right)\frac{1}{\lambda_6^3}\frac{d^3}{d{\eta_T}^3}(\lambda_5 f_T)+\frac{m-1}{2}\lambda_5 f_T\frac{1}{\lambda_6^2}\frac{d^2}{d{\eta_T}^2}(\lambda_5 f_T)\\ =m\left[\frac{1}{\lambda_6}\frac{d}{d\eta_T}(\lambda_5 f_T)\right]^2+2m\bar{p}\frac{R}{p_{res}}\bar{T}(\lambda_4\vartheta_T),\end{aligned}$$

or the ordinary differential equations in terms of f as

$$\frac{\gamma C p_{res}}{R}\frac{\lambda_5}{\lambda_6^3}{f_T}'''+\frac{m-1}{2}\left(\frac{\lambda_5}{\lambda_6}\right)^2 f_T{f_T}''=m\left[\frac{\lambda_5}{\lambda_6}{f_T}'\right]^2+\frac{2m\bar{p}R\lambda_4}{p_{res}}\vartheta_T.$$

Also the equation (3.26)

$$\frac{\gamma C}{\sigma}\frac{R}{p_{res}}\frac{1}{\lambda_6^2}\frac{d^2}{d{\eta_T}^2}(\lambda_4\vartheta_T)+\frac{m-1}{2}\lambda_5 f_T\frac{1}{\lambda_6}\frac{d^2}{d\eta_T}(\lambda_4\vartheta_T)=0,$$

or

$$\frac{\gamma C}{\sigma}\frac{R}{p_{res}}\frac{\lambda_4}{\lambda_6^2}{\vartheta_T}''+\frac{m-1}{2}\frac{\lambda_4\lambda_5}{\lambda_6}f_T{\vartheta_T}''=0.$$

Therefore the coefficients λ_4, λ_5, λ_6 are related to the constants above as follows:

$$\frac{\gamma C p_{res}}{R}\frac{\lambda_5}{\lambda_6^3}=1,\quad \frac{m-1}{2}\left(\frac{\lambda_5}{\lambda_6}\right)^2=1,\quad m\left[\frac{\lambda_5}{\lambda_6}\right]^2=\beta,\quad \frac{2m\bar{p}R\lambda_4}{p_{res}}=\beta,$$

$$\frac{\gamma C}{\sigma}\frac{R}{p_{res}}\frac{\lambda_4}{\lambda_6^2}=1,\quad \frac{m-1}{2}\frac{\lambda_4\lambda_5}{\lambda_6}=1.$$

Hence the suggestion is that there exists a similarity solution for the boundary layer equations if λ_4, λ_5, λ_6 satisfy the conditions above.

We now introduce the coordinate

$$\hat{\eta} = \frac{\tilde{y}}{|x|^{\frac{m+1}{2}}},$$

in view of the above arguments. Expanding the variables with respect to $\hat{\eta}$ as $x \longrightarrow \infty$ then gives

$$\begin{aligned} \tilde{\psi} &= |x|^{\frac{1-m}{2}} \bar{\psi}(\hat{\eta}), \\ \vartheta &= \hat{\vartheta}(\hat{\eta}). \end{aligned}$$

Since $\tilde{\psi} = |\tilde{x}|^{\frac{1-m}{2}} F + \cdots$, the derivatives of the stream function are as follows:

$$\begin{aligned} \tilde{\psi} &= |\tilde{x}|^{\frac{1-m}{2}} F, \\ \tilde{\psi}_{\tilde{x}\tilde{y}} &= -\tilde{\psi}_{|\tilde{x}|\tilde{y}} = -\left[-m|\tilde{x}|^{-m-1}F' - \left(\frac{m+1}{2}\right)\hat{\eta}F''|\tilde{x}|^{-m-1}\right], \\ \tilde{\psi}_{\tilde{x}} &= -\tilde{\psi}_{|\tilde{x}|} = -\left[\left(\frac{1-m}{2}\right)|\tilde{x}|^{\frac{-1-m}{2}}F - \left(\frac{m+1}{2}\right)\hat{\eta}F'|\tilde{x}|^{\frac{-1-m}{2}}\right], \\ \tilde{\psi}_{\tilde{y}\tilde{y}} &= |\tilde{x}|^{\frac{-1-3m}{2}}F'', \\ \tilde{\psi}_{\tilde{y}\tilde{y}\tilde{y}} &= |\tilde{x}|^{-1-2m}F'''. \end{aligned}$$

Substituting them into the Illingworth-Stewartson form, the momentum equation (3.9) becomes

$$\begin{aligned} +mF'^2|\tilde{x}|^{-2m-1} + \left(\frac{1-m}{2}\right)FF''|\tilde{x}|^{-2m-1} &= \tilde{u}_1\tilde{u}_{1\tilde{x}}(1+\vartheta) + \nu_0|\tilde{x}|^{-1-2m}F''' \\ &= (1+\vartheta)m\hat{u}_1^2|\tilde{x}|^{-2m-1} + \nu_0|\tilde{x}|^{-1-2m}F''', \end{aligned}$$

and hence

$$mF'^2 + \left(\frac{1-m}{2}\right)FF'' = (1+\vartheta)m\hat{u}_1^2 + \nu_0 F''', \tag{3.27}$$

and similarly the energy equation (3.14) becomes

$$-F\hat{\vartheta}_{\hat{\eta}} = \frac{\nu_0}{\sigma}\hat{\vartheta}_{\hat{\eta}\hat{\eta}}. \tag{3.28}$$

The Illingworth-Stewartson equations then take the form

$$\nu_0 F_{\hat{\eta}\hat{\eta}\hat{\eta}} + FF_{\hat{\eta}\hat{\eta}} = F_{\hat{\eta}}{}^2 - \hat{u}_1^2(1+\vartheta), \tag{3.29}$$

$$\frac{\nu_0}{\sigma}\hat{\vartheta}_{\hat{\eta}\hat{\eta}} - F\hat{\vartheta}_{\hat{\eta}} = 0. \tag{3.30}$$

The similarity variable is introduced with the following assumptions,

$$\begin{aligned} 1+\hat{\vartheta} &= \lambda_1\vartheta_T, \\ F &= \lambda_2 f_T, \\ \hat{\eta} &= \lambda_3\eta_T \qquad \text{or} \qquad \frac{d}{d\hat{\eta}} = \frac{1}{\lambda_3}\frac{d}{d\eta_T}. \end{aligned}$$

Then the equation (3.29) becomes

$$\frac{\nu_0}{\lambda_3^3}\frac{d^3}{d\eta_T^3}(\lambda_2 f_T) + \lambda_2 f_T \cdot \frac{1}{\lambda_3^2}\frac{d^2}{d\eta_T^2}(\lambda_2 f_T) = \left[\frac{1}{\lambda_3}\frac{d}{d\eta_T}(\lambda_2 f_T)\right]^2 - \hat{u}_1^2(\lambda_2 \vartheta_T),$$

or in the form of an ordinary differential equation in f,

$$\frac{\lambda_2}{\lambda_3^3}\nu_0 f_T''' + \frac{\lambda_2^2}{\lambda_3^2} f_T f_T'' = \left[\frac{\lambda_2}{\lambda_3} f_T'\right]^2 - \hat{u}_1^2(\lambda_2 \vartheta_T).$$

Also, the equation (3.30) is now

$$\nu_0 \frac{1}{\lambda_3^2}\frac{d^2}{d\eta_T^2}(\lambda_1 \vartheta_T - 1) - \lambda_2 f_T \frac{1}{\lambda_3}\frac{d}{d\eta_T}(\lambda_1 \vartheta_T - 1) = 0,$$

or

$$\frac{\nu_0 \lambda_1}{{\lambda_3}^2}\vartheta_T'' + \left(\frac{-\lambda_1 \lambda_2}{\lambda_3}\right) f_T \vartheta_T' = 0.$$

Then the coefficients λ_1, λ_2, λ_3 are related to the constants as follows:

$$\nu_0 \frac{\lambda_2}{\lambda_3^3} = 1, \quad \left(\frac{\lambda_2}{\lambda_3}\right)^2 = 1, \quad \left(\frac{\lambda_2}{\lambda_3}\right)^2 = \beta, \quad {\hat{u_1}}^2 \lambda_2 = \beta,$$

$$\frac{\nu_0 \lambda_1}{{\lambda_3}^2} = 1, \quad -\frac{\lambda_1 \lambda_2}{\lambda_3} = 1.$$

This is similar to the suggestion for the boundary-layer equations, that there exists a similarity solution for the Illingworth-Stewartson equations if λ_1, λ_2, λ_3 satisfy the conditions above.

Chapter 4

Exact Similarity Solutions

In the previous chapter we examined the possibility of self-similarity flow when the geometry takes the form of a power of the coordinate x. In this chapter the effects of changes in the values of the coefficients are observed analytically and numerically.

4.1 The Similarity Equations

To set up the exact similarity equations the number of variables is reduced by means of a similarity assumption and a transformation. The flow geometry is assumed to take the form $y \sim x^m$. Then the primary orders of the variables are expected to be

$$\psi \sim 1, \quad u \sim x^{\frac{m-1}{2}}, \quad v \sim x^{\frac{3(m-1)}{2}},$$
$$p \sim x^{\frac{-m-1}{2}}, \quad T \sim \mu \sim x^{m-1}, \quad \varrho \sim x^{\frac{1-3m}{2}}.$$

These orders of magnitude are given by the mass flow constraint and by the core solution.

In terms of a new coordinate $\eta \equiv y/x^m$ of order one, or independent of x, the variables are expressed as

$$\psi = \tilde{\psi}(\eta), \quad u = x^{\frac{m-1}{2}}\tilde{u}(\eta), \quad v = x^{\frac{3(m-1)}{2}}\tilde{v}(\eta),$$
$$p = x^{\frac{-m-1}{2}}\tilde{p}(\eta), \quad T = x^{m-1}\tilde{T}(\eta), \quad \mu = x^{m-1}\gamma C\tilde{T}(\eta), \quad \varrho = x^{\frac{1-3m}{2}}\tilde{\varrho}(\eta),$$

and the differential operators become

$$\frac{\partial}{\partial y} \longrightarrow x^{-m}\frac{\partial}{\partial \eta},$$
$$\frac{\partial}{\partial x} \longrightarrow \frac{\partial}{\partial x} - m\frac{\eta}{x}\frac{\partial}{\partial \eta}.$$

Then the boundary layer equations can be expressed in terms of η and powers of x. First of all the continuity equation is written in terms of η as follows :

$$\frac{\partial(\varrho u)}{\partial x}+\frac{\partial(\varrho v)}{\partial y}=0,$$

implying

$$m\tilde{u}\tilde{\varrho}+m\eta\left(\tilde{u}\tilde{\varrho}\right)'-\left(\tilde{v}\tilde{\varrho}\right)'=0,$$

and hence

$$m\eta\tilde{u}=\tilde{v}. \tag{4.1}$$

Here we have integrated in η, and used the conditon that $\tilde{u}$, $\tilde{v}$ vanish at $\eta = 0$. Alternatively the continuity equation can be expressed in terms of the stream function

$$\tilde{u}\tilde{\varrho}=\tilde{\psi}', \tag{4.2}$$

$$\tilde{v}\tilde{\varrho}=-m\eta\tilde{\psi}'. \tag{4.3}$$

The momentum equation is

$$\varrho\left(u\frac{\partial u}{\partial x}+v\frac{\partial u}{\partial y}\right)=-\frac{dp}{dx}+\frac{\partial}{\partial y}\left(\mu\frac{\partial u}{\partial y}\right),$$

which becomes now

$$\tilde{\varrho}\left\{\tilde{u}\left[\frac{m-1}{2}\tilde{u}-m\eta\tilde{u}'\right]+\tilde{v}\tilde{u}'\right\}=\frac{m+1}{2}\tilde{p}+\gamma C\left(\tilde{T}\tilde{u}'\right)',$$

so that

$$\frac{m-1}{2}\tilde{\varrho}\tilde{u}^2-m\eta\tilde{\varrho}\tilde{u}\tilde{u}'+\tilde{\varrho}\tilde{v}\tilde{u}'=\frac{m+1}{2}\tilde{p}+\gamma C\left(\tilde{T}\tilde{u}'\right)'.$$

Hence we have

$$\frac{m-1}{2}\tilde{\varrho}\tilde{u}^2=\frac{m+1}{2}\tilde{p}+\gamma C\left(\tilde{T}\tilde{u}'\right)', \tag{4.4}$$

since the continuity equation gives $\tilde{v}=m\eta\tilde{u}$ in (4.1). Finally the energy equation is

$$\varrho c_p\left(u\frac{\partial T}{\partial x}+v\frac{\partial T}{\partial y}\right)=u\frac{dp}{dx}+\frac{\partial}{\partial y}\left(k\frac{\partial T}{\partial y}\right)+\mu\left(\frac{\partial u}{\partial y}\right)^2,$$

and this becomes

$$\tilde{\varrho}c_p\left\{\tilde{u}\left(k-1\right)\tilde{T}-m\eta\tilde{u}\tilde{T}'+\tilde{v}\tilde{T}'\right\}=\frac{-m-1}{2}\tilde{u}\tilde{p}+\frac{c_p}{\sigma}\gamma C\left(\tilde{T}\tilde{T}'\right)'+\gamma C\tilde{T}\left(\tilde{u}'\right)^2,$$

and in consequence

$$\left(k-1\right)\tilde{\varrho}c_p\tilde{u}\tilde{T}=\frac{-m-1}{2}\tilde{u}\tilde{p}+\frac{c_p}{\sigma}\gamma C\left(\tilde{T}\tilde{T}'\right)'+\gamma C\tilde{T}\left(\tilde{u}'\right)^2. \tag{4.5}$$

Therefore the governing equations of concern here can be written as

$$m\eta\tilde{u} = \tilde{v},$$

$$\frac{m-1}{2}\tilde{\varrho}\tilde{u}^2 = \frac{m+1}{2}\tilde{p} + \gamma C\left(\tilde{T}\tilde{u}'\right)',$$

$$(k-1)\,\tilde{\varrho}c_p\tilde{u}\tilde{T} = \frac{-m-1}{2}\tilde{u}\tilde{p} + \frac{c_p}{\sigma}\gamma C\left(\tilde{T}\tilde{T}'\right)' + \gamma C\tilde{T}\left(\tilde{u}'\right)^2.$$

Since the state equation yields $\tilde{\varrho} = \tilde{p}/R\tilde{T}$, the governing equations can now be re-written in terms of $\tilde{u}$, $\tilde{T}$,

$$\frac{m-1}{2R}\tilde{u}^2 = \frac{m+1}{2}\tilde{T} + \frac{\gamma C}{\tilde{p}}\tilde{T}\left(\tilde{T}\tilde{u}'\right)', \tag{4.6}$$

$$\frac{c_p(k-1)}{R}\tilde{u}\tilde{p} + \frac{m+1}{2}\tilde{u}\tilde{p} = \frac{c_p}{\sigma}\gamma C\left(\tilde{T}\tilde{T}'\right)' + \gamma C\tilde{T}\left(\tilde{u}'\right)^2, \tag{4.7}$$

with the boundary conditions

$$\tilde{u} = 0, \quad \tilde{T} = T_w \qquad \text{at} \quad \eta = 0, \tag{4.8}$$

$$\tilde{u}' = \tilde{T}' = 0 \qquad \text{at} \quad \eta = 1. \tag{4.9}$$

Also from the mass-flow constraint, $\psi = 1$ at $\eta = 1$, we obtain

$$\int_0^1 \tilde{\varrho}\tilde{u}d\eta = \frac{\tilde{p}}{R}\int_0^1 \frac{\tilde{u}}{\tilde{T}}d\eta = 1. \tag{4.10}$$

The system to be solved for $\tilde{u}$, $\tilde{T}$ is thus (4.6), (4.7), together with the above boundary conditions and integral property.

4.2 Numerical Treatment

In order to obtain numerical solutions, the new coordinate of the Howarth-Dorodnitsyn transformation z is introduced by the definition

$$z = \int_0^y \frac{d\eta}{\tilde{T}},$$

so that

$$dz = \frac{d\eta}{\tilde{T}}, \qquad \tilde{T}\frac{d}{d\eta} = \frac{d}{dz}$$

formally. Then the governing equations (4.6), (4.7) become

$$\frac{m-1}{2R}\tilde{u}^2 = \frac{m+1}{2}\tilde{T} + \frac{\gamma C}{\tilde{p}}\frac{d^2\tilde{u}}{dz^2}, \tag{4.11}$$

$$\left[\frac{c_p(m-1)}{R} + \frac{m+1}{2}\right]\tilde{u}\tilde{p} = \frac{c_p}{\sigma}\gamma C\frac{1}{\tilde{T}}\frac{d^2\tilde{T}}{dz^2} + \gamma C\frac{1}{\tilde{T}}\left(\frac{d\tilde{u}}{dz}\right)^2, \tag{4.12}$$

with the boundary conditions, from (4.8), (4.9),

$$\begin{aligned} &\tilde{u} = 1, \quad \tilde{T} = 0 \qquad \text{at} \qquad z = 0, \\ &\tilde{u}' = \tilde{T}' = 0 \qquad \text{at} \qquad z = z_0, \end{aligned} \tag{4.13}$$

where z_0 is unknown. The mass-flow constraint, relation (4.10) yields two equations in effect,

$$\frac{\tilde{p}}{R}\int_0^{z_0}\tilde{u}dz = 1, \tag{4.14}$$

and

$$\int_0^1 d\eta = \int_0^{z_0}\tilde{T}dz = 1. \tag{4.15}$$

Therefore the equations to be solved can be expressed now as

$$\frac{d\tilde{u}}{dz} = r, \tag{4.16}$$

$$\frac{d^2\tilde{u}}{dz^2} = \frac{\tilde{p}}{\gamma C}\left[\frac{m-1}{2R}\tilde{u}^2 - \frac{m+1}{2}\tilde{T}\right], \tag{4.17}$$

$$\frac{d\tilde{T}}{dz} = s, \tag{4.18}$$

$$\frac{d^2\tilde{T}}{dz^2} = \frac{\sigma\tilde{T}}{c_p\gamma C}\left\{\left[\frac{c_p(m-1)}{R} + \frac{m+1}{2}\right]\tilde{u}\tilde{p}\frac{\gamma C}{\tilde{T}}r^2\right\}. \tag{4.19}$$

The solution of these nonlinear equations was computed by use of the Runge-Kutta method of order four, combined with shooting in z.

Figure 4.1 shows the results obtained for $C = 0.2$, 1.0, 5.0, when the wall temperature $T_{wall} = 0.5$, the pressure $\tilde{p} = 1.0$ and the Prandtl number $\sigma = 1$. As C increases, i.e. the viscosity increases in effect, the range of solution broadens in terms of power of m. At $m = -1.0$ the velocity u and temperature T along the centre-line have the values as $u = 0.0$ and $T = 0.5$. This special case will be discussed in the following section. There is one peculiar feature that near a maximum value of the exponent m there is observed an additional branch which, when m is then reduced, seems to approach asymptotically close to zero as $m \longrightarrow 0+$. This however is not easy to obtain numerically. It is assumed that as $m \longrightarrow 0+$ this branch produces

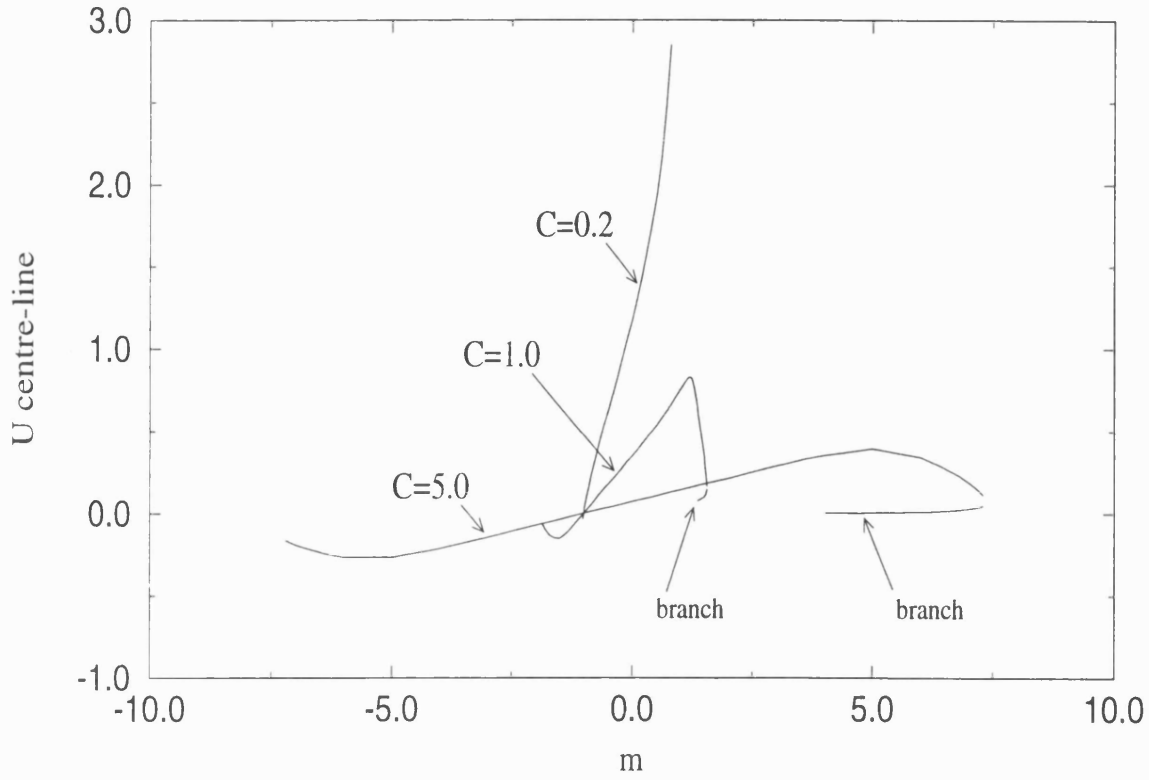

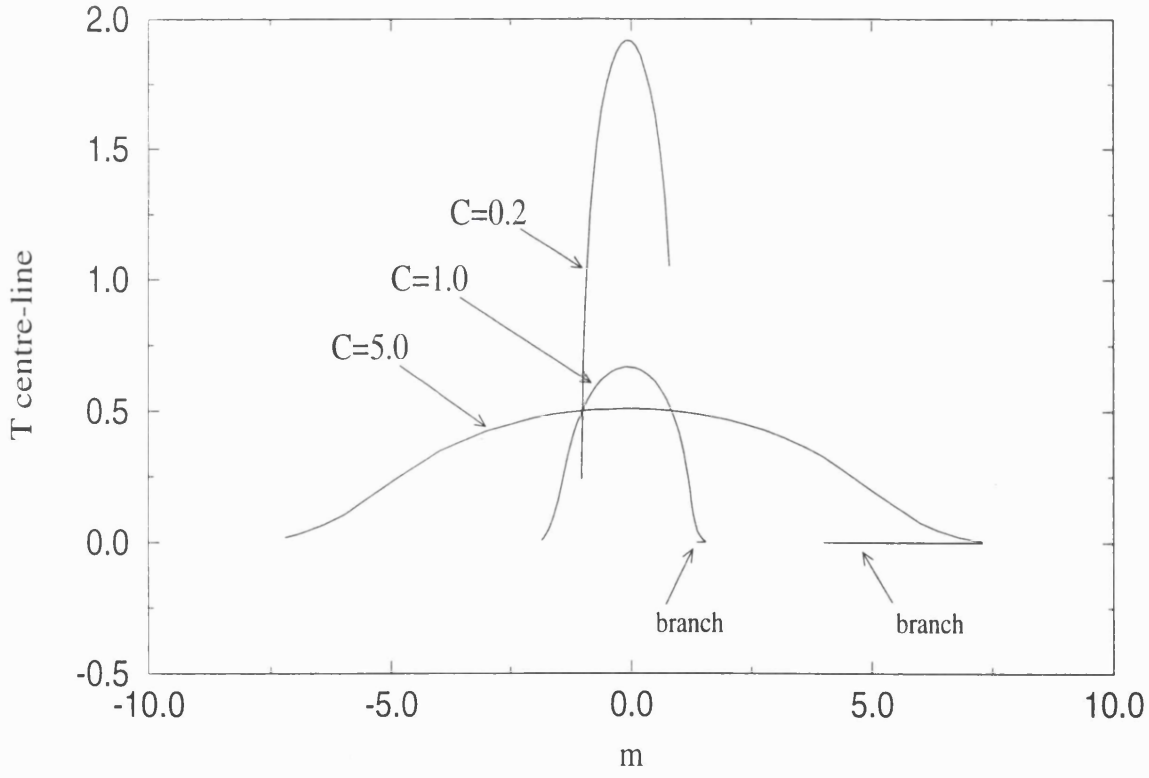

Figure 4.1: Velocity u and temperature T along the centre-line with $C = 0.2$, 1.0, 5.0.

zeroes in the velocity u_{cl} and the temperature T_{cl} along the centre-line. This thesis does not pursue that particular detailed feature further.

4.3 Special Cases

4.3.1 $m = -1$ and $\sigma \ll 1$

When $m = -1$, certain terms in the governing equations vanish and the results the values of u and T appear to become invariant to the viscosity or the value of the effective Chapman constant, as shown in figure 4.1. The momentum equation and the energy equation are now

$$\frac{m-1}{2R}\tilde{u}^2 = \frac{\gamma C}{\tilde{p}}\frac{d^2\tilde{u}}{dz^2}, \tag{4.20}$$

$$\frac{-2c_p}{R}\tilde{u}\tilde{p} = \frac{c_p}{\sigma}\frac{\gamma C}{\tilde{T}}\frac{d^2\tilde{T}}{dz^2} + \gamma C\frac{1}{\tilde{T}}\left(\frac{d\tilde{u}}{dz}\right)^2, \tag{4.21}$$

from (4.11), (4.12), or

$$-\frac{\tilde{u}^2}{R} = \lambda\frac{d^2\tilde{u}}{dz^2}, \tag{4.22}$$

$$-2\frac{\tilde{u}\tilde{T}}{R} = \frac{\lambda}{\sigma}\frac{d^2\tilde{T}}{dz^2} + \frac{\lambda}{c_pR}\left(\frac{d\tilde{u}}{dz}\right)^2, \tag{4.23}$$

where $\lambda = \gamma C/\tilde{p}$. The equation (4.22) can be integrated in terms of $\tilde{u}$ and gives

$$\frac{\lambda}{2}\left(\frac{d\tilde{u}}{dz}\right)^2 = -\frac{\tilde{u}^3}{3R} + \frac{\lambda}{2}{c_1}^2,$$

so that

$$\left(\frac{d\tilde{u}}{dz}\right)^2 = -\frac{2\tilde{u}^3}{3R\lambda} + {c_1}^2, \tag{4.24}$$

from which an implicit solution is obtained (as in a phase plane diagram). Here c_1 is a constant of integration. The centre-line boundary condition $\tilde{u}'(1) = 0$ fixes ${c_1}^2$ from

$$\frac{2\tilde{u}^3(1)}{3R\lambda} = {c_1}^2.$$

Then the equation (4.23) becomes

$$\frac{\lambda}{\sigma}\frac{d^2\tilde{T}}{dz^2} + \frac{2\tilde{u}\tilde{T}}{R} = -\frac{\lambda}{c_pR}\left[{c_1}^2 - \frac{2\tilde{u}^3}{3R\lambda}\right], \tag{4.25}$$

which is a linear equation for $\tilde{T}$ given $\tilde{u}$ and can be solved analytically in principle. Since

$$\frac{d}{dz} = \frac{d\tilde{u}}{dz}\frac{d}{d\tilde{u}},$$

the equation (4.25) becomes

$$\left[\left(\frac{d\tilde{u}}{dz}\right)^2 \frac{d^2\tilde{T}}{d\tilde{u}^2} + \frac{d^2\tilde{u}}{dz^2}\frac{d\tilde{T}}{d\tilde{u}}\right] + \frac{2\tilde{u}}{R}\tilde{T}\frac{\sigma}{\lambda} = -\frac{\lambda}{c_p R}\left[{c_1}^2 - \frac{2\tilde{u}^3}{3R\lambda}\right]\frac{\sigma}{\lambda},$$

or from (4.22), (4.24),

$$\left({c_1}^2 - \frac{2\tilde{u}^3}{3R\lambda}\right)\frac{d^2\tilde{T}}{d\tilde{u}^2} - \frac{\tilde{u}^2}{R\lambda}\frac{d\tilde{T}}{d\tilde{u}} + \frac{2\sigma}{R\lambda}\tilde{u}\tilde{T} = -\frac{\sigma}{c_p R}\left[{c_1}^2 - \frac{2\tilde{u}^3}{3R\lambda}\right]. \tag{4.26}$$

However, from the equation (4.22)

$$\lambda\frac{d^3\tilde{u}}{dz^3} = -\frac{2\tilde{u}}{R}\frac{d\tilde{u}}{dz}. \tag{4.27}$$

Therefore the complimentary function is

$$\tilde{T} = \frac{d\tilde{u}}{dz},$$

for the case of the Prandtl number being unity. Then assuming that

$$\tilde{T} = \left({c_1}^2 - \frac{2\tilde{u}^3}{3R\lambda}\right)^{\frac{1}{2}} Q, \tag{4.28}$$

or

$$\tilde{T} = G^{\frac{1}{2}}Q,$$

the derivatives of $\tilde{T}$ are

$$\frac{d\tilde{T}}{d\tilde{u}} = Q'G^{\frac{1}{2}} + Q\frac{1}{2}G^{-\frac{1}{2}}\left(\frac{-2\tilde{u}^2}{R\lambda}\right),$$

and

$$\frac{d^2\tilde{T}}{d\tilde{u}^2} = Q''G^{\frac{1}{2}} + 2Q'\frac{1}{2}G^{-\frac{1}{2}}\left(-\frac{2\tilde{u}^2}{R\lambda}\right) + Q\left[-\frac{1}{4}G^{-\frac{3}{2}}\frac{4\tilde{u}^4}{R^2\lambda^2}\right] + Q\frac{1}{2}G^{-\frac{1}{2}}\left(-\frac{4\tilde{u}}{R\lambda}\right).$$

So the equation (4.26) becomes

$$G\left[Q''G^{\frac{1}{2}} - \frac{2\tilde{u}^2}{R\lambda}Q'G^{-\frac{1}{2}} - \frac{\tilde{u}^4}{R^2\lambda^2}QG^{-\frac{3}{2}} - \frac{2\tilde{u}}{R\lambda}QG^{-\frac{1}{2}}\right] -$$
$$-\frac{\tilde{u}^2}{R\lambda}\left[Q'G^{\frac{1}{2}} - \frac{2\tilde{u}^2}{R\lambda}QG^{-\frac{1}{2}}\right] + \frac{2\tilde{u}}{R\lambda}G^{\frac{1}{2}}Q = \frac{1}{c_p R}G \tag{4.29}$$

provided

$$G\left[-\frac{\tilde{u}^4}{R^2\lambda^2}G^{-\frac{3}{2}}-\frac{2\tilde{u}}{R\lambda}G^{-\frac{1}{2}}\right]+\frac{\tilde{u}^4}{R^2\lambda^2}G^{\frac{1}{2}}+\frac{2\tilde{u}}{R\lambda}G^{\frac{1}{2}}=0.$$

From the assumption for the complimentary function,

$$\frac{Q''}{Q'}=\frac{3\tilde{u}^2}{R\lambda G}, \tag{4.30}$$

giving

$$\ln Q'=-\frac{3}{2}\ln G+\text{constant}.$$

Since

$$G\equiv {c_1}^2-\frac{2\tilde{u}^3}{3R\lambda},$$

it follows that

$$\left[Q'\left({c_1}^2-\frac{2\tilde{u}^3}{3R\lambda}\right)^{\frac{3}{2}}\right]'=-\frac{1}{c_pR}\left({c_1}^2-\frac{2\tilde{u}^3}{3R\lambda}\right).$$

Hence

$$Q'\left({c_1}^2-\frac{2\tilde{u}^3}{3R\lambda}\right)^{\frac{3}{2}}=-\frac{1}{c_pR}\left({c_1}^2\tilde{u}-\frac{\tilde{u}^4}{6R\lambda}\right)+c_2, \tag{4.31}$$

where c_2 is a constant of integration. Consequently the temperature solution is giving by

$$\tilde{T}=\left({c_1}^2-\frac{2\tilde{u}^3}{3R\lambda}\right)^{\frac{1}{2}}\left\{c_3+\int_0^{\tilde{u}}\frac{c_2-\frac{1}{c_pR}\left({c_1}^2\tilde{u}-\frac{\tilde{u}^4}{6R\lambda}\right)}{\left({c_1}^2-\frac{2\tilde{u}^3}{3R\lambda}\right)^{\frac{3}{2}}}d\tilde{u}\right\}. \tag{4.32}$$

Therefore one of the boundary conditions requires

$$c_1c_3=1.$$

When the Prandtl number $\sigma \ll 1$ then the equation (4.25) is approximated as

$$\frac{d^2\tilde{T}}{dz^2}=0. \tag{4.33}$$

In terms of the derivatives of $\tilde{u}$ it becomes

$$\left(\frac{d\tilde{u}}{dz}\right)^2\frac{d^2\tilde{T}}{d\tilde{u}^2}+\frac{d^2\tilde{u}}{d\tilde{u}^2}\frac{d\tilde{T}}{d\tilde{u}}=0$$

and then from (4.24)

$$\left({c_1}^2 - \frac{2\tilde{u}^3}{3R\lambda}\right)\frac{d^2\tilde{T}}{d\tilde{u}^2} - \frac{\tilde{u}^2}{R\lambda}\frac{d\tilde{T}}{d\tilde{u}} = 0. \tag{4.34}$$

With the assumption (4.28), $\tilde{T} = G^{\frac{1}{2}}Q$, it becomes

$$G\left[Q''G^{\frac{1}{2}} - \frac{2\tilde{u}^2}{R\lambda}Q'G^{-\frac{1}{2}} - \frac{\tilde{u}^4}{R^2\lambda^2}QG^{-\frac{3}{2}} - \frac{2\tilde{u}}{R\lambda}QG^{-\frac{1}{2}}\right] - \frac{\tilde{u}^2}{R\lambda}\left[Q'G^{\frac{1}{2}} - \frac{2\tilde{u}^2}{R\lambda}QG^{-\frac{1}{2}}\right] = 0, \tag{4.35}$$

or

$$G^2Q'' - \frac{3\tilde{u}^2}{R\lambda}GQ' + \left(\frac{u^4}{R^2\lambda^2} - \frac{2\tilde{u}}{R\lambda}G\right)Q = 0. \tag{4.36}$$

Hence

$$\begin{aligned} 2G^2Q &= \frac{3\tilde{u}^2}{R\lambda}G \pm \left[\frac{9\tilde{u}^4}{R^2\lambda^2}G^2 - 4G^2\left(\frac{\tilde{u}^4}{R^2\lambda^2} - \frac{2\tilde{u}}{R\lambda}G\right)\right]^{\frac{1}{2}}, \\ 2G\,Q &= \frac{3\tilde{u}^2}{R\lambda} \pm \left[\frac{5\tilde{u}^4}{R^2\lambda^2} + \frac{8\tilde{u}}{R\lambda}G\right]^{\frac{1}{2}}. \end{aligned}$$

Therefore the temperature solution for $\sigma \ll 1$ is given by

$$\tilde{T} = \frac{1}{2}\left({c_1}^2 - \frac{2\tilde{u}^3}{3R\lambda}\right)^{-\frac{1}{2}}\left\{\frac{3\tilde{u}^2}{R\lambda} \pm \left[\frac{5\tilde{u}^4}{R^2\lambda^2} + \frac{8\tilde{u}}{R\lambda}\left({c_1}^2 - \frac{2\tilde{u}^3}{3R\lambda}\right)\right]^{\frac{1}{2}}\right\}. \tag{4.37}$$

4.3.2 High Wall Temperature

The wall temperature also affects the flow solution significantly. Figure 4.2 shows the results of the velocity u_{cl} and the temperature T_{cl} for the wall temperature $T_w = 0.45$, 0.50, 0.55. As the wall temperature increases the maximum temperature along the centre-line also increases, as a result, the possible first-branch range of m for T_{cl} broadens and so does that for u_{cl}.

It is then worth discussing the case when the wall temperature is very high, $T_w \gg 1$. If $T_w \gg 1$ then the velocity u and temperature T are assumed to take expansions as follows,

$$\begin{aligned} T &= T_w + {T_w}^{-2}T_1 + {T_w}^{-3}T_2 + \cdots, \\ u &= {T_w}^{-1}u_1 + {T_w}^{-2}u_2 + \cdots. \end{aligned} \tag{4.38}$$

These expansions are deduced from the equations (4.6) to balance the orders of the terms. From the primary equation of the first equation

$$0 = \left(\frac{1+m}{2}\right)T_w + \left(\frac{\gamma C}{\pi}\right){T_w}^2{u_1}''{T_w}^{-1} + 0,$$

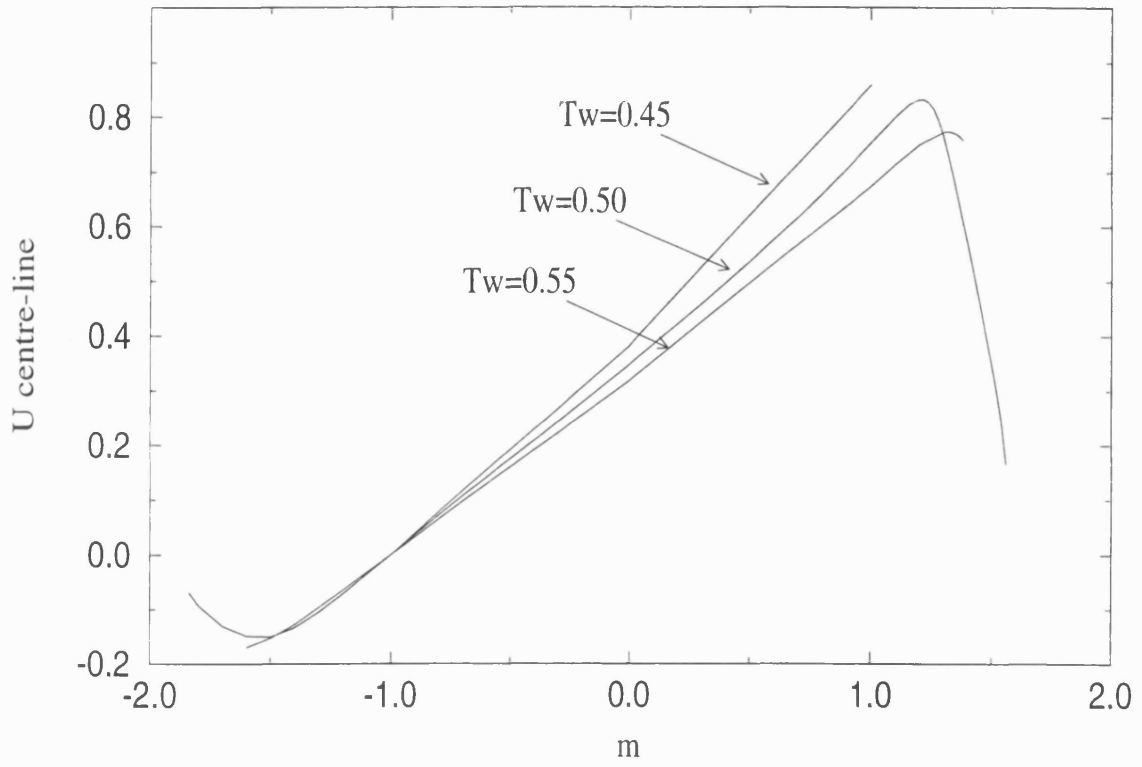

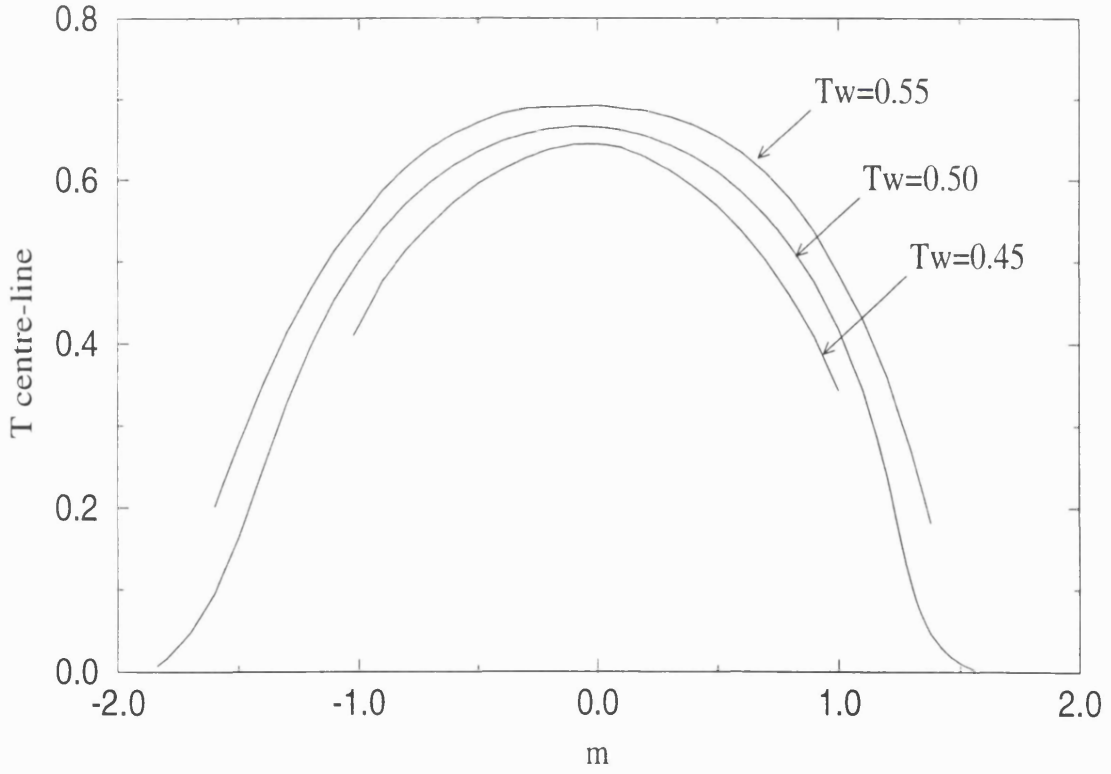

Figure 4.2: Velocity u and temperature T with various wall temperature $T_{wall} = 0.45$, 0.50, 0.55.

or

$$0 = \left(\frac{1+m}{2}\right) + \left(\frac{\gamma C}{\pi}\right) u_1'', \tag{4.39}$$

which yields a linear equation for u_1. From the second equation

$$\left(\frac{m-1}{R}\right)\frac{u_1}{T_w} = -\left(\frac{1+m}{2}\right)\frac{u_1}{c_p T_w} + \frac{1}{\sigma}\left(\frac{\gamma C}{\pi}\right) T_w \frac{T_1''}{{T_w}^2} + \frac{1}{c_p}\left(\frac{\gamma C}{\pi}\right) T_w \frac{{u_1'}^2}{{T_w}^2},$$

and so

$$\left(\frac{m-1}{R}\right) u_1 = -\left(\frac{1+m}{2}\right)\frac{u_1}{c_p} + \frac{1}{\sigma}\left(\frac{\gamma C}{\pi}\right) T_1'' + \frac{1}{c_p}\left(\frac{\gamma C}{\pi}\right) {u_1'}^2, \tag{4.40}$$

yielding T_1 likewise. The boundary conditions are now

$$\begin{aligned} u_1'(1) &= 0 \quad \text{and} \quad u_1(0) = 0, \\ T_1'(1) &= 0 \quad \text{and} \quad T_1(0) = 0. \end{aligned}$$

In order to find $u_1(1)$ the equation (4.39) is integrated and in this analysis the case where $p = 1.0$, $\gamma = 1.4$ and $C = 1.0$ is applied. Thus

$$u_1'' = -\left(\frac{1+m}{2}\right)\frac{\pi}{\gamma C},$$

yielding

$$u_1' = -\frac{5(1+m)}{14} y + \frac{5(1+k)}{14},$$

and hence

$$u_1 = -\frac{5(1+m)}{14}\frac{1}{2} y^2 + \frac{5(1+m)}{14} y.$$

Therefore

$$u_1(1) = \frac{5}{28}((1+m)). \tag{4.41}$$

Similarly to find T_1 the same case is applied and the equation (4.40) becomes

$$\frac{3m-1}{2} u_1 - \frac{7}{5} {u_1'}^2 = \frac{7}{5} T_1''.$$

The working proceeds in the following manner,

$$T_1'' = -\frac{5(1+m)}{14^2}\frac{5}{2}\left[(5m+1)y^2 - 2(5m+1)y + 2(m+1)\right],$$

giving

$$T_1' = -\frac{25(1+m)}{14^2 \cdot 2}\left[\frac{5m+1}{3} y^3 - (5m+1)y^2 + 2(m+1)y + \frac{4}{3}(k-1)\right],$$

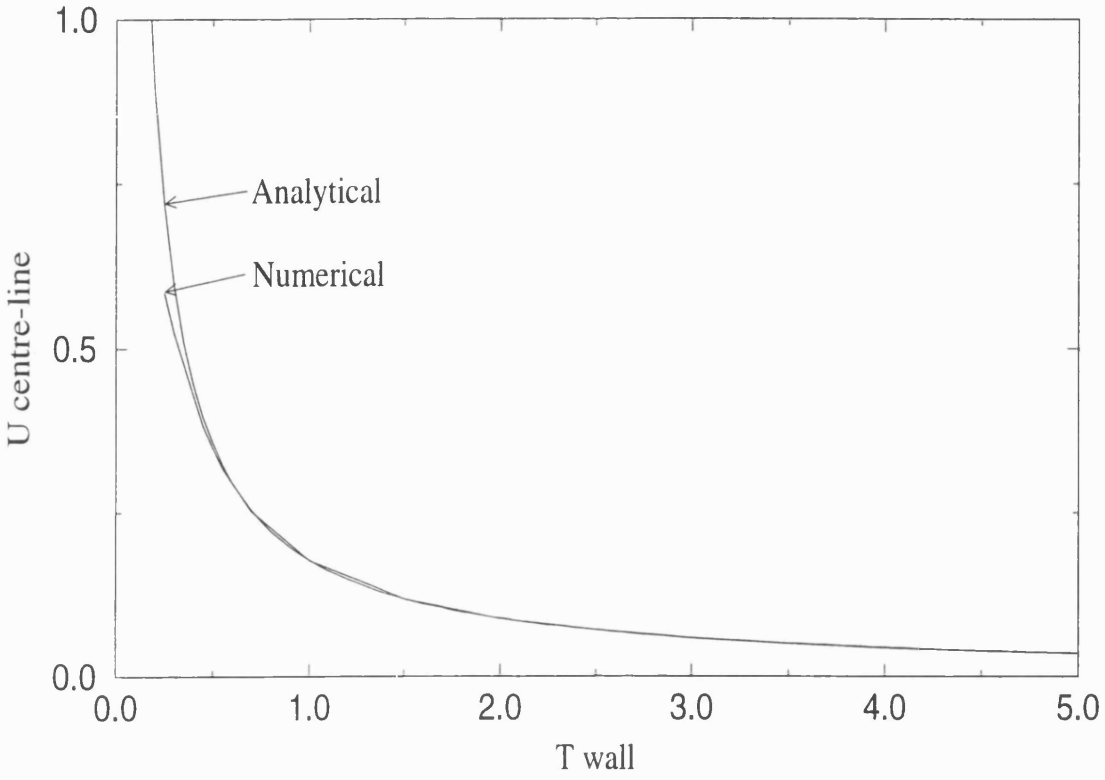

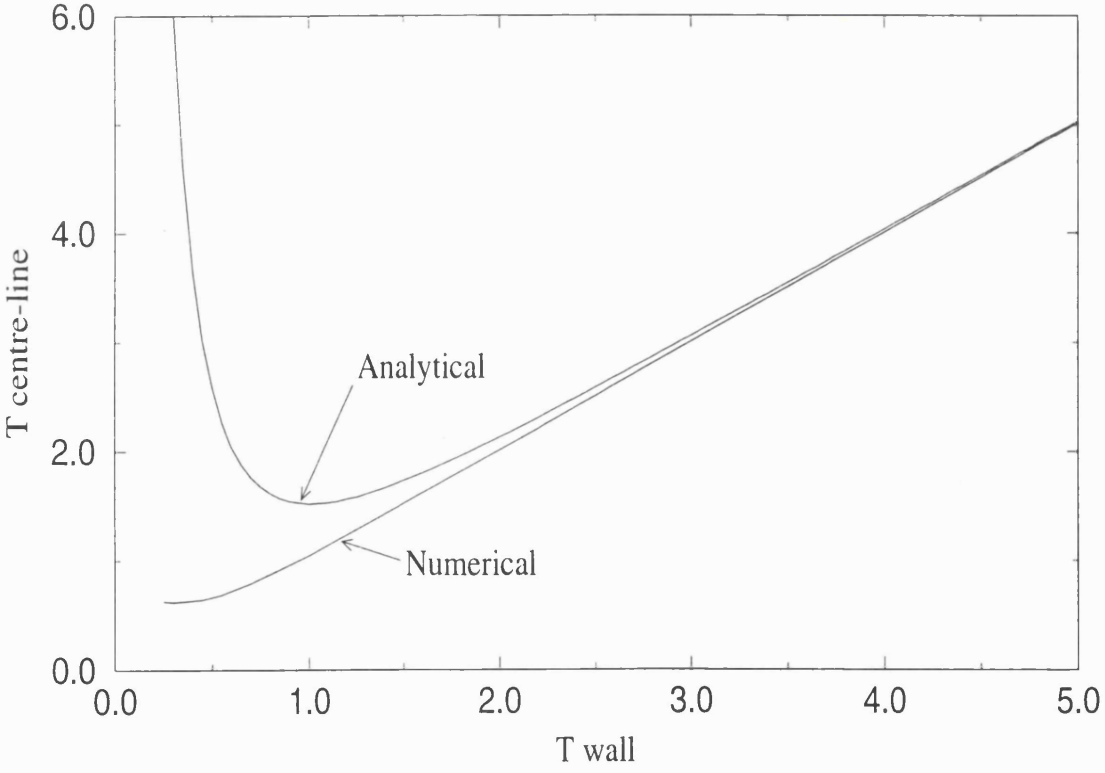

Figure 4.3: Analytical and Numerical values of velocity u and temperature T with various wall temperature T_{wall}.

and so

$$T_1 = -\frac{25(1+m)}{14^2 \cdot 2}\left[\frac{5m+1}{12}y^4 - \frac{5m+1}{3}y^3 + (m+1)y^2 + \frac{4}{3}(m-1)y\right].$$

Therefore

$$T_1(1) = \frac{-25(m+1)(13m-7)}{336} \tag{4.42}$$

is the prediction for large T_{wall}

Figure 4.3 presents the results obtained analytically and numerically for the velocity u_{cl} and the temperature T_{cl} along the centre-line, for various wall temperatures. The trend seems clear: the wall temperature increases the analytical and numerical values tend towards agreement and these results seem to confirm the assumption taken for the form of the expansion.

4.3.3 $C \gg 1$

Here we consider not only similarity solutions but also a general form of the nozzle shape. When the effective viscosity is very high, $C \gg 1$, we have in the original partial differential equations of chapter 3

$$0 = -p' + \gamma C\left(T_y u_y + T u_{yy}\right), \tag{4.43}$$

$$0 = up' + \frac{c_p}{\sigma}\gamma C\left({T_y}^2 + T T_{yy}\right) + \gamma C T\left(u_y\right)^2, \tag{4.44}$$

from neglect of the inertia terms. The system (4.43), (4.44) will be re-considered later. The variables can now be expressed in terms of functions of η,

$$u = x^{\frac{m-1}{2}}\tilde{u}(\eta), \qquad T = x^{m-1}\tilde{T}(\eta), \qquad p = x^{\frac{-m-1}{2}}\tilde{\pi}(\eta),$$
$$\varrho = x^{\frac{1-3m}{2}}\tilde{\varrho}(\eta), \qquad \psi = F(\eta), \qquad v = x^{\frac{3(m-1)}{2}}\tilde{v}(\eta), \qquad \mu = x^{m-1}\gamma C\tilde{T}(\eta),$$

with $\eta = y/x^m$. The x-momentum equation therefore yields

$$0 = \frac{m+1}{2}x^{\frac{-m-3}{2}}\tilde{\pi} + \gamma C\left(\frac{x^{m-1}}{x^m}\tilde{T}' \cdot \frac{x^{\frac{m-1}{2}}}{x^m}\tilde{u}' + x^{m-1}\tilde{T} \cdot \frac{x^{\frac{m-1}{2}}}{x^{2m}}\tilde{u}''\right),$$

so that

$$0 = \frac{m+1}{2}\tilde{\pi} + \gamma C\left(\tilde{T}'\tilde{u}' + \tilde{T}\tilde{u}''\right). \tag{4.45}$$

The energy equation becomes

$$0 = x^{\frac{m-1}{2}}\tilde{u} \cdot \frac{-m-1}{2}x^{\frac{-m-3}{2}}\tilde{\pi} + \frac{c_p}{\sigma}\gamma C\left(\frac{x^{2(m-1)}}{x^{2m}}\tilde{T}'^2 + \tilde{T}\tilde{T}''\right) + \gamma C \cdot x^{m-1}\tilde{T} \cdot \left(\frac{x^{\frac{m-1}{2}}}{x^{2m}}\tilde{u}'\right)^2,$$

and so

$$0 = \frac{-m-1}{2}\tilde{u}\tilde{\pi} + \frac{c_p}{\sigma}\gamma C\left(\tilde{T}'^2 + \tilde{T}\tilde{T}''\right) + \gamma C\tilde{T}\left(\tilde{u}'\right)^2. \tag{4.46}$$

The equations here agree with the full similarity case for large C values. In addition, however, $\tilde{u} = O(C^{-1})$, $\tilde{T} = O(1)$, if $\tilde{\pi}$ is $O(1)$. So the energy equation becomes simply

$$0 = \frac{c_p}{\sigma}\gamma C\left(\tilde{T}'^2 + \tilde{T}\tilde{T}''\right) \tag{4.47}$$

instead of (4.46). To solve the equations, we obtain from the x-momentum equation

$$0 = \frac{m+1}{2}\tilde{\pi} + \gamma C\left(\tilde{T}\tilde{u}'\right)'$$

and hence, on integration

$$(m+1)\,\tilde{\pi}\eta + 2\gamma C\left(\tilde{T}\tilde{u}'\right) = A_1$$

where A_1 is a constant. However, at $\eta = 1$ (the centre-line), $u' = 0$. Therefore the constant $A_1 = (m+1)\,\tilde{\pi}$. Since the energy equation (4.47) yields $T =$ constant $= T_w$, the current equation becomes

$$2\gamma C\tilde{T}_w \cdot \tilde{u}' = (m+1)\,\tilde{\pi}\,(1-\eta),$$

which is a linear equation for $\tilde{u}$. Integrating this yields

$$u = \frac{(m+1)\,\pi}{2\gamma C T_w}\left(\eta - \frac{1}{2}\eta^2 + A_2\right)$$

where A_2 is a constant. Again, however, $\tilde{u} = 0$ at $\eta = 0$. Therefore the constant $A_2 = 0$.

The predictions from this large-C analysis agree with the computations as the value of C is increased.

Figures in chapter 4

Fig 4.1 : the values of the velocity u and the temperature T at the centre-line, for the various effective Chapman constants $C = 0.2$, 1.0, 5.0, are plotted over the value of exponent m. The wall temperature $T_{wall} = 0.5$, the pressure $\tilde{p} = 1.0$ and the Prandtl number $\sigma = 1.0$.

Fig 4.2 : the values of u and T along the centre-line against m, for the various wall temperatures $T_w = 0.45$, 0.50, 0.55.

Fig 4.3 : showing the result obtained analytically and numerically for the velocity u and the temperature T at the the centre-line, for various wall temperature.

Chapter 5

Upstream Influence

5.1 Governing Equations

As was shown in section 4.2, there are at least two solution branches for the similarity flow profile and that provides one form of non-uniqueness possible in the local flow. Another form of non-uniqueness in the flow is due to upstream influence within the original composite partial-differential system as follows.

The flow components now are expressed again in terms of the streamwise dependence. A small perturbation term associated with upstream influence in the stream function is assumed to be proportional to x^α; therefore the expression of the whole solution is of the form

$$\begin{aligned}(\psi, u, v, p, \varrho, T) = &\left(\psi_0,\ x^{-1/2}u_0,\ x^{-3/2}v_0,\ x^{-1/2}p_0,\ x^{1/2}\varrho_0,\ x^{-1}T_0\right) + \\ &+\left(x^\alpha\psi_1,\ x^{\alpha-1/2}u_1,\ x^{\alpha-3/2}v_1,\ x^{\alpha-1/2}p_1,\ x^{\alpha+1/2}\varrho_1,\ x^{\alpha-1}T_1\right) + \cdots \end{aligned} \tag{5.1}$$

where the constant α is unknown and to be determined. The leading terms in parentheses on the right in (5.1) are the basic solutions found in the previous chapter, for the specific case $m = 0$ for definiteness.

In order to determine the exponent α, the equations of the perturbation terms with certain boundary conditions are required, and these are obtained from substitution into the composite system (3.1) - (3.7). Our concern here is mostly with the possibility of positive values of α, corresponding to eigenfunctions (branchings) at small x.

The resulting similarity equations for the basic flow are as in chapter 4,

$$\varrho_0 u_0 = \psi_0', \quad \varrho_0 v_0 = 0, \tag{5.2}$$

$$\varrho_0\left[u_0\left(-\frac{1}{2}u_0\right)\right] = +\frac{1}{2}p_0 + \gamma C\left(T_0 u_0'\right)', \tag{5.3}$$

$$\varrho_0 c_p \left(u_0 \left(-T_0\right)\right) = -\frac{1}{2} u_0 p_0 + \frac{c_p \gamma C}{\sigma} \left(T_0 T_0'\right)' + \gamma C T_0 {u_0'}^2, \tag{5.4}$$

$$p_0 = R \varrho_0 T_0, \tag{5.5}$$

with the boundary conditions being

$$\psi_0 = u_0 = 0, \quad T_0 = T_w(x) \qquad \text{at} \quad y = 0 \quad \text{(wall)}, \tag{5.6}$$

$$u_0' = T_0' = 0 \qquad \text{at} \quad y = y_0 \quad \text{(centre)}. \tag{5.7}$$

The similarity-type equations at the order of x^α then yield the governing equations

$$\varrho_0 u_1 + \varrho_1 u_0 = \psi_1', \quad \varrho_0 v_1 + \varrho_1 v_0 = -\alpha \psi_1, \tag{5.8}$$

$$\begin{aligned} \varrho_0 \left[u_0 \left(\alpha - \frac{1}{2}\right) u_1 + u_1 \left(-\frac{1}{2} u_0\right) + v_1 u_0'\right] + \varrho_1 \left(-\frac{1}{2} {u_0}^2\right) = \\ = -\left(\alpha - \frac{1}{2}\right) p_1 + \gamma C \left(T_0 u_1' + T_1 u_0'\right)', \end{aligned} \tag{5.9}$$

$$\begin{aligned} \varrho_0 c_p \left[u_0 \left(\alpha - 1\right) T_1 + u_1 \left(-T_0\right) + v_1 T_0'\right] + \varrho_1 c_p \left[u_0 \left(-T_0\right)\right] = \\ = u_0 \left(\alpha - \frac{1}{2}\right) p_1 + u_1 \left(-\frac{1}{2} p_0\right) + \frac{c_p \gamma C}{\sigma} \left(T_0 T_1' + T_1 T_0'\right)' \\ + \gamma C \left(T_1 {u_0'}^2 + 2 T_0 u_0' u_1'\right), \end{aligned} \tag{5.10}$$

$$p_1 = R\left(\varrho_0 T_1 + \varrho_1 T_0\right), \tag{5.11}$$

while the boundary conditions are

$$\psi_1 = u_1 = T_1 = 0 \qquad \text{at} \quad y = 0, \tag{5.12}$$

$$u_1' = T_1' = 0 \quad \text{and} \quad \psi_1 = 0 \qquad \text{at} \quad y = y_0. \tag{5.13}$$

Here (5.12), (5.13) hold because of the complete wall and centre-line conditions respectively. In order to find the eigenvalues α, the equations (5.8) - (5.12) are to be solved, yielding a non-trivial solution, with $p_1 = 1$ as a convenient normalisation. This is done in the current work essentially by solving all the above equations for various α values and then examining the dependence of $\psi_1(y_0)$ on α, to determine the value(s) of α. The necessary further details are given below.

The equations in terms of the second derivatives of u and T are, from above,

$$\begin{aligned} \gamma C T_0 u_1'' \;=\; & \gamma C \left(T_0' u_1' + T_1' u_0' + T_1 u_0''\right) + \left(\alpha - \frac{1}{2}\right) p_1 \\ & + \varrho_0 \left[u_0 \left(\alpha - \frac{1}{2}\right) u_1 + u_1 \left(-\frac{1}{2} u_0\right) + v_1 u_0'\right] + \varrho_1 \left(-\frac{1}{2} {u_0}^2\right), \end{aligned} \tag{5.14}$$

$$\begin{aligned}\frac{c_p\gamma C}{\sigma}T_0T_1'' &= -\frac{c_p\gamma C}{\sigma}\left(2T_0'T_1' + T_1T_0''\right) - u_0\left(\alpha - \frac{1}{2}\right)p_1 - u_1\left(-\frac{1}{2}p_0\right) \\ &\quad -\gamma C\left(T_1u_0'^2 + 2T_0u_0'u_1'\right) + \varrho_1 c_p\left[u_0\left(-T_0\right)\right] \\ &\quad +\varrho_0 c_p\left[u_0\left(\alpha - 1\right)T_1 + u_1\left(-T_0\right) + v_1T_0'\right]. \qquad (5.15)\end{aligned}$$

In order to compute v_1, variables ϱ_0 and v_1 have to be kept amalgamated since $\varrho_0 v_1 = -\alpha\psi_1$ and from the state equation

$$\begin{aligned}\varrho_1 &= \frac{p_1 - R\varrho_0 T_1}{T_0 R} \\ &= \frac{p_1}{RT_0} - \frac{T_1}{T_0}\frac{p_0}{RT_0}.\end{aligned}$$

Therefore a set of five equations of first order is obtained,

$$\psi_1' = \varrho_0 u_1 + \varrho_1 u_0 \qquad \left(\text{and } \psi_1 = -\frac{\varrho_0 v_1}{\alpha}\right), \qquad (5.16)$$

$$\begin{aligned}\frac{\partial R}{\partial \eta} = u_1'' &= \frac{1}{\gamma C T_0}\left\{\gamma C\left(T_0'u_1' + T_1'u_0' + T_1u_0''\right) + \left(\alpha - \frac{1}{2}\right)p_1\right. \\ &\quad \left. +\varrho_0\left[u_0\left(\alpha - \frac{1}{2}\right)u_1 + u_1\left(-\frac{1}{2}u_0\right) + v_1u_0'\right] + \varrho_1\left(-\frac{1}{2}u_0^2\right)\right\} \qquad (5.17)\end{aligned}$$

$$R = u_1', \qquad (5.18)$$

$$\begin{aligned}\frac{\partial S}{\partial \eta} = T_1'' &= \frac{\sigma}{c_p\gamma C}\left\{-\frac{c_p\gamma C}{\sigma}\left(2T_0'T_1' + T_1T_0''\right) - u_0\left(\alpha - \frac{1}{2}\right)p_1\right. \\ &\quad -u_1\left(-\frac{1}{2}p_0\right) - \gamma C\left(T_1u_0'^2 + 2T_0u_0'u_1'\right) + \varrho_1 c_p\left[u_0\left(-T_0\right)\right] \\ &\quad \left. +\varrho_0 c_p\left[u_0\left(\alpha - 1\right)T_1 + u_1\left(-T_0\right) + v_1T_0'\right]\right\}, \qquad (5.19)\end{aligned}$$

$$S = T_1'. \qquad (5.20)$$

These are used below.

5.2 Numerical Results

The five equations just mentioned were solved numerically by use of a four-stage Runge-Kutta scheme, along with the appropriate boundary conditions. The figures 5.1 - 5.6 show the values of $\psi_1(y_0)$ versus α (from which α is fixed by $\psi_1(y_0) = 0$), numerically solved for various values of the scaled Chapman constant C. Sudden changes of pattern in the graphs were observed around $C = 0.005$. The following are some sample results in tabular form; see also figure 5.7.

C	α	α	C	α	α
5.0	0.99	-72.21	0.002	13.88	-0.92
2.0	0.97	-11.83	0.001	12.84	-0.71
1.0	1.04	-2.89	0.0005	9.99	-0.65
0.5	1.30	-0.53	0.0002	7.39	-0.61
0.2	2.28	0.26	0.0001	6.15	-0.59
0.1	3.60	0.40	0.00005	5.23	-0.58
0.05	5.59	0.49	0.00002	4.09	-0.55
0.02	9.87	0.85			
0.01	15.24	1.41			
0.005	24.74	3.07			

When the scaled Chapman constant C is sufficiently large, $C > 0.005$ approx., an eigenvalue for α of positive value decreases but apparently converges to unity from above as C tends to infinity.

When the scaled Chapman constant C is sufficiently small, $C < 0.005$ approx., this positive eigenvalue for α decreases but seems to tend to an $O(1)$ positive value, as C tends to zero.

However, it should be noted that the computational results became questionable for $C < 0.00001$ and the value of the eigenvalue is not determined accurately there.

The main point suggested by the above computational work is that there are positive eigenvalues α, associated with the local expansion (5.1). This is borne out by the subsequent analytical properties, for large C and small C in turn (the former also provides the basis for chapter 6).

5.3 Analysis for Large C

When the scaled Chapman constant C is large, $C \gg 1$, T_0 is expected to be $O(1)$ since the wall temperature T_w is $O(1)$ and u_0 is $O(C^{-1})$ since p_0 is $O(1)$. Similarly it can be argued that $\varrho_0 = O(1)$, $\psi_0 = O(C^{-1})$. Therefore from the primary equations (5.2) - (5.5) we are left now with the system

$$\varrho_0 u_0 = \psi_0', \tag{5.21}$$

$$0 = +\frac{1}{2}p_0 + \gamma C\,(T_0 u_0')', \tag{5.22}$$

$$0 = \frac{c_p \gamma C}{\sigma}(T_0 T_0')', \tag{5.23}$$

$$p_0 = R\varrho_0 T_0, \tag{5.24}$$

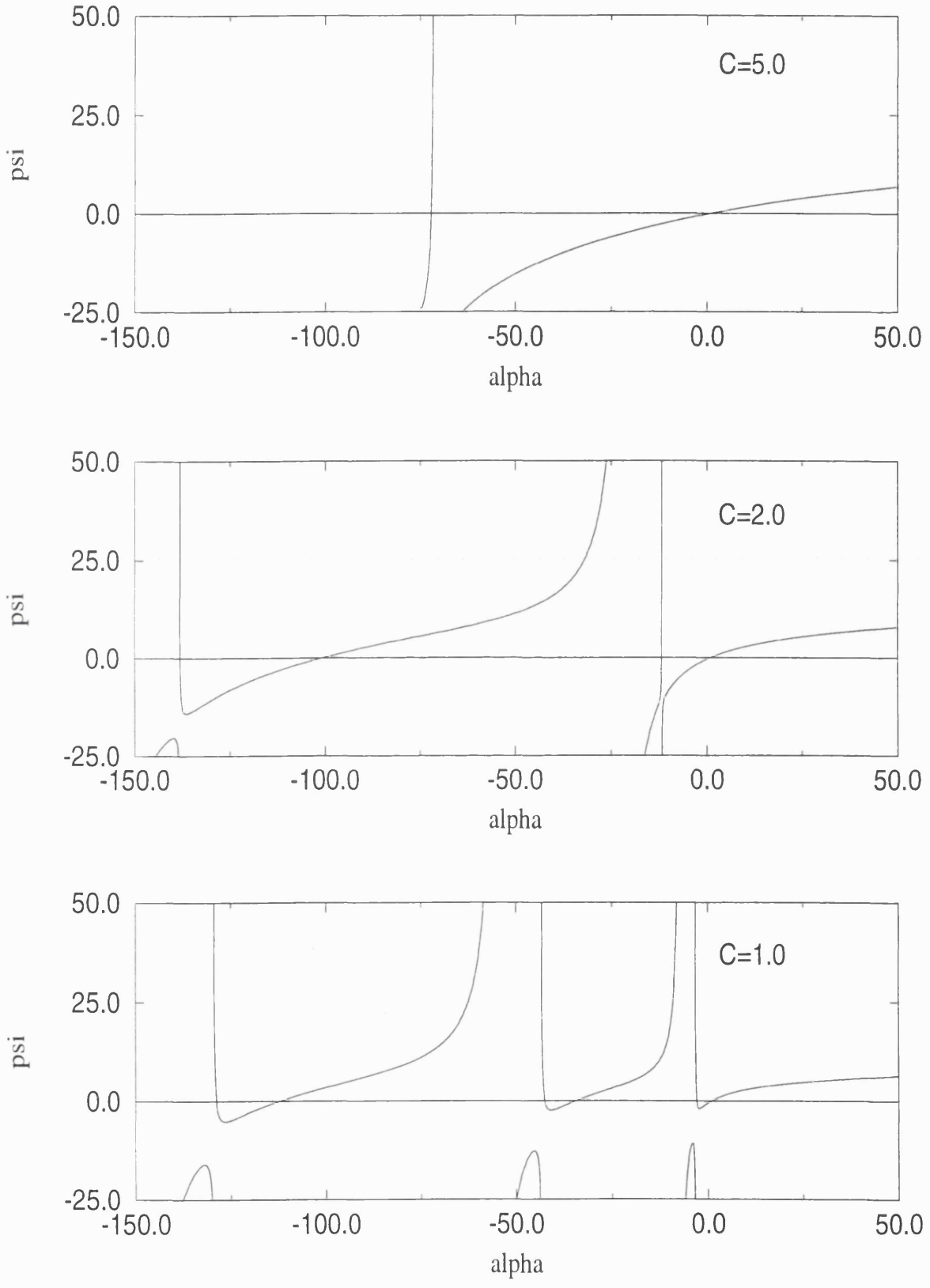

Figure 5.1: Seeking eigenvalues α

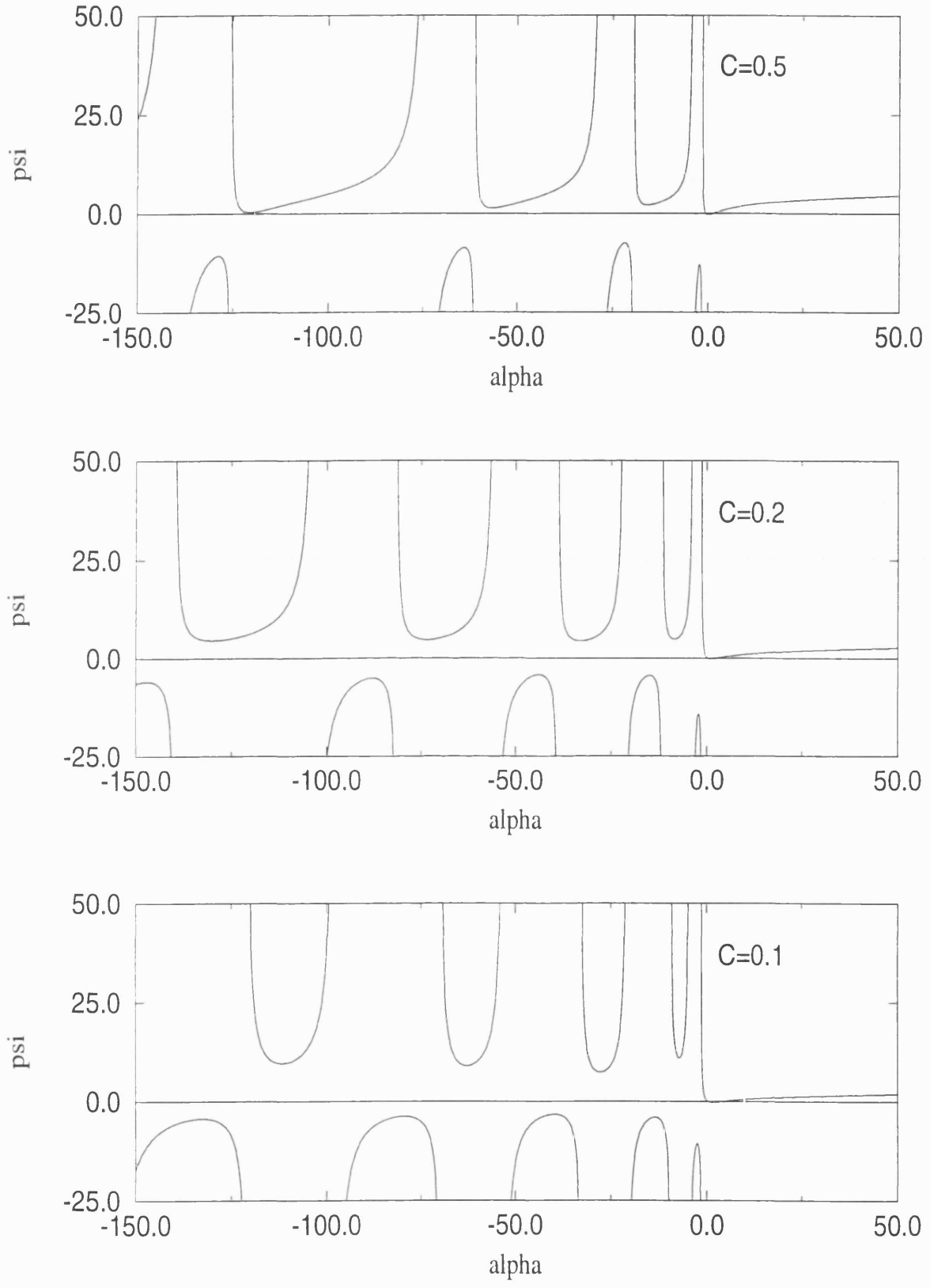

Figure 5.2: Seeking eigenvalues α

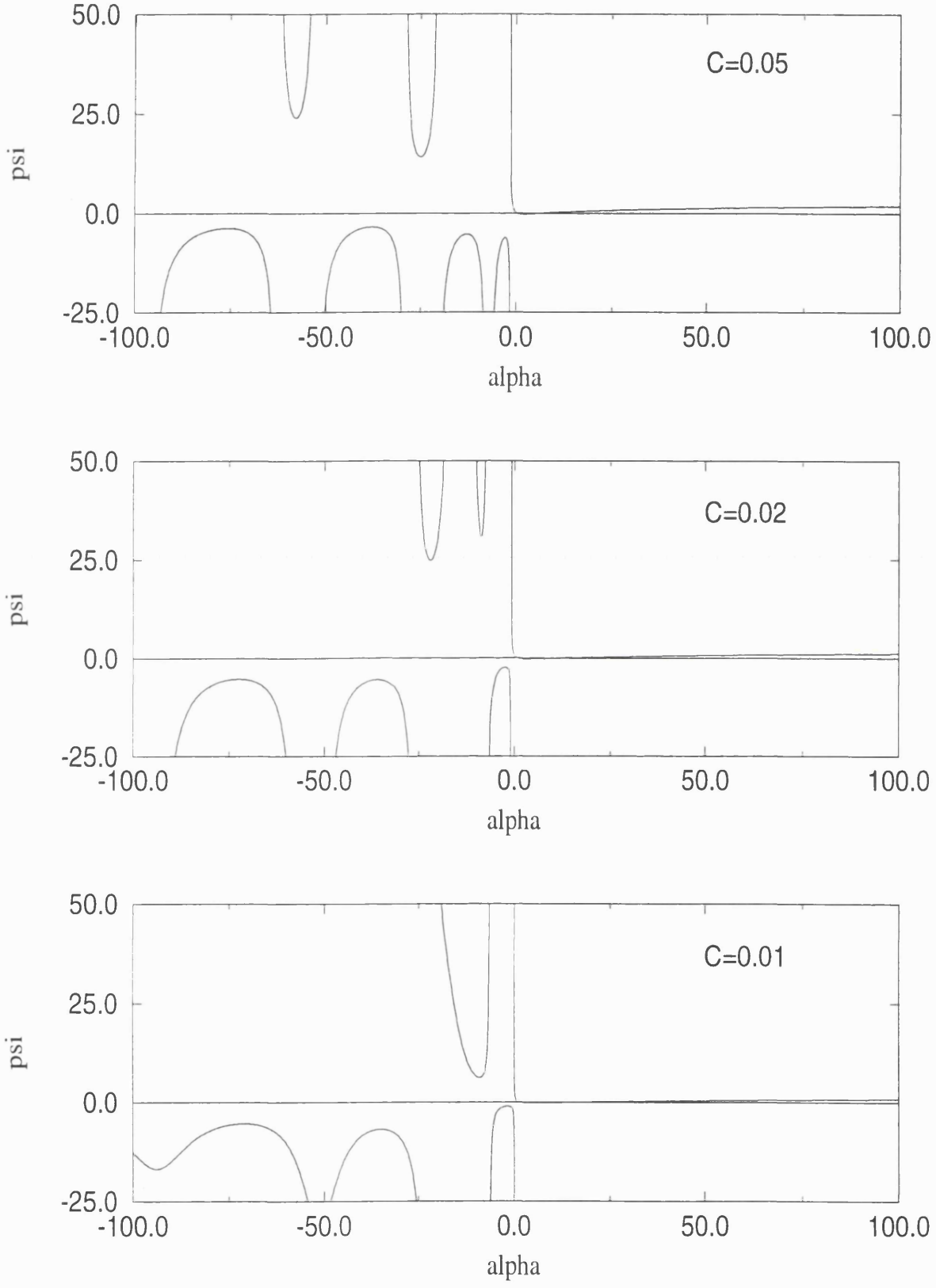

Figure 5.3: Seeking eigenvalues α

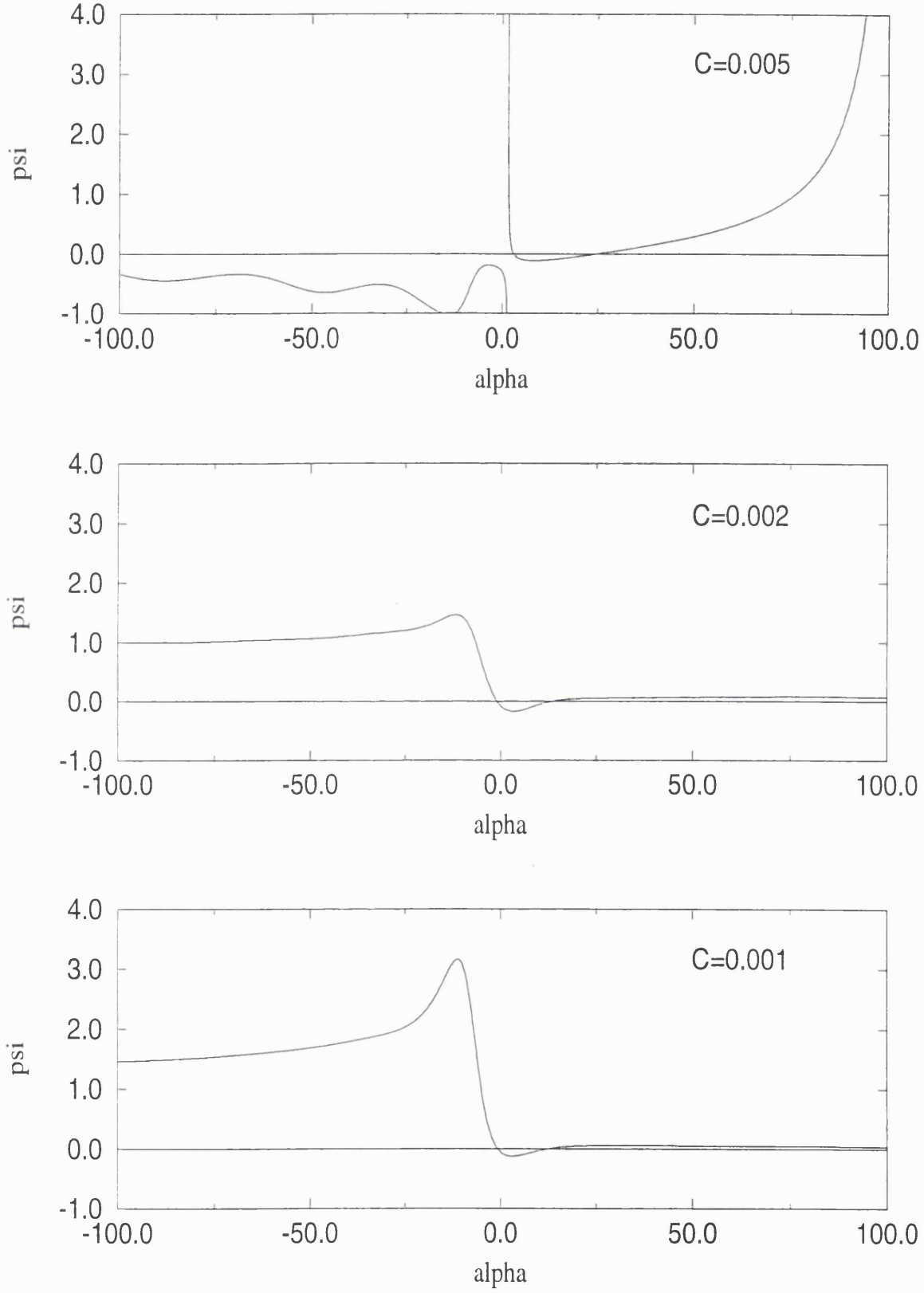

Figure 5.4: Seeking eigenvalues α

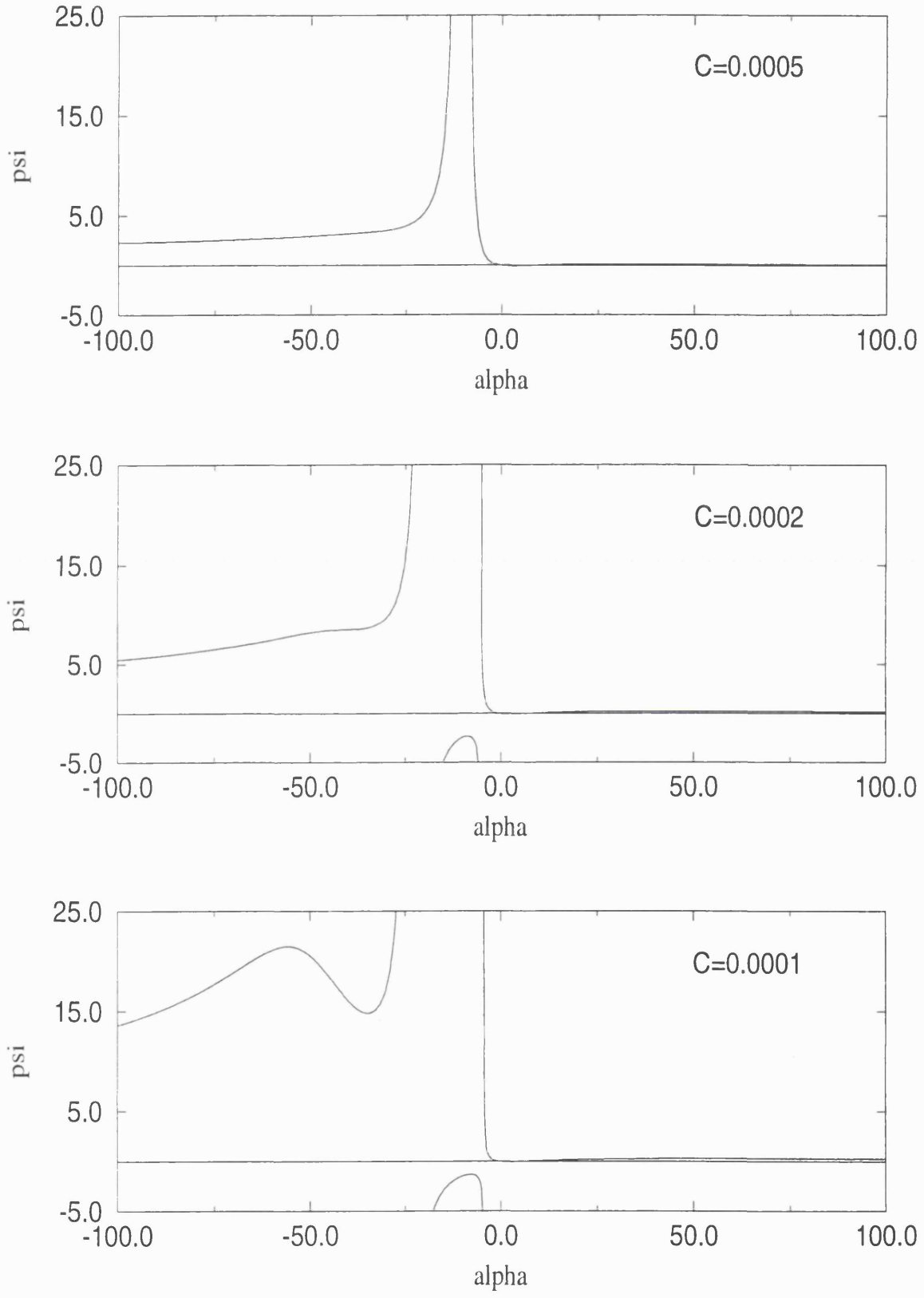

Figure 5.5: Seeking eigenvalues α

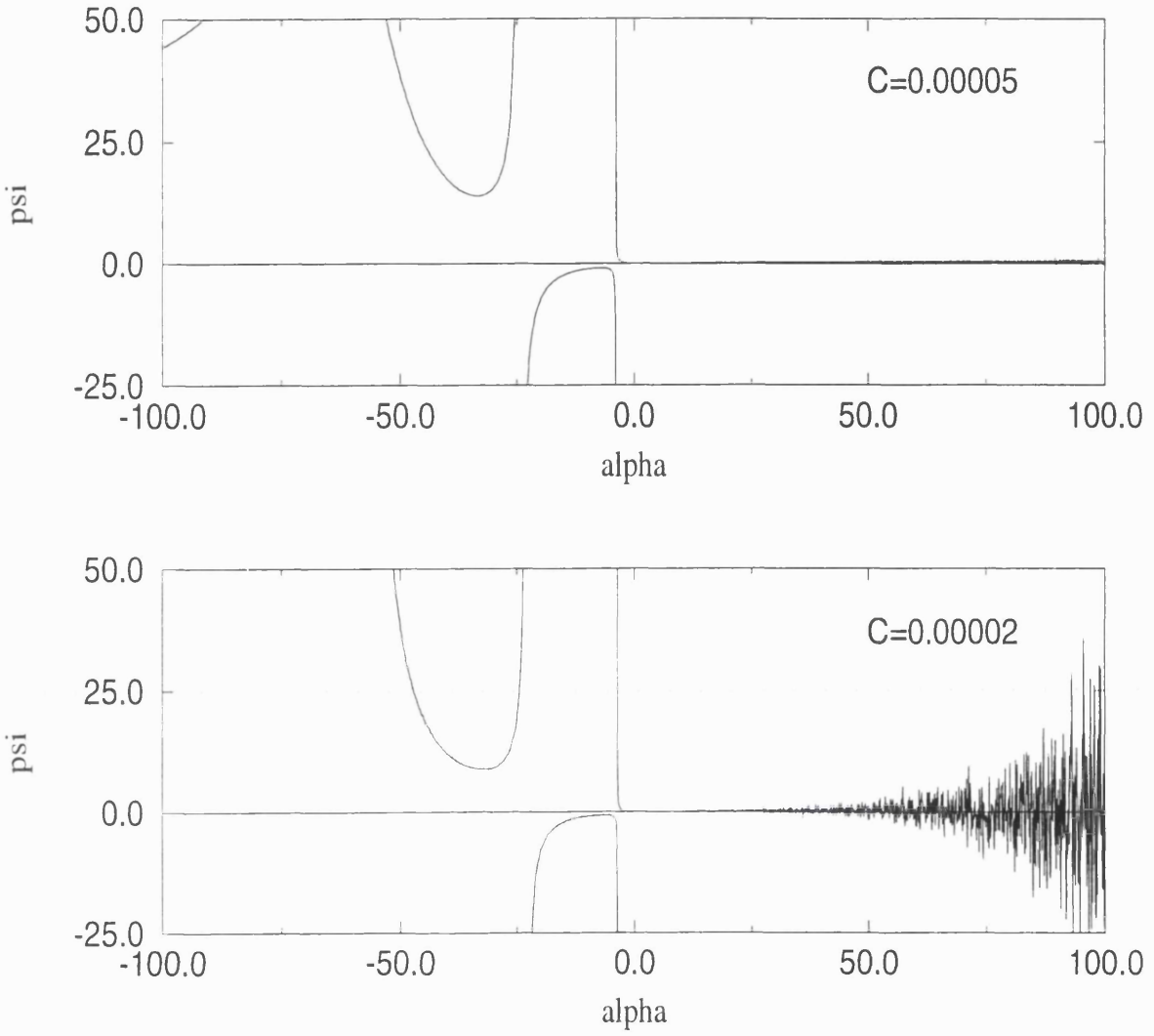

Figure 5.6: Seeking eigenvalues α

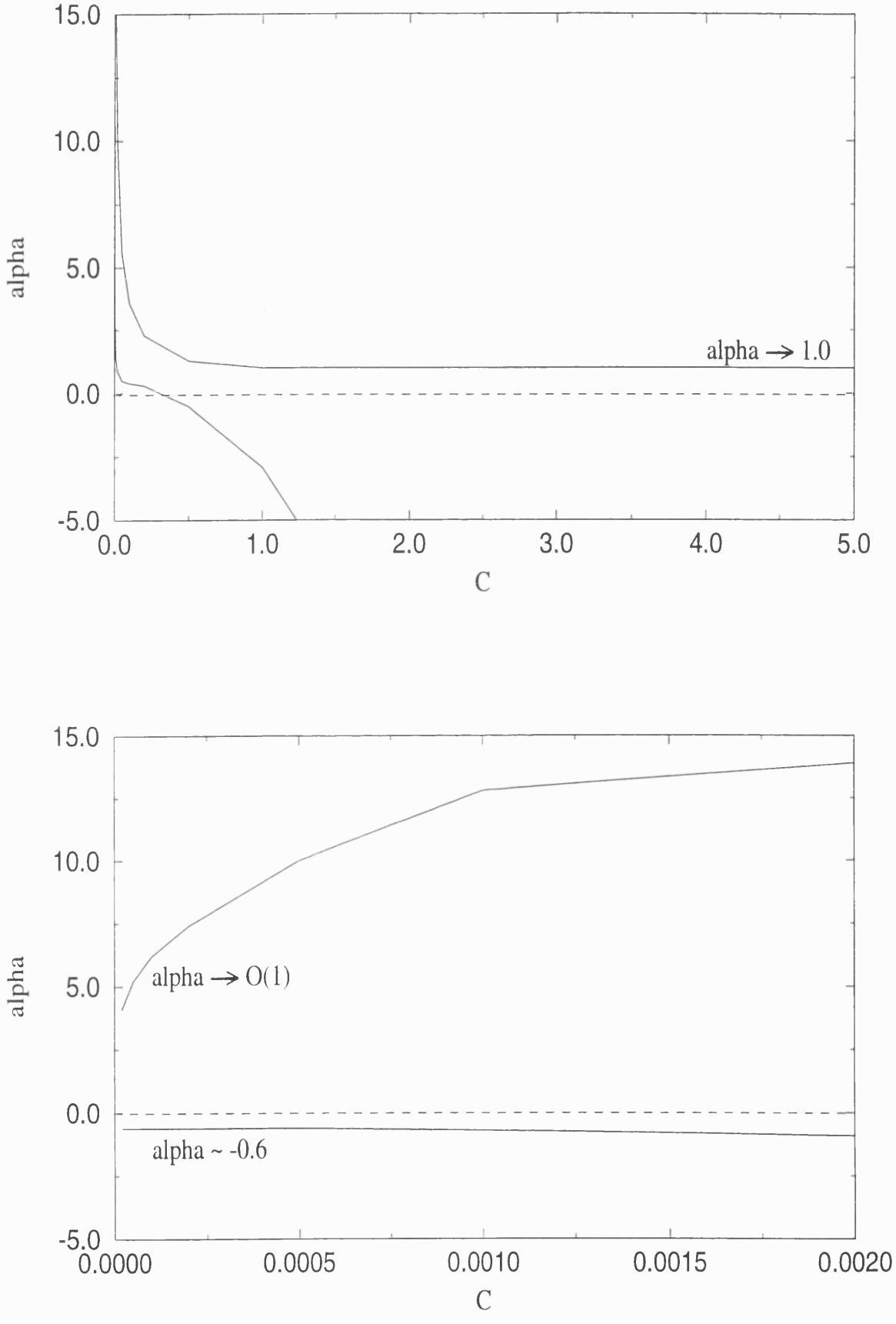

Figure 5.7: Eigenvalue α for large C and small C

for the leading terms. Then from the energy equation (5.23) $T_0 = \text{constant} = T_w$, while from the x-momentum equation (5.22)

$$\gamma C T_w u_0'' = -\frac{1}{2} p_0.$$

After integration we therefore obtain the form, with unknown constants A, B,

$$u_0 = \frac{-\frac{1}{4}p_0}{\gamma C T_w}\, y^2 + Ay + B.$$

From the boundary conditions, however, $u_0 = 0$ at $y = 0$ and $u_0' = 0$ at $y = y_0$, the solution becomes

$$u_0 = \left(\frac{-\frac{1}{4}p_0}{\gamma C T_w}\right)\left(y^2 - 2yy_0\right), \tag{5.25}$$

for u_0. For the secondary equations, employing a similar argument in terms of the orders of magnitude gives $T_1 = O(1)$ since $p_1 = 1$ (normalisation) and $\varrho_1 = O(1)$ from the state equation, and $u_1 = O(C^{-1})$ since $p_1 = 1$ and $u_0 = O(C^{-1})$ from the momentum equation. Thence the equations (5.8) - (5.11) become, with α assumed to be $O(1)$,

$$\begin{aligned}
\varrho_0 u_1 + \varrho_1 u_0 &= \psi_1', && (5.26)\\
\varrho_0 v_1 &= -\alpha \psi_1', && (5.27)\\
0 &= -(\alpha - 1/2)\, p_1 + \gamma C\,(T_0 u_1' + T_1 u_0')', && (5.28)\\
0 &= \frac{c_p \gamma C}{\sigma}\,(T_0 T_1' + T_1 T_0')', && (5.29)\\
p_1 &= R(\varrho_0 T_1 + \varrho_1 T_0). && (5.30)
\end{aligned}$$

Hence $T_1 = 0$ is the solution here, leaving the equation (for u_1)

$$\gamma C T_w u_1'' = (\alpha - 1/2)\, p_1.$$

Therefore

$$u_1 = \frac{\frac{1}{2}(\alpha - 1/2)\, p_1}{\gamma C T_w} + A_1 y + B_1,$$

with the constants A, B, to be found. From the boundary conditions, $u_1 = 0$ at $y = 0$ and $u_1' = 0$ at $y = y_0$, it follows that

$$u_1 = \left(\frac{\frac{1}{2}(\alpha - 1/2)\, p_1}{\gamma C T_w}\right)\left(y^2 - 2yy_0\right). \tag{5.31}$$

Then from the state equation $p_1 = R\varrho_1 T_w$, $\varrho_1 = p_1/RT_w$ which is constant, and therefore the stream fuction ψ_1 satisfies

$$\begin{aligned}\psi_1{}' &= \frac{p_0}{RT_w}\frac{-\frac{1}{2}(\alpha-1/2)\,p_1}{\gamma C T_w}\left(y^2-2yy_0\right)+\frac{p_1}{RT_w}\frac{-\frac{1}{4}p_0}{\gamma C T_w}\left(y^2-2yy_0\right)\\ &= \frac{\frac{1}{4}p_0 p_1}{RT_w\cdot\gamma C T_w}\left(y^2-2yy_0\right)\cdot(2\alpha-2)\,.\end{aligned}$$

Therefore we have, on integration,

$$\psi_1 = \frac{\frac{1}{4}p_0 p_1}{RT_w\cdot\gamma C T_w}\left(y^3/3-y_0y^2/2\right)\cdot(2\alpha-2)\,, \tag{5.32}$$

after using the boundary condition $\psi_1 = 0$ at $y = 0$. Also, however, $\psi_1 = 0$ at $y = y_0$; so (5.32) requires that

$$\alpha = 1 \tag{5.33}$$

Therefore as $C \longrightarrow \infty$, the eigenvalue $\alpha \longrightarrow 1$, a prediction which agrees well with the numerical results of the previous section.

5.4 Analysis for Small C

When the scaled Chapman constant is very small the velocity u and temperature T are assumed to take the power-law forms

$$u_0 = C^{-L}\hat{u_0} + \cdots, \tag{5.34}$$

$$T_0 = C^{-M}\hat{T_0} + \cdots, \tag{5.35}$$

for $y \sim 1$, with L, M being positive values to be found. From the state equation the density ϱ is therefore of the form

$$\varrho_0 = C^{L}\hat{\varrho_0} + \cdots\,. \tag{5.36}$$

These expressions are substituted into the momentum equation and the energy equation, and then the resulting orders of magnitude are, in turn,

$$C^{M-2L} \sim 1 \sim C^{1-L-M}, \tag{5.37}$$

$$C^{-L} \sim C^{-L} \sim C^{1-2M} \sim C^{1-2L-M}. \tag{5.38}$$

Therefore the implied values of the powers are $L = 1/3$ and $M = 2/3$. Then the momentum equation effectively stays in full, when the expansion forms in powers of

C are inserted. Indeed the whole problem remains as it was, with C replaced by 1 and T_w replaced by zero in effect.

The figure 5.8 shows $C^{2/3}T_0|_{centre}$ vs. C, and $C^{1/3}u_0|_{centre}$ vs. C, for small C, as a check on the behaviour proposed just above. The corresponding tabular form is the following.

C	$u_0\|_{centre}$	$T_0\|_{centre}$	$C^{1/3}u_0$	$C^{2/3}T_0$
0.1	1.7097	2.9544	0.7933	0.6348
0.05	2.2948	4.8201	0.8454	0.6523
0.02	3.2611	9.0761	0.8855	0.6666
0.01	4.1891	14.5484	0.9029	0.6730
0.005	5.3413	23.2363	0.9138	0.6771
0.002	7.3161	43.0060	0.9223	0.6803
0.001	9.2545	68.4106	0.9260	0.6817
0.0005	11.6892	108.7380	0.9278	0.6826
0.0002	15.8956	200.5021	0.9296	0.6857
0.0001	20.0443	318.4202	0.9304	0.6860
0.00005	25.2678	505.6036	0.9309	0.6862
0.00002	34.3080	931.5348	0.9313	0.6864
0.00001	43.2333	1478.8623	0.9314	0.6864

The behaviour very near the wall, where T_w makes its presence felt significantly, is similar to that analysed by Seddougui *et al.* (1991).

For the secondary (eigenfunction) equations the orders of magnitudes in the continuity, momentum, energy and state equations are follows, respectively.

$$\begin{aligned}
\varrho_0 u_1 \sim \varrho_1 u_0 \sim \psi_1, \qquad & \varrho_0 v_1 \sim \psi_1, \\
\varrho_0 u_0 \alpha T_1 \sim \alpha \sim \; & C T_0 u_1 \sim C T_1 u_0, \\
\varrho_0 u_0 \alpha T_1 \sim \varrho_1 u_0 T_0 \sim \alpha u_0 \sim u_1 \sim \; & C T_0 T_1 \sim C T_1 u_0^2 \sim C T_0 u_0 u_1, \\
1 \sim \varrho_0 T_1 \sim \; & \varrho_1 T_0.
\end{aligned}$$

Hence from the state equation (and from the orders of magnitude of ϱ_0, T_0 earlier) $\varrho_1 \sim C^{2/3}$ and $T_1 \sim C^{-2/3}$, while from the momentum equation similarly $u_1 \sim C^{-1/3}$ and $\alpha \sim 1$. Therefore for small C the suggestion is that the eigenvalue α has a positive value of $O(1)$.

From these scalings the secondary equations of motion remain in full, as do the primary equations, along with $\psi_1 \sim C^{1/3}$, $v_1 \sim C^{-1/3}$.

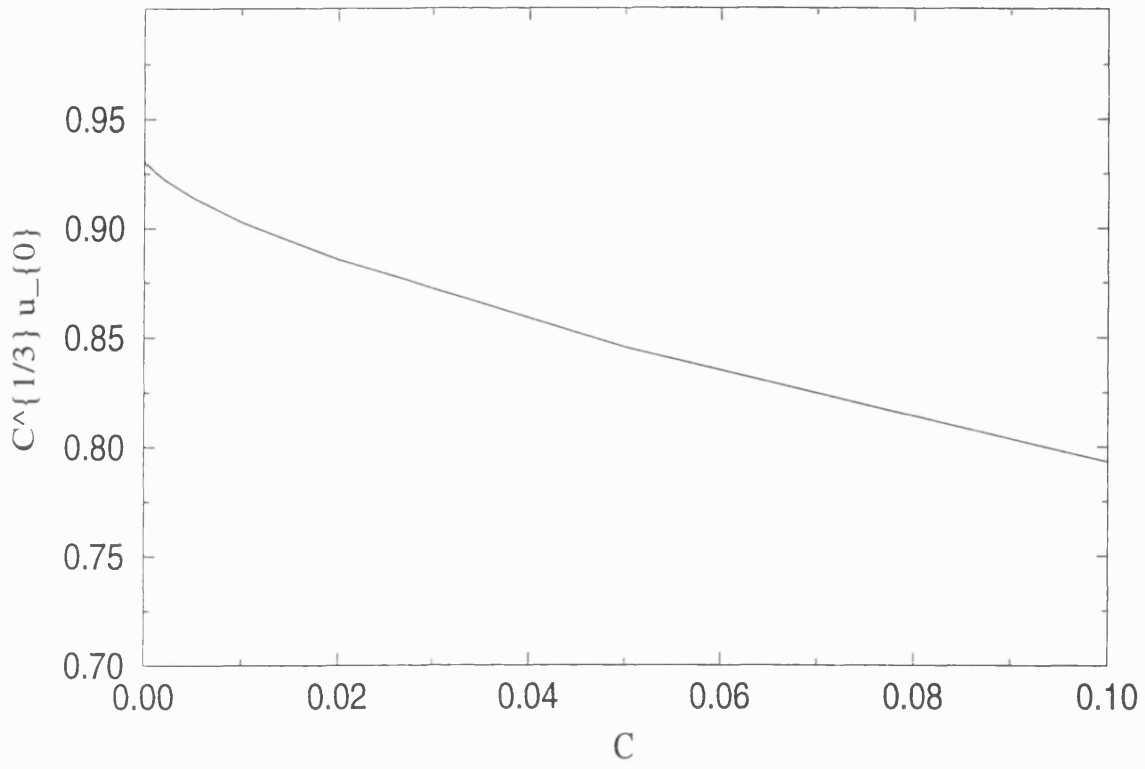

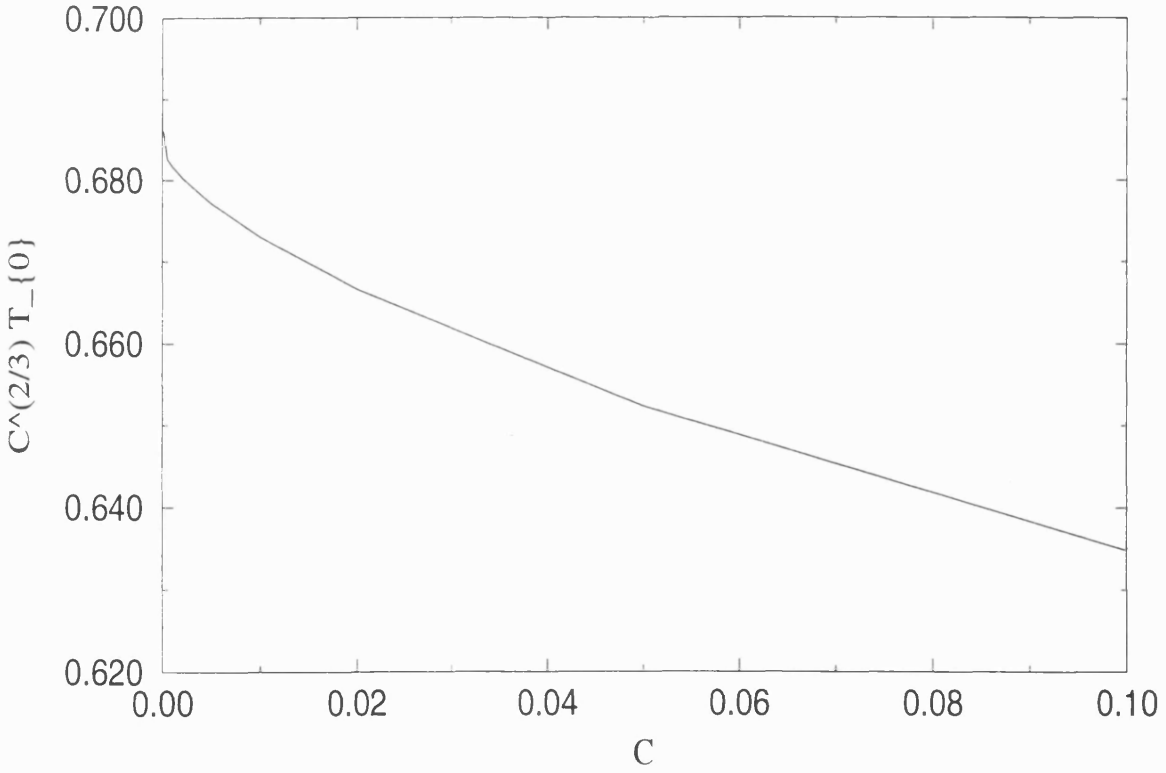

Figure 5.8: $C^{1/3}u_0|_{centre}$ vs. C and $C^{2/3}T_0|_{centre}$ vs. C

Figures in chapter 5

Figures 5.1 - 5.6 : the value of ψ_1 at the centre-line is plotted against α, from (5.16) - (5.20), to determine those values of α for which (5.13) is completely satisfied.

Fig 5.7 : showing α versus C, over different ranges of C.

Fig 5.8 : plotting scaled values of the centre-line velocity and temperature, against C.

Chapter 6

Lubrication Results for the Entire Flow Solution

6.1 The Pressure Equation

In this chapter our attention is focused particularly on the near-throat stage when the change in the pressure and other flow quantities through the nozzle is due to complete lubrication theory. This follows from extending the analysis of the previous chapter for large effective C values to incorporate the entire flow solution rather than the small disturbances of chapter 5 alone. In the current study, compressible lubrication theory, corresponding to neglect of the inertial effects in the original non-linear governing equations of chapter 3, is generally applied to the viscous flow passing through a narrow and variable nozzle shape. As the effective Chapman constant becomes large the viscous terms and the pressure gradient become dominant. Thus in the streamwise momentum equation the typical inertia term is negligible provided

$$\varrho u \frac{\partial u}{\partial x} \ll \mu \frac{\partial^2 u}{\partial y^2},$$

which is approximately, i.e. in terms of orders of magnitude, the requirement that

$$\varrho u \frac{u}{x} \ll \mu \frac{u}{y^2},$$

or

$$\frac{\varrho u x}{\mu} \frac{y^2}{x^2} \ll 1.$$

Hence the Reynolds number (in effect $\varrho ux/\mu$ here) can be large provided that the typical width of the throat of a nozzle is very narrow compared with the typical length, so that $|y/x|$ is sufficiently small.

In the full boundary-layer equations, approximating similarly, we therefore obtain for large effective C values the controlling equations

$$\varrho u = \psi_y, \quad \varrho v = -\psi_x, \tag{6.1}$$

$$0 = -p' + \gamma C \left(T u_y\right)_y, \tag{6.2}$$

$$0 = \frac{c_p}{\sigma} \gamma C \left(T T_y\right)_y, \tag{6.3}$$

$$p = R\varrho T. \tag{6.4}$$

From the energy equation $T = T_w$ and therefore the x-momentum equation is

$$\gamma C T_w u_{yy} = p'(x), \qquad u_{yy} = \frac{p'(x)}{\gamma C T_w}.$$

Therefore the velocity profile u is given, on integration, by the following development,

$$u_y = \frac{p'}{\gamma C T_w}(y + S_0) + A, \qquad \text{with} \quad A = -\frac{p' S_0}{\gamma C T_w}.$$

It follows that

$$u = \frac{p'}{\gamma C T_w}\frac{(y+S_0)^2}{2} - \frac{p'}{\gamma C T_w}(y + S_0) + B, \qquad \text{but} \quad B = 0.$$

Hence the velocity profile u is

$$u = \frac{p'(x)}{2\gamma C T_w}\left[(y+S_0)^2 - 2S_0(y+S_0)\right],$$

after use of the boundary conditions $u' = 0$ at $y = 0$ and $u = 0$ at $y = S_0$. From the state equation $\varrho = p/RT_w$, which is a function of x only, and from the continuity equation

$$\psi_y = \frac{p}{RT_w}\frac{p'}{2\gamma C T_w}\left[y^2 - {S_0}^2\right],$$

and so

$$\psi = \frac{p}{RT_w}\frac{p'}{2\gamma C T_w}\left[\frac{1}{3}y^3 - {S_0}^2 y - \frac{2}{3}{S_0}^3\right],$$

since $\psi = 0$ at $y = -S_0$. Then the streamfunction ψ is a constant D, which is unknown and to be found, at $y = 0$.

$$D = \frac{pp'}{2\gamma C R {T_w}^2}\left[-\frac{2}{3}{S_0}^3\right].$$

Hence the pressure $p(x)$ is governed by

$$pp' = -\lambda \frac{{T_w}^2(x)}{{S_0}^3(x)} \tag{6.5}$$

where the constant $\lambda \equiv 3D\gamma CR$. Then

$$\frac{1}{2}p^2 = \frac{1}{2}p^2(x_0) - \lambda \int_{x_0}^{x} \frac{{T_w}^2(x)}{{S_0}^3(x)} dx \tag{6.6}$$

where $p(x_0)$ is the starting pressure. But actually D is unknown and $p(x_1)$ is given. Therefore we need

$$\frac{1}{2}p^2(x_1) = \frac{1}{2}p^2(x_0) - \lambda \int_{x_0}^{x_1} \frac{{T_w}^2(x)}{{S_0}^3(x)} dx \tag{6.7}$$

which fixes λ and hence D from the definition above.

Another way to regard the solution is to eliminate λ from the equation (6.5),

$$pp' = -\lambda \frac{{T_w}^2(x)}{{S_0}^3(x)},$$

by differentiating to give

$$\frac{d}{dx}\left[\frac{{S_0}^3(x)}{{T_w}^2(x)}\frac{d}{dx}p^2\right] = 0, \tag{6.8}$$

and this gives a second order ordinary differential equation for $p(x)$, in which two boundary conditions are required to determine the pressure profile through the nozzle. That tends to confirm the existence of upstream influence, with one boundary condition being associated with the upstream end of the nozzle and the other with the downstream end.

6.2 Sample Solutions

We restrict attention here to representative results. The two graphs of Fig. 6.1 show the pressure profiles along x, with various shape of nozzle $S_0(x)$ which is a function defined as

$$S_0(x) = 1 + ax^2$$

with variable a ($25 > a > 0.04$). The upper graph shows the case in which the fixed pressure $p_{(x_0=-1)} = 5.0$ and $p_{(x_1=1)} = 1.0$ are imposed, and the lower shows fixed pressure $p_{(x_0=-1)} = 1.0$ and $p_{(x_1=1)} = 0.5$. When a becomes large, the equation (6.7) becomes

$$\frac{1}{2}p^2 = \frac{1}{2}p^2(x_0) - \lambda \int_{-\infty}^{x} \frac{{T_w}^2(x)}{{S_0}^3(x)} dx$$

and hence, for $x > 0$, in effect

$$\frac{1}{2}p^2 = \frac{1}{2}p^2(x_0) - \lambda \int_{-\infty}^{\infty} \frac{{T_w}^2(x)}{{S_0}^3(x)} dx,$$

Thus the pressure decreases rapidly. In both cases the pressure profiles are determined by the fixed pressures downstream *and* upstream; therefore there is upstream influence in the flow system.

Fig. 6.2 show the pressure profiles with different wall temperature $T_w(x)$ functions. Decrease of the wall temperature along x causes faster decrease of the pressure compared to increase of the wall temperature.

The results thus confirm the existence of concise exact solutions for the nozzle-wall pressure, and likewise for other representative quantities, when the effective Chapman constant is large. The results also verify the presence of upstream influence in the system (as implied by chapter 5) in view of the two boundary conditions appropriate in solving (6.8).

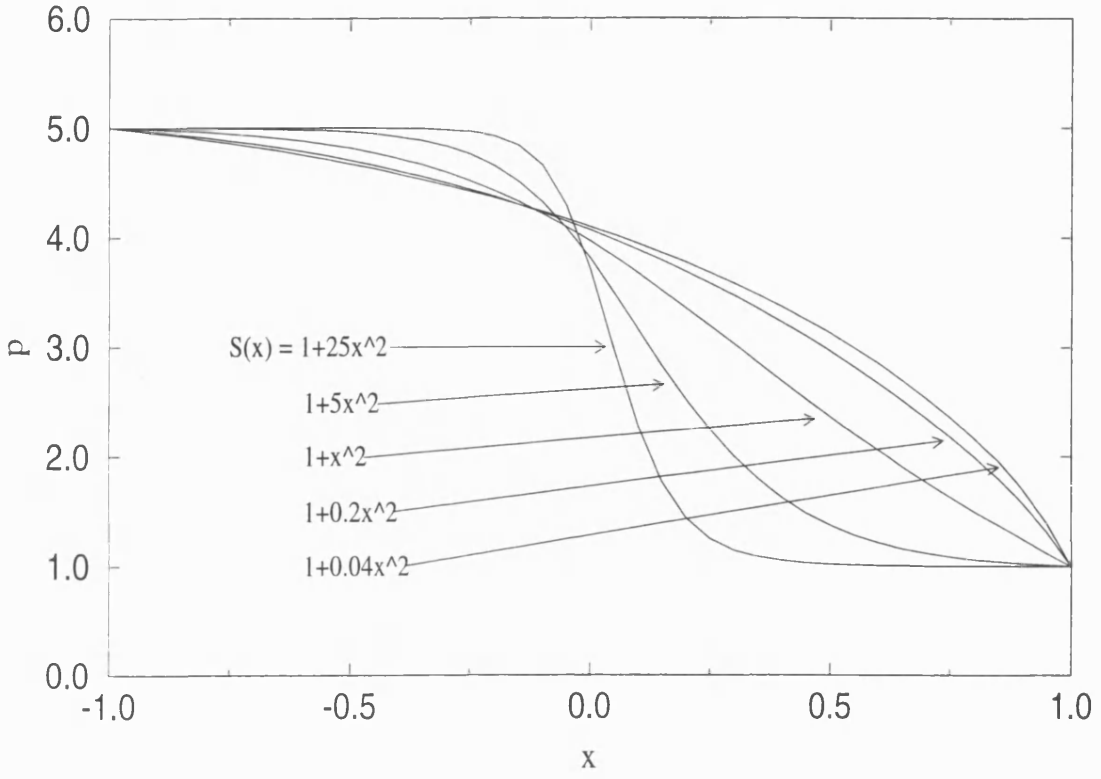

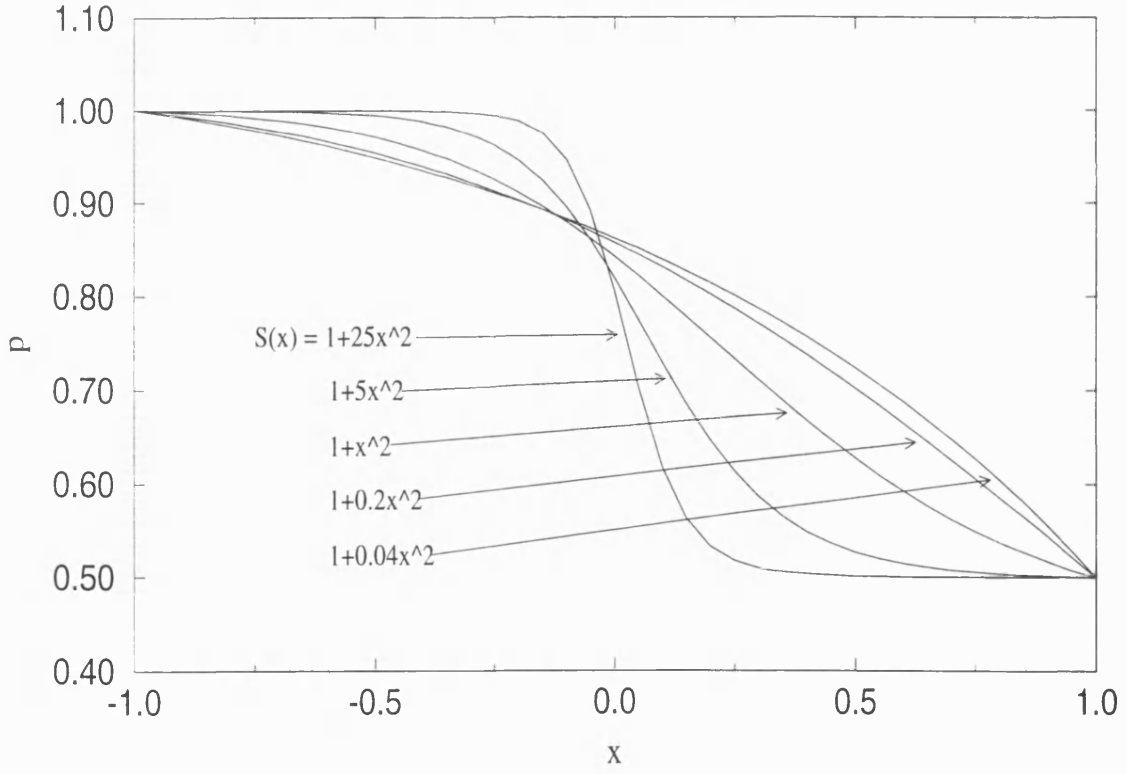

Figure 6.1: Pressure equation : $T_0 = 1.0$, $T_1 = 2.0$ with various $S(x)$.

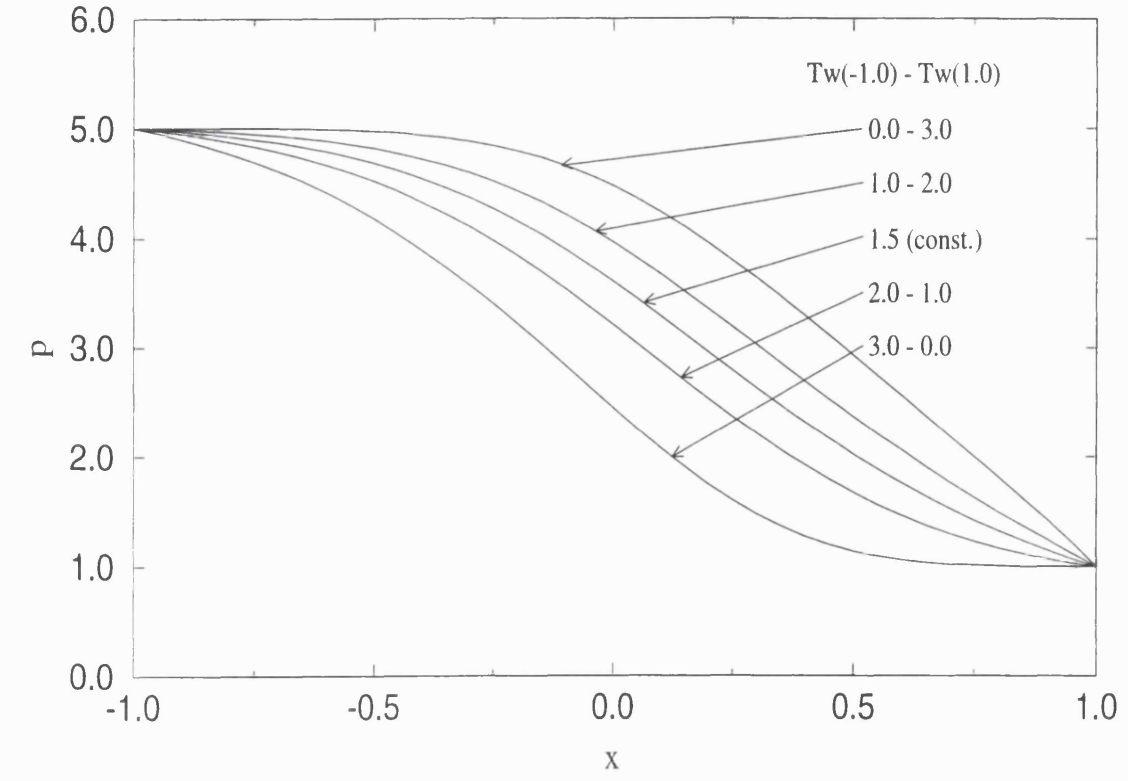

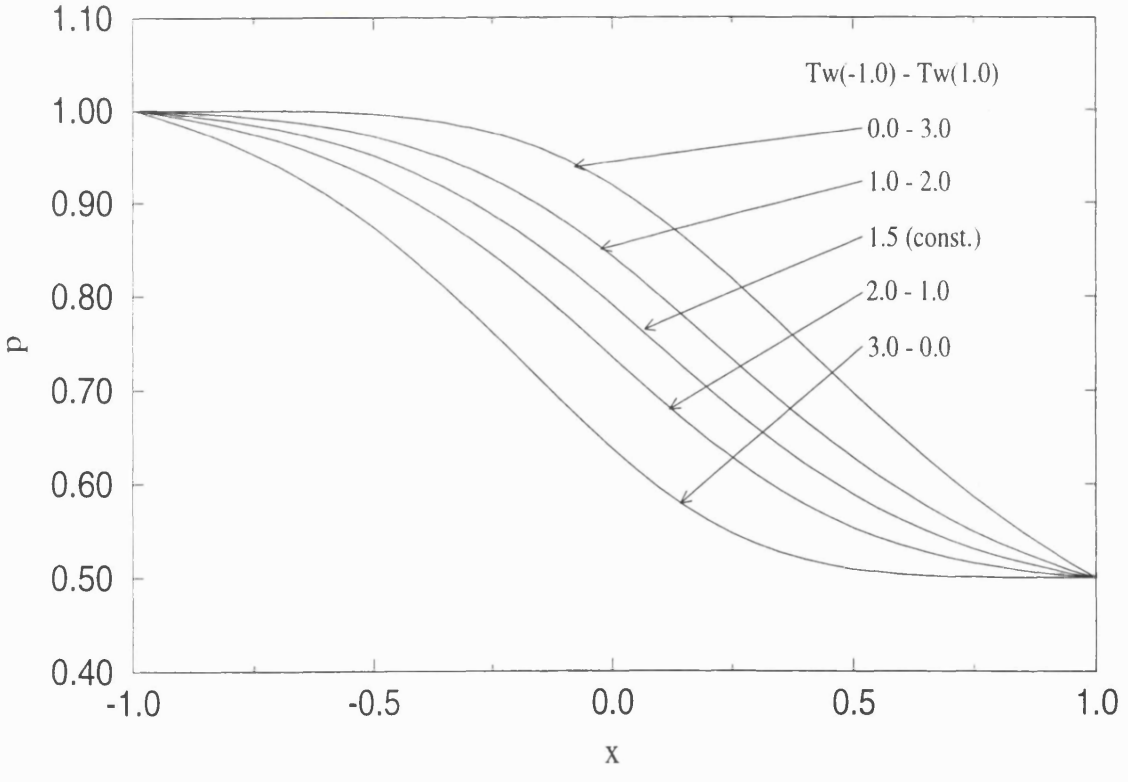

Figure 6.2: Pressure equation : fixed $S(x)$ with various T_w

Figures in chapter 6

Fig 6.1 : the pressure profiles with various shapes of the nozzle $S(X)$ along x. The upper graph shows the case in which the fixed pressures $p_{(x_0=-1)} = 5.0$ and $p_{(x_1=1)} = 1.0$ are imposed, and the lower shows fixed pressures $p_{(x_0=-1)} = 1.0$ and $p_{(x_1=1)} = 0.5$. The nozzle shapes $S(x)$ taken are, in turn,

$$\begin{aligned} S(x) &= 1 + 25x^2 \\ &= 1 + 5x^2 \\ &= 1 + x^2 \\ &= 1 + 0.2x^2 \\ &= 1 + 0.04x^2. \end{aligned}$$

Fig 6.2 : the pressure profiles with various wall temperatures $T_w(x)$ along x. The fixed pressures are imposed as Fig. 6.1. The wall temperatures imposed are

$T_w(x = -1.0)$	–	$T_w(x = 1.0)$
0.0	–	3.0
1.0	–	2.0
1.5	–	1.5
2.0	–	1.0
3.0	–	0.0.

Chapter 7

On the P.D.E. Sweeping Problem

Here we describe a preliminary attempt at incorporating the findings in the previous chapters, on upstream influence, into a method for solving the original partial-differential system. This is a simple first such trial. Section 7.1 below considers the semi-implicit algorithm that was used, section 7.2 gives its effect on the partial differential equations of concern, and section 7.3 describes the resulting tridiagonal matrix algorithm. Then section 7.4 goes through the local solution procedure for the velocities and temperatures, followed by section 7.5 on determining the other quantities required. Finally sample solutions are discussed in section 7.6, along with some comments and recommendations.

7.1 Semi-Implicit Algorithm

In the previous chapter the solution of the ordinary-differential system applying for certain similarity shapes of nozzle and suitable boundary conditions was computed by means of a fourth-order Runge-Kutta method, for various parameter values. This chapter extends the previous similarity or limit results to more general cases where the original partial-differential system holds in full and streamwise marching in one form or another is required. In order to determine the solution of the flow system fully now, all the terms of the composite equations (3.1)-(3.7) have to be taken into account in the numerical approach.

The finite-difference method which was used to discretise the governing equations is described in the sections that follow. In particular, in this work the differences are taken as effectively forward-time (in x) and centred in space (y), giving a method which is referred to by Roache (1976) as the FTCS method and which can be readily made second-order accurate in both x and y.

Generally there are two different types of marching scheme to solve parabolic

partial differential equations; explicit methods and implicit methods. In an explicit method the downstream profiles are computed directly from the known neighbouring upstream profiles. Explicit methods are simple but often require small step sizes in the corresponding computations to achieve numerical stability. In an implicit method the downstream-profile solutions are determined simultaneously, typically by iteration and matrix inversion. The advantage in implicit methods tends to be that there is no or reduced numerical instability and hence the step sizes can be taken much larger than those in explicit methods. On the other hand, it can take many iterations to solve those steps in an implicit method.

In order to minimise or reduce the disadvantages of the two approaches above, a semi-implicit method is introduced as an algorithm to solve the partial differential equations for the flow solution numerically. While an implicit method requires iteration and matrix inversion, a semi-implicit method requires only matrix inversion, without iteration.

We consider first below a single forward march streamwise in x, before addressing subsequently the issue of multi-sweeping in x which is clearly necessary in view of the upstream influence established in previous chapters.

7.2 The System of Flow Equations

A convenient system of coordinates is introduced to account for the normalised nozzle shape. The new coordinate $\hat{y}$ is defined as

$$\hat{y} = y/S \tag{7.1}$$

where $S(x)$ is the given width of the normalised nozzle shape and y is the original Cartesian coordinate. Hence the $\hat{y}$-ordinate is confined to the region of $0 < |\hat{y}| < 1$ regardless of the width of the nozzle. Then as the system is transformed, $(x, y) \longrightarrow (x, \hat{y})$, the derivatives with respect to x and y transform according to

$$\frac{\partial}{\partial x} \longrightarrow \frac{\partial}{\partial x} - \frac{S_x}{S}\,\hat{y}\,\frac{\partial}{\partial \hat{y}}\,, \quad \frac{\partial}{\partial y} \longrightarrow \frac{1}{S}\frac{\partial}{\partial \hat{y}}$$

respectively.

Therefore the momentum and the energy equations become

$$\varrho\, u \left(u_x - \frac{S_x}{S}\,\hat{y}\,u_{\hat{y}}\right) + \varrho\, v\,\frac{1}{S}\,u_{\hat{y}} = -p'(x) + \frac{\mu}{S^2}\,u_{\hat{y}\hat{y}} + \frac{1}{S^2}\,\mu_{\hat{y}}\,u_{\hat{y}}, \tag{7.2}$$

$$\varrho\, c_p \left(u \left(T_x - \frac{S_x}{S}\,\hat{y}\,T_{\hat{y}}\right) + v\,\frac{1}{S}\,T_{\hat{y}}\right) = u\,p'(x) + k\,\frac{1}{S^2}\,T_{\hat{y}\hat{y}} + \frac{1}{S^2}\,k_{\hat{y}}\,T_{\hat{y}} + \mu\,\frac{1}{S^2}\,(u_{\hat{y}})^2\,, \tag{7.3}$$

in turn.

In order to discretise the derivatives in (7.2), (7.3) with respect to x first, effectively a forward-differencing method is applied to $\partial u/\partial x$ in the x-momentum equation and to $\partial T/\partial x$ in the energy equation. First, at the current calculation step $i+1$, in the x-momentum equation all the non-derivative terms are set to their values at the previous step i where the variables are assumed to have been numerically determined already, while the x-derivative term is expressed in finite differences. The form is as follows.

$$\bar{\varrho}\,\bar{u}\left(u_x - \frac{S_x}{S}\,\hat{y}\,u_{\hat{y}}\right) + \bar{\varrho}\,\bar{v}\,\frac{1}{S}\,u_{\hat{y}} = -p'(x) + \frac{\bar{\mu}}{S^2}\,u_{\hat{y}\hat{y}} + \frac{1}{S^2}\,\bar{\mu}_{\hat{y}}\,u_{\hat{y}}.$$

The bars above denote their values at the previous step i. Likewise, in the energy equation the x-derivative of T is expressed as

$$\bar{\varrho}\,c_p\,\left(\,\bar{u}\left(T_x - \frac{S_x}{S}\,\hat{y}\,T_{\hat{y}}\right) + \bar{v}\,\frac{1}{S}\,T_{\hat{y}}\right) = \bar{u}\,p'(x) + \bar{k}\,\frac{1}{S^2}\,T_{\hat{y}\hat{y}} + \frac{1}{S^2}\,\bar{k}_{\hat{y}}\,T_{\hat{y}} + \bar{\mu}\,\frac{1}{S^2}\,(\bar{u_{\hat{y}}})^2\,.$$

In the last term $(\bar{u_{\hat{y}}})^2$ can be expressed as $\bar{u_{\hat{y}}}u_{\hat{y}}$ instead. The x momentum equation above can then be rearranged to display the x-derivative term on the left hand side and the other variables on the right hand side,

$$\bar{\varrho}\,\bar{u}\cdot u_x = \left(\,\bar{\varrho}\,\bar{u}\,\frac{S_x}{S}\,\hat{y} - \bar{\varrho}\,\bar{v}\,\frac{1}{S} + \frac{1}{S^2}\,\bar{\mu}_{\hat{y}}\right)u_{\hat{y}} + \frac{\bar{\mu}}{S^2}\,u_{\hat{y}\hat{y}} - p'(x).$$

Using FTCS differencing in the y-derivatives also, the finite-difference analogue of the momentum equation is thus, with steps $j\,\Delta y$ in the y direction,

$$\begin{aligned}\bar{\varrho}\,\bar{u}\cdot\frac{u_j - \bar{u_j}}{\Delta x} \;=\; & \left(\,\bar{\varrho}\,\bar{u}\,\frac{S_x}{S}\,\hat{y} - \bar{\varrho}\,\bar{v}\,\frac{1}{S} + \frac{1}{S^2}\,\bar{\mu}_{\hat{y}}\right)\frac{u_{j+1} - u_{j-1}}{2\Delta y} \\ & + \frac{\bar{\mu}}{S^2}\,\frac{u_{j+1} - 2u_j + u_{j-1}}{(\Delta y)^2} - p'(x). \qquad (7.4)\end{aligned}$$

Similarly the energy equation becomes

$$\bar{\varrho}\,c_p\,\bar{u}\,T_x = \left(\bar{\varrho}\,c_p\,\bar{u}\,\frac{S_x}{S}\,\hat{y} - \bar{\varrho}\,c_p\,\bar{v}\,\frac{1}{S} + \frac{1}{S^2}\,\bar{k}_{\hat{y}} + \bar{\mu}\,\frac{1}{S}\,\bar{u_{\hat{y}}}\right)T_{\hat{y}} + \bar{k}\,\frac{1}{S^2}\,T_{\hat{y}\hat{y}} + \bar{u}\,p'(x),$$

and its finite-difference analogue is then

$$\begin{aligned}\bar{\varrho}\,c_p\,\bar{u}\,\frac{T_j - \bar{T_j}}{\Delta x} \;=\; & \left(\bar{\varrho}\,c_p\,\bar{u}\,\frac{S_x}{S}\,\hat{y} - \bar{\varrho}\,c_p\,\bar{v}\,\frac{1}{S} + \frac{1}{S^2}\,\bar{k}_{\hat{y}} + \bar{\mu}\,\frac{1}{S}\,\bar{u_{\hat{y}}}\right)\frac{T_{j+1} - T_{j-1}}{2\Delta y} \\ & + \frac{\bar{k}}{S^2}\cdot\frac{T_{j+1} - 2T_j + T_{j-1}}{(\Delta y)^2} + \bar{u}\,p'(x). \qquad (7.5)\end{aligned}$$

In the above, (7.4) is regarded as determining the u_j, (7.5) the T_j, and then ϱ_j are to be found from the equation of state, v_j from the continuity, and so on. More details are provided below.

7.3 Tridiagonal Matrix Algorithm

As the finite-difference analogue of the momentum equation (for instance) consists of three consecutive discretised variables u_{j+1}, u_j, u_{j-1}, the notation can be simplified here by denoting the coefficients involved by α, β, γ and R, leaving the form

$$\alpha_j\, u_{j-1} + \beta_j\, u_j + \gamma_j\, u_{j+1} = R_j \tag{7.6}$$

where R denotes the entire rest of the terms in (7.4). From the boundary condition u_1 is known, $u_1 = u_w$ (at the wall). Then the complete system of finite-difference equations representing (7.4) can be written in matrix form as

$$\begin{pmatrix} 1 & & & & & \\ \alpha_2 & \beta_2 & \gamma_2 & & & \\ & \alpha_3 & \beta_3 & \gamma_3 & & \\ & & \ddots & \ddots & \ddots & \\ & & & \alpha_{J-1} & \beta_{J-1} & \gamma_{J-1} \\ & & & & \alpha_J + \gamma_J & \beta_J \end{pmatrix} \begin{pmatrix} u_1 \\ u_2 \\ u_3 \\ \vdots \\ u_{J-1} \\ u_J \end{pmatrix} = \begin{pmatrix} u_w \\ R_2 \\ R_3 \\ \vdots \\ R_{J-1} \\ R_J \end{pmatrix}.$$

Here the last equation in the system represented by the equation (7.6) is

$$\alpha_J u_{J-1} + \beta_J u_J + \gamma_J u_{J+1} = R_J \tag{7.7}$$

originally. However, $u_{J-1} = u_{J+1}$ from an interpretation of the symmetry condition along the centre line; thus the equation becomes

$$(\alpha_J + \gamma_J)\; u_{J-1} + \beta_J u_J = R_J.$$

This is incorporated in the matrix equation above.

The coefficient matrix is a tridiagonal matrix, having non-zero elements only along the diagonal, the superdiagonal and the subdiagonal. The solution of the system of equations can therefore be obtained by matrix inversion or Gaussian elimination.

In more detail, the equation (7.4) is

$$\begin{aligned} \bar{\varrho}_j\, \bar{u}_j \cdot \frac{u_j - \bar{u}_j}{\Delta x} \;=\; & \left(\bar{\varrho}\, \bar{u}\, \frac{S_x}{S}\, \hat{y} - \bar{\varrho}\, \bar{v}\, \frac{1}{S} + \frac{1}{S^2}\, \bar{\mu}_{\hat{y}} \right) \frac{u_{j+1} - u_{j-1}}{2\Delta y} \\ & + \frac{\bar{\mu}_j}{S^2}\, \frac{u_{j+1} - 2u_j + u_{j-1}}{(\Delta y)^2} - p'(x), \end{aligned} \tag{7.8}$$

and this can be written in the above form (7.6) with

$$\begin{aligned}
\alpha_j &= \frac{\bar{\mu}_j}{S^2(\Delta y)^2} - \Big(\bar{\varrho}\,\bar{u}\,\frac{S_x}{S}\,\hat{y} - \bar{\varrho}\,\bar{v}\,\frac{1}{S} + \frac{1}{S^2}\,\bar{\mu}_{\hat{y}} \Big) \frac{1}{2\Delta y}, \\
\beta_j &= -2\frac{\bar{\mu}_j}{S^2(\Delta y)^2} - \frac{\bar{\varrho}_j\,\bar{u}_j}{\Delta x}, \\
\gamma_j &= \frac{\bar{\mu}_j}{S^2(\Delta y)^2} + \Big(\bar{\varrho}\,\bar{u}\,\frac{S_x}{S}\,\hat{y} - \bar{\varrho}\,\bar{v}\,\frac{1}{S} + \frac{1}{S^2}\,\bar{\mu}_{\hat{y}} \Big) \frac{1}{2\Delta y}, \\
R_j &= -\frac{\bar{\varrho}_j\,\bar{u}_j^{\,2}}{\Delta x} + p'(x).
\end{aligned}$$

Likewise for T, the equation (7.5) becomes

$$\begin{aligned}
\bar{\varrho}_j\,c_p\,\bar{u}_j\,\frac{T_j - \bar{T}_j}{\Delta x} &= \Big(\bar{\varrho}\,c_p\,\bar{u}\,\frac{S_x}{S}\,\hat{y} - \bar{\varrho}\,c_p\,\bar{v}\,\frac{1}{S} + \frac{1}{S^2}\,\bar{k}_{\hat{y}} + \bar{\mu}\,\frac{1}{S}\,\bar{u}_{\hat{y}} \Big) \frac{T_{j+1} - T_{j-1}}{2\Delta y} \\
&\quad + \frac{\bar{k}}{S^2} \cdot \frac{T_{j+1} - 2T_j + T_{j-1}}{(\Delta y)^2} + \bar{u}_j\,p'(x), \qquad (7.9)
\end{aligned}$$

and this reduces to the form

$$\delta_j\,T_{j-1} + \varepsilon_j\,T_j + \zeta_j\,T_{j+1} = Q_j, \qquad (7.10)$$

similarly as (7.6), where

$$\begin{aligned}
\delta_j &= \frac{\bar{k}_j}{S^2(\Delta y)^2} - \Big(\bar{\varrho}\,c_p\,\bar{u}\,\frac{S_x}{S}\,\hat{y} - \bar{\varrho}\,c_p\,\bar{v}\,\frac{1}{S} + \frac{1}{S^2}\,\bar{k}_{\hat{y}} + \bar{\mu}\,\frac{1}{S}\,\bar{u}_{\hat{y}} \Big) \frac{1}{2\Delta y}, \\
\varepsilon_j &= -2\frac{\bar{k}_j}{S^2(\Delta y)^2} - \frac{\bar{\varrho}_j\,c_p\,\bar{u}_j}{\Delta x}, \\
\zeta_j &= \frac{\bar{k}_j}{S^2(\Delta y)^2} + \Big(\bar{\varrho}\,c_p\,\bar{u}\,\frac{S_x}{S}\,\hat{y} - \bar{\varrho}\,c_p\,\bar{v}\,\frac{1}{S} + \frac{1}{S^2}\,\bar{k}_{\hat{y}} + \bar{\mu}\,\frac{1}{S}\,\bar{u}_{\hat{y}} \Big) \frac{1}{2\Delta y}, \\
Q_j &= -\frac{\bar{\varrho}_j\,c_p\,\bar{u}_j\,\bar{T}_j}{\Delta x} - \bar{u}_j\,p'(x).
\end{aligned}$$

The method of solution of (7.7), (7.10) is described, for completeness, in the next section.

7.4 Gaussian Elimination

The numerical procedure starts with the elimination of the γ_j 's by Gaussian elimination. The last equation of the system can be written as

$$u_J = \frac{R_J - (\alpha_J + \gamma_J)\,u_{J-1}}{\beta_J}.$$

Then the second last equation can be represented as

$$\alpha_{J-1}u_{J-2} + \beta_{J-1}u_{J-1} - \gamma_{J-1} \cdot \frac{R_J - (\alpha_J + \gamma_J)\, u_{J-1}}{\beta_J} = R_{J-1}$$

$$\alpha_{J-1}u_{J-2} + \left(\beta_{J-1} - \gamma_{J-1} \cdot \frac{\alpha_J + \gamma_J}{\beta_J}\right) u_{J-1} = R_{J-1} - \frac{\gamma_{J-1}}{\beta_J} R_J$$

Therefore the factor for Gaussian elimination is

$$\begin{aligned} \tilde{\beta}_{J-1} &= \beta_{J-1} - \gamma_{J-1} \cdot \frac{\alpha_J + \gamma_J}{\beta_J}, \\ \tilde{R}_{J-1} &= R_{J-1} - \frac{\gamma_{J-1}}{\beta_J} \cdot R_J. \end{aligned}$$

This will result in a bidiagonal form of equation given by

$$\alpha_{J-1}u_{J-2} + \tilde{\beta}_{J-1} \cdot u_{J-1} = \tilde{R}_{J-1}.$$

Likewise, the other equations can be solved as

$$\begin{aligned} \alpha_j u_{j-1} + \beta_j u_j + \gamma_j u_{j+1} &= R_j, \\ \alpha_{j+1} u_j + \tilde{\beta}_{j+1} u_{j+1} &= \tilde{R}_j. \end{aligned}$$

In order to eliminate γ_j, multiply the second equation by $\gamma_j/\tilde{\beta}_{j+1}$, then the coefficient of u_j is replaced by $\tilde{\beta}$ upward in the system

$$\tilde{\beta}_j = \beta_j - \frac{\gamma_j}{\tilde{\beta}_{j+1}} \cdot \alpha_{j+1},$$

$$\tilde{R}_j = R_j - \frac{\gamma_j}{\tilde{\beta}_{j+1}} \cdot \tilde{R}_{j+1}.$$

Although the γ 's are eliminated from the equations, the effect of γ 's remains in the system.

The first equation of the system is $u_1 = u_w$ and therefore the solution of the remaining equations is obtained by back-substitution in the system and determination of u_j by the general recursion formula

$$u_j = \frac{\tilde{R}_j - \alpha_j \cdot u_{j-1}}{\tilde{\beta}_j}, \tag{7.11}$$

for the calculation of u_j where u_{j-1} has already been determined by the previous application of the formula, and the sequence ends with the last equation solved by

$$u_J = \frac{R_J - (\alpha_J + \gamma_J)\, u_{J-1}}{\tilde{\beta}_J} \tag{7.12}$$

7.5 Determining the Other Quantities

After the computation of the x-momentum and energy equations, u_j's and T_j's are determined. In similar fashion, expanding backwards the x-derivative in the continuity equation gives its finite-difference analogue here as

$$(\varrho u)_x = \frac{\varrho u - \bar{\varrho}\bar{u}}{\Delta x}, \tag{7.13}$$

and similarly for $\partial(\varrho u)/\partial\hat{y}$ and $\partial(\varrho v)/\partial\hat{y}$, namely

$$(\varrho_j\, u_j)_{\hat{y}} = \frac{\varrho_j\, u_j - \varrho_{j-1}\, u_{j-1}}{\Delta\hat{y}},$$

$$(\varrho_j\, v_j)_{\hat{y}} = \frac{\varrho_j\, v_j - \varrho_{j-1}\, v_{j-1}}{\Delta\hat{y}}.$$

Then using the discrete values for j and $j-1$ a central difference can be evaluated with $j-\frac{1}{2}$ (as in a so-called box method). The product term at the midpoint $\varrho_{j-\frac{1}{2}}\, u_{j-\frac{1}{2}}$ can be derived as the average of the products at the neighbouring points,

$$\varrho_{j-\frac{1}{2}}\, u_{j-\frac{1}{2}} = \frac{1}{2}\left[\varrho_j\, u_j + \varrho_{j-1}\, u_{j-1}\right].$$

The x-derivative in the continuity equation can likewise be written as

$$\left(\varrho_{j-\frac{1}{2}}\, u_{j-\frac{1}{2}}\right)_x = \frac{\frac{1}{2}(\varrho_j\, u_j + \varrho_{j-1}\, u_{j-1}) - \frac{1}{2}(\bar{\varrho}_j\, \bar{u}_j + \bar{\varrho}_{j-1}\, \bar{u}_{j-1})}{\Delta x}$$

$$= \frac{(\varrho_j\, u_j - \bar{\varrho}_j\, \bar{u}_j)(\varrho_{j-1}\, u_{j-1} - \bar{\varrho}_{j-1}\, \bar{u}_{j-1})}{2\Delta x}.$$

Therefore the entire continuity equation in finite-difference form becomes

$$\frac{\frac{1}{2}\left[(\rho_j\, u_j - \bar{\rho}_j\, \bar{u}_j) + (\rho_{j-1}\, u_{j-1} - \bar{\rho}_{j-1}\, \bar{u}_{j-1})\right]}{\Delta x} + \frac{\left[(\rho_j\, v_j) - (\rho_{j-1}\, v_{j-1})\right]}{\Delta y} = 0,$$

so that v_j is given by

$$v_j = \frac{\Delta y}{\rho_j}\left[\frac{\rho_{j-1}\, v_{j-1}}{\Delta y} - \frac{(\rho_j\, u_j - \bar{\rho}_j\, \bar{u}_j) + (\rho_{j-1}\, u_{j-1} - \bar{\rho}_{j-1}\, \bar{u}_{j-1})}{2\Delta x}\right]. \tag{7.14}$$

The value of the density ϱ above, in (7.11), can be computed by using the state equation, for example $\varrho_j = R\, T_j/p$, as p and T_j are determined (or guessed) earlier in

the computational process. Further, the coefficient of viscosity is assumed to be given by the Chapman viscosity law, $\mu_i = \gamma C T_j$, where the constants γ and C are known.

In this numerical treatment, the pressure p appears partly through its gradient, the derivative with respect to x, and partly through the equation of state. As shown in previous chapters, there exists upstream influence and so branchings can disturb the stability of any computation in a purely forward-marching solution, which results in a departure from the main solution. This phenomenon is as in recent external hypersonic-flow studies by Khorrami and Smith (1994) and references therein, dating back to Neiland (1969), Stewartson and Williams (1969) in particular. The numerical treatment here accordingly adopts as a first simple trial a multi-sweeping technique (in x), in view of the inherent upstream influence present. The derivative of p is therefore discretised in forward-differenced form to bring in the upstream influence directly, an approach which is associated with numerical work by Prof. R.T. Davis and colleagues in the 1970s (also work by Prof. S.G. Rubin and collaborators at Cincinnati, e.g. Rubin (1982)); see for instance Davis and Werle (1982), Brown *et al.* (1991), Khorrami and Smith (1994) and references therein; earlier studies are by Davis (1970), Patankar and Spalding (1972). The forward-differenced pressure method effectively allows for the effects of branching by incorporating upstream influence gradually per outer x-sweep (whereas backward-differencing of the pressure gradient tends to retain the unstable branching as above). Quite simply, we set

$$p'(x) = \frac{p_{i+1} - p_i}{\Delta x}. \tag{7.15}$$

In the current approach, the pressure difference is calculated through outer iteration sweeps, by first inserting a guessed value for the forward pressure p_{i+1} and then updating it after each sweep in x. The sweeping process in x is repeated until (hopefully) the overall solution converges, subject to a prescribed pressure value at the downstream end of the computational domain.

Results from this first trial method are presented in the following section.

7.6 Sample Solutions

Solutions were obtained by using the numerical methods described above, and some results are shown in Figures 7.1 - 7.9. The initial profiles u, T are given by

$$u = \left(y - \frac{1}{2S_0}y^2\right)\frac{2}{S_0},$$

$$T = T_w + \left(y - \frac{1}{2S_0}y^2\right)\frac{1}{2S_0}$$

The normal step size used was $\Delta y = 0.01$, with a nozzle shape $S = S_0 = 1.0$, giving a constant parallel wall, for simplicity. The pressure guess p is prescribed as

$$p = \frac{p_0}{(1+x)^{1/2}}$$

for all x. The computations are applied to a parallel sided duct since there exists similarity solution derived earlier.

First we consider the effect of the step size Δx of the computations, on which the accuracy of the computation partly depends as well as the iterative convergence. Fig 7.1 demonstrates the iteration sequence at a relatively large value of spacing, $\Delta x = 0.1$, with the initial wall temperature $T_w|_{x=0} = 0.75$, downstream temperature $T_w|_{x=10} = 0.25$, and the initial pressure $p_{x=0} = 5$. Here the wall temperature variation $T_w(x)$ was specified as

$$T_w(x) = \frac{T_w|_{x=0}}{1+ax} \qquad (\text{a is } a \text{ constant})$$

throughout, while $u_w(x)$, the wall streamwise velocity, was set to zero, as was the normal velocity component $v_w(x)$. Plotted in the figures are representative quantities along the centre-line, $u(x,1)$, $T(x,1)$. After 100 iterations the solution appears to be convergent although there appear also minor barely noticeable fluctuations in u near $x = 0$ and these are found to remain essentially as they are even after 2000 iterations.

As the step size is reduced these fluctuations reduce. Fig 7.2 shows the result for a finer grid size, $\Delta x = 0.05$. The method now takes more iterations to achieve convergence, where the computational results of u and T settle into certain profiles, around 200 iterations, but the overall solution seems more acceptable, smooth and accurate.

Further, when the step size is reduced to $\Delta x = 0.005$ and double precision is applied to the variables in the programme, more iterations are required to achieve comparable convergence as shown in Fig 7.3.

Results for various temperature gradients are presented in Figures 7.4 - 7.8. With the initial wall temperature $T_w|_{x=0} = 0.5$ and $T_w|_{x=10} = 0.25$, Fig 7.4 gives the result

obtained with step size $\Delta x = 0.05$ and single precision, while Fig 7.5 gives the result with $\Delta x = 0.005$ and double precision. With this smaller temperature gradient both achieve rather slower convergence, and the solution remains steady in Fig 7.4 with a certain degree of fluctuations in it.

Figures 7.6 and 7.7 demonstrate the iteration sequence at larger wall temperature gradients. With the initial wall temperature $T_w|_{x=0} = 1.25$ and final wall temperature $T_w|_{x=10} = 0.25$, Fig 7.6 shows the result for a step size $\Delta x = 0.05$ and single precision, and Fig 7.7 shows the result with $\Delta x = 0.005$ and double precision. The solution again shows noticeable fluctuations in u near $x = 0$ (and further downstream), even with a finer grid size, and in Fig 7.7 unsteadiness appears after 1500 iterations.

In contrast, Fig 7.8 shows/suggests the failure of the iteration sequence at the constant wall temperature $T_w = 0.25$. Clearly the convergence, if any, is poor.

Results for smaller initial pressure, $p_{x=0} = 1$, are presented in Figures 7.9 - 7.11. The initial wall temperatures are taken to be $T_w|_{x=0} = 0.5$ for Fig 7.9, $T_w|_{x=0} = 0.75$ for Fig 7.10 and $T_w|_{x=0} = 1.25$ for Fig 7.11, but the final ones are $T_w|_{x=10} = 0.25$ for all three cases. It is interesting that Fig 7.9 and Fig 7.10 again show unsteadiness (oscillations), after 700 iterations for Fig 7.9 and after 1000 iterations for Fig 7.10, while Fig 7.11 shows none as far as 2000 iterations and the solution appears to be convergent. This suggests that with the smaller temperature gradient the solution seems to become more well-behaved and convergent.

The unsteadiness found in Figures 7.7 - 7.10 starts to appear from the downstream end of the computational domain after a certain number of iterations and then gradually spreads upstream.

We have shown the above results, convergent or divergent as they are, to bring out the point that a better method is (or methods are) perhaps required to be developed, in order to handle rapidly the underlying ellipticity of the present partial-differential problem. The current first, trial, method can surely be improved upon. Faster stable methods are described by Brotherton-Ratcliffe (1986) for example, including methods originating from earlier research by R.T. Davis and by J.E. Carter. An improved or alternative downstream boundary condition may also be necessary, for instance of the similarity or limit form studied earlier in the present thesis.

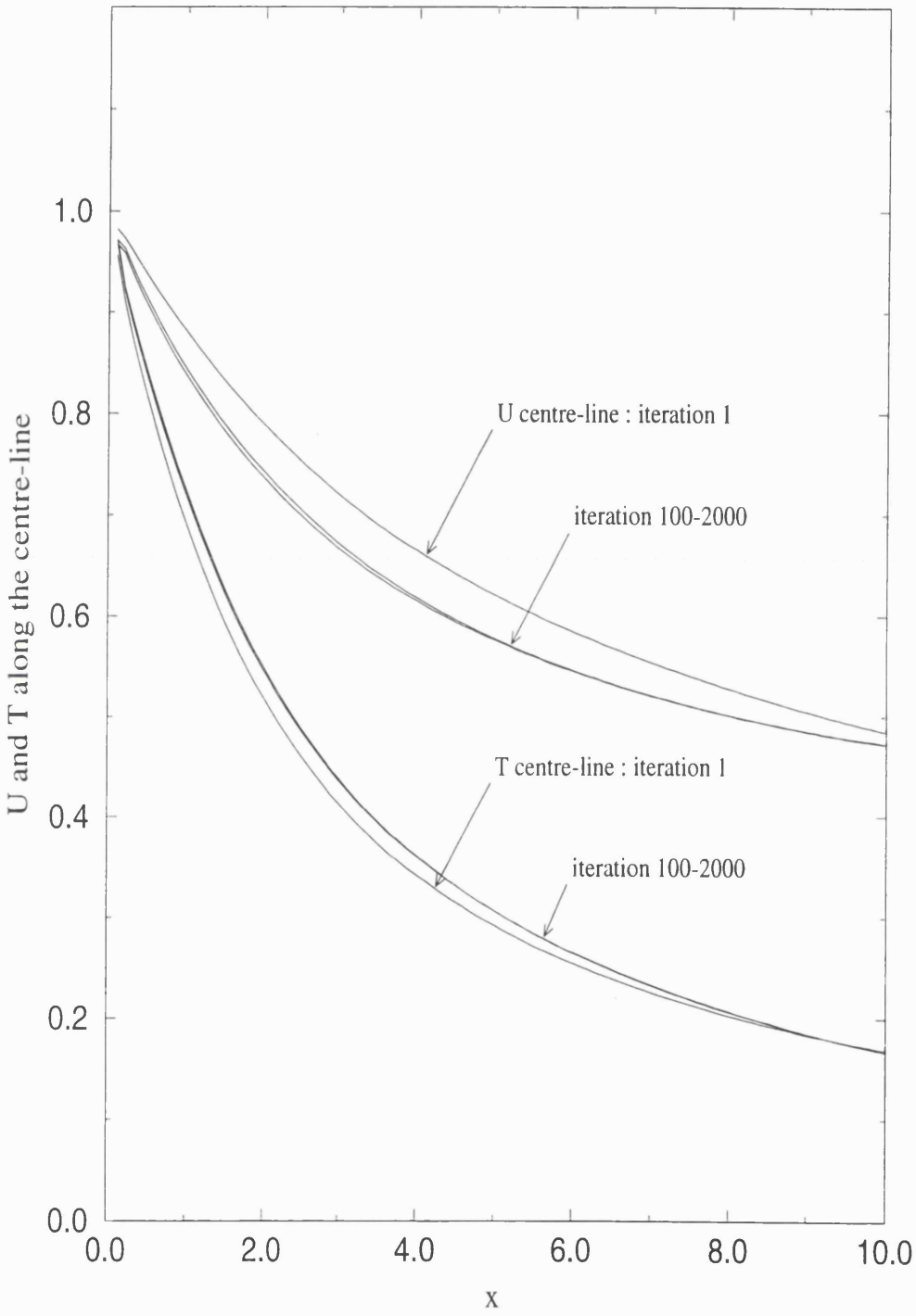

Figure 7.1: $p = 5.0$, $T_w|_{x=0} = 0.75$, $T_w|_{x=10} = 0.25$, $\Delta x = 0.1$.

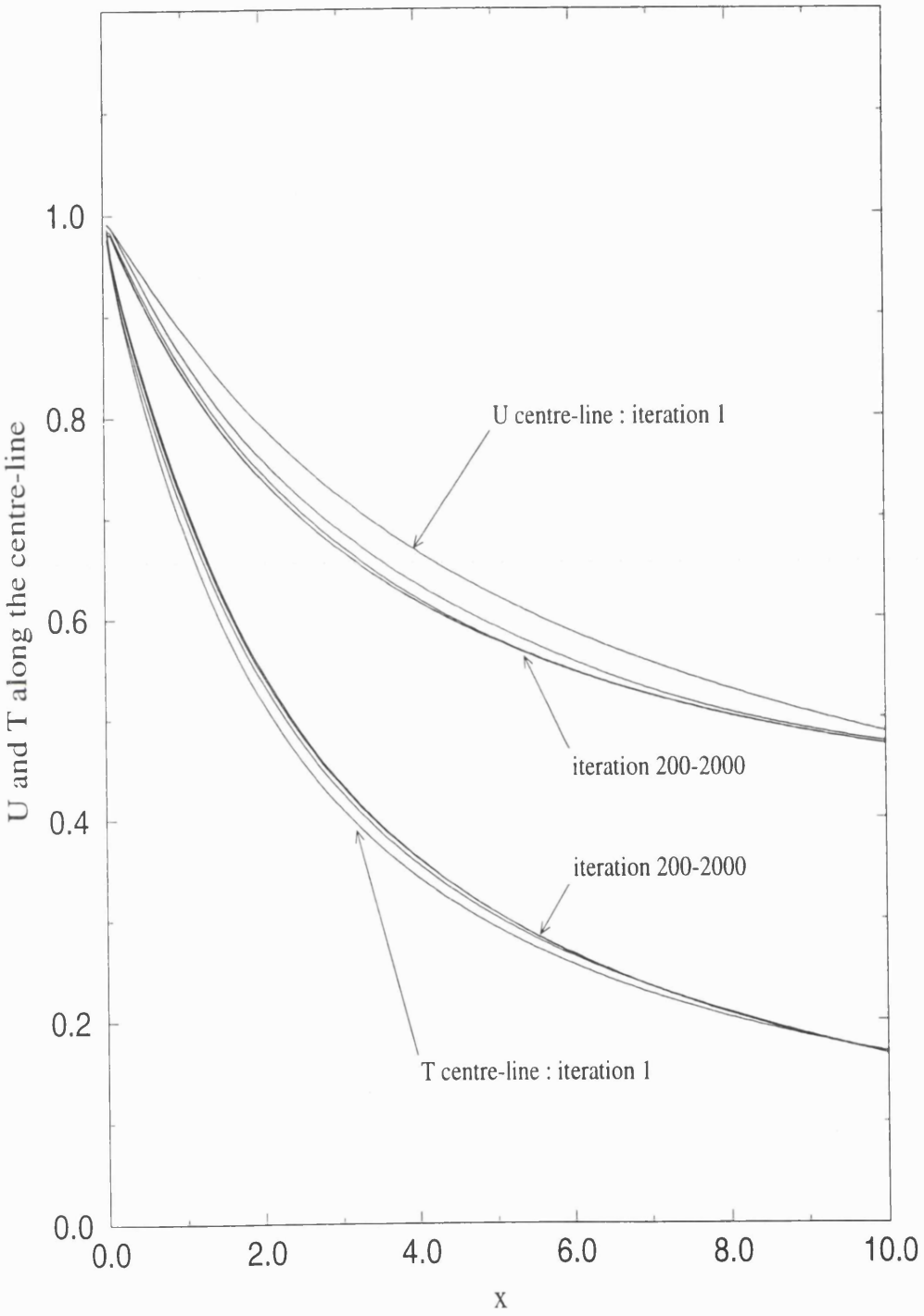

Figure 7.2: $p = 5.0$, $T_w|_{x=0} = 0.75$, $T_w|_{x=10} = 0.25$, $\Delta x = 0.05$.

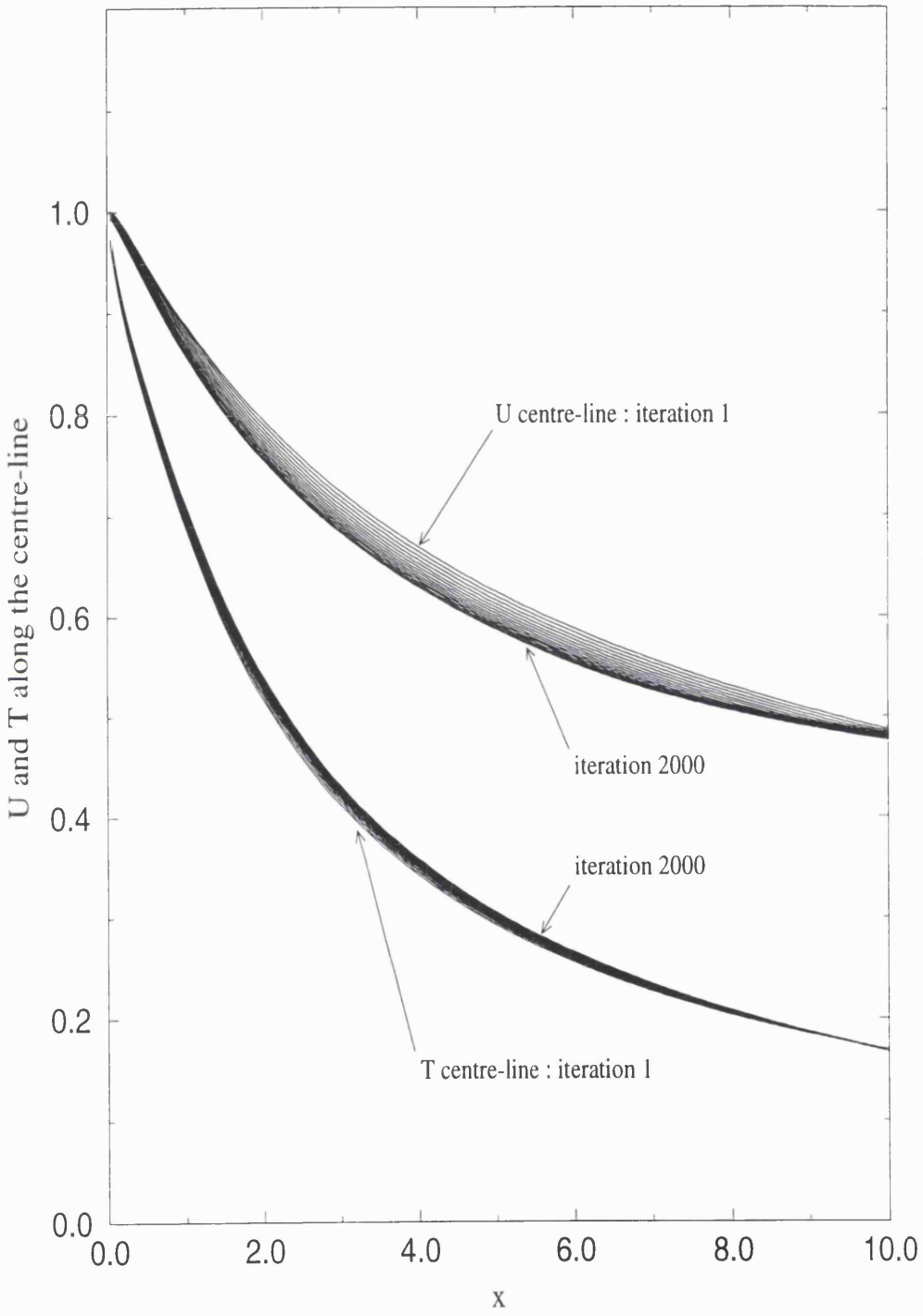

Figure 7.3: $p = 5.0$, $T_w|_{x=0} = 0.75$, $T_w|_{x=10} = 0.25$, $\Delta x = 0.005$.

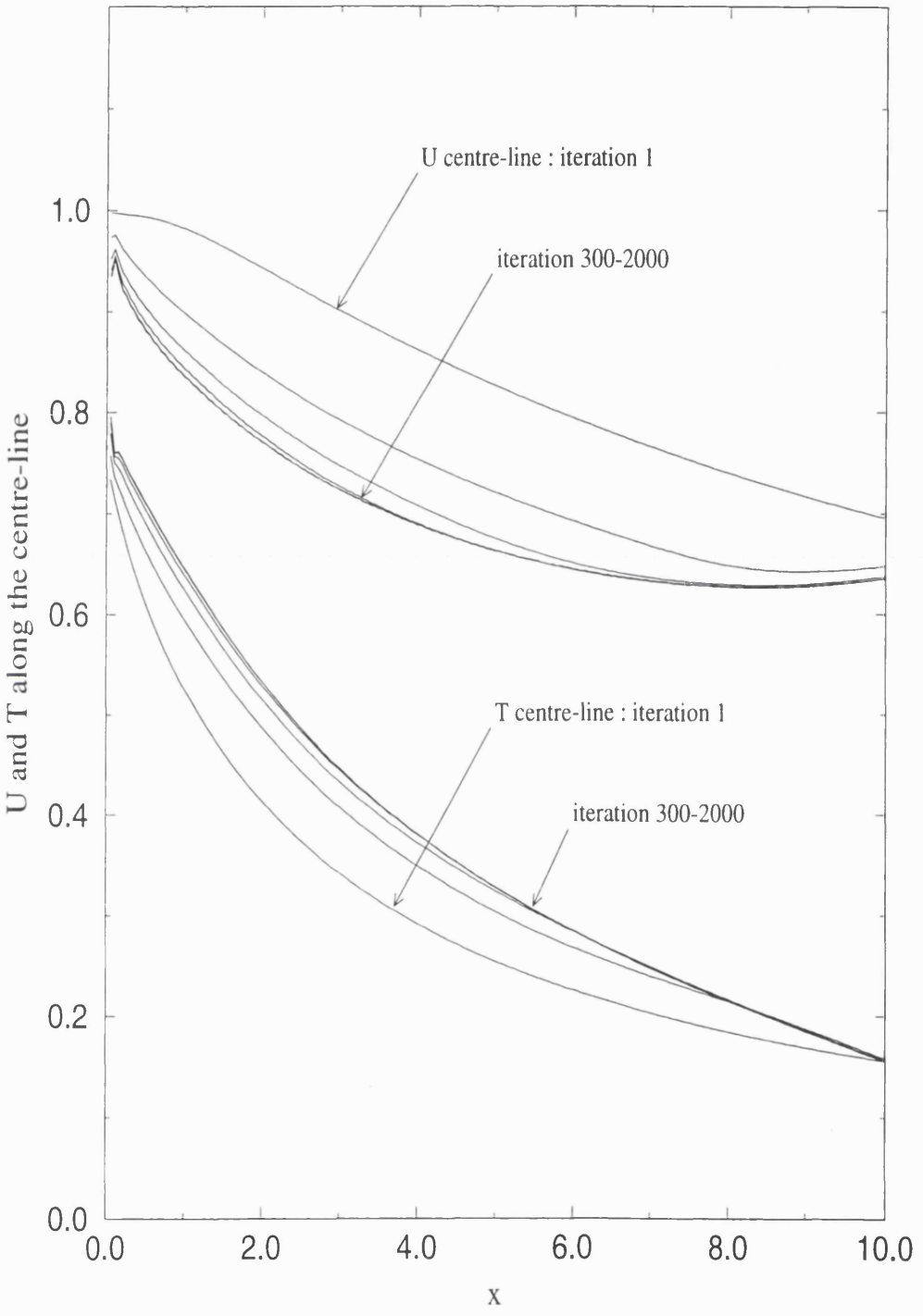

Figure 7.4: $p = 5.0$, $T_w|_{x=0} = 0.5$, $T_w|_{x=10} = 0.25$, $\Delta x = 0.05$.

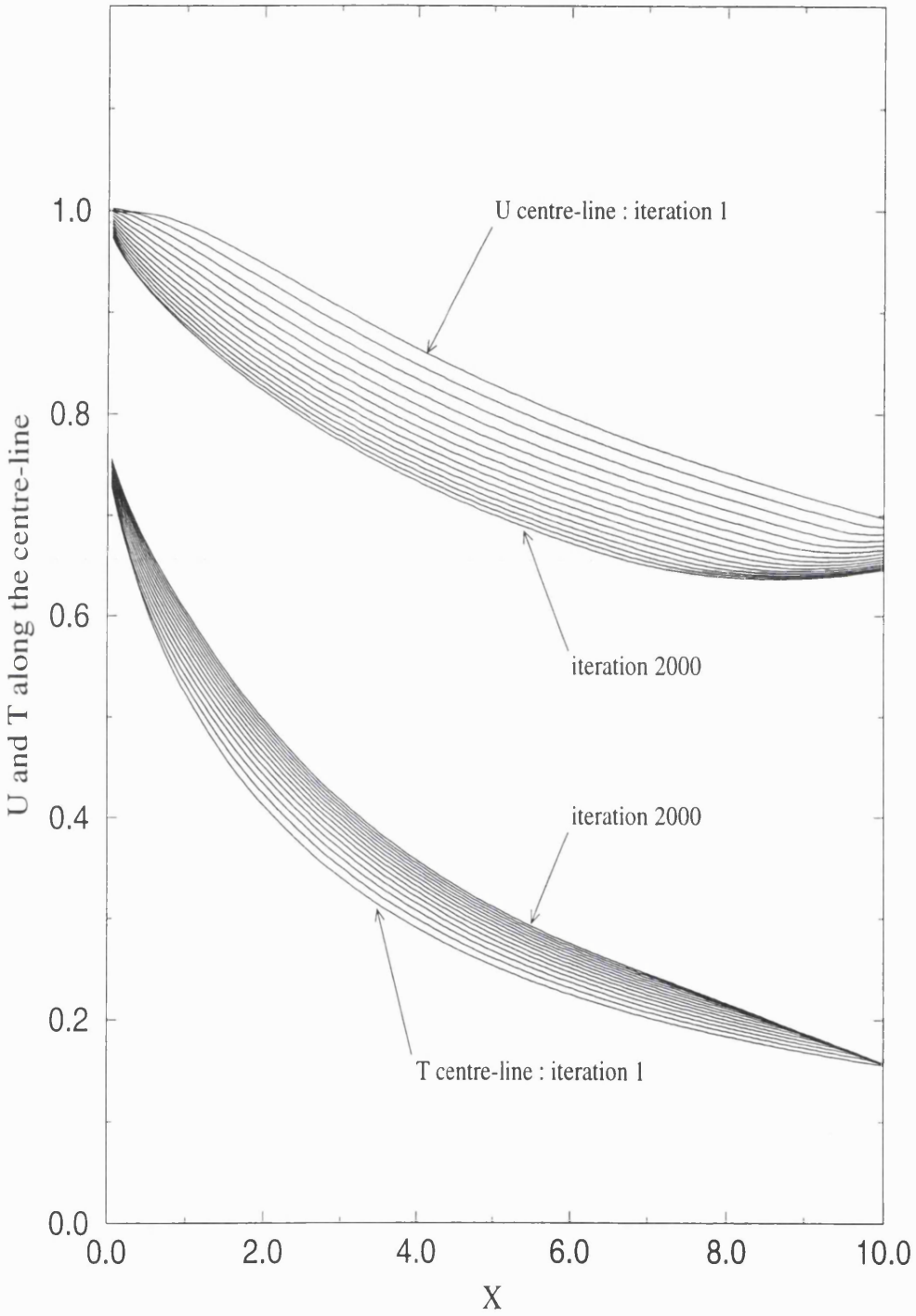

Figure 7.5: $p = 5.0$, $T_w|_{x=0} = 0.5$, $T_w|_{x=10} = 0.25$, $\Delta x = 0.005$.

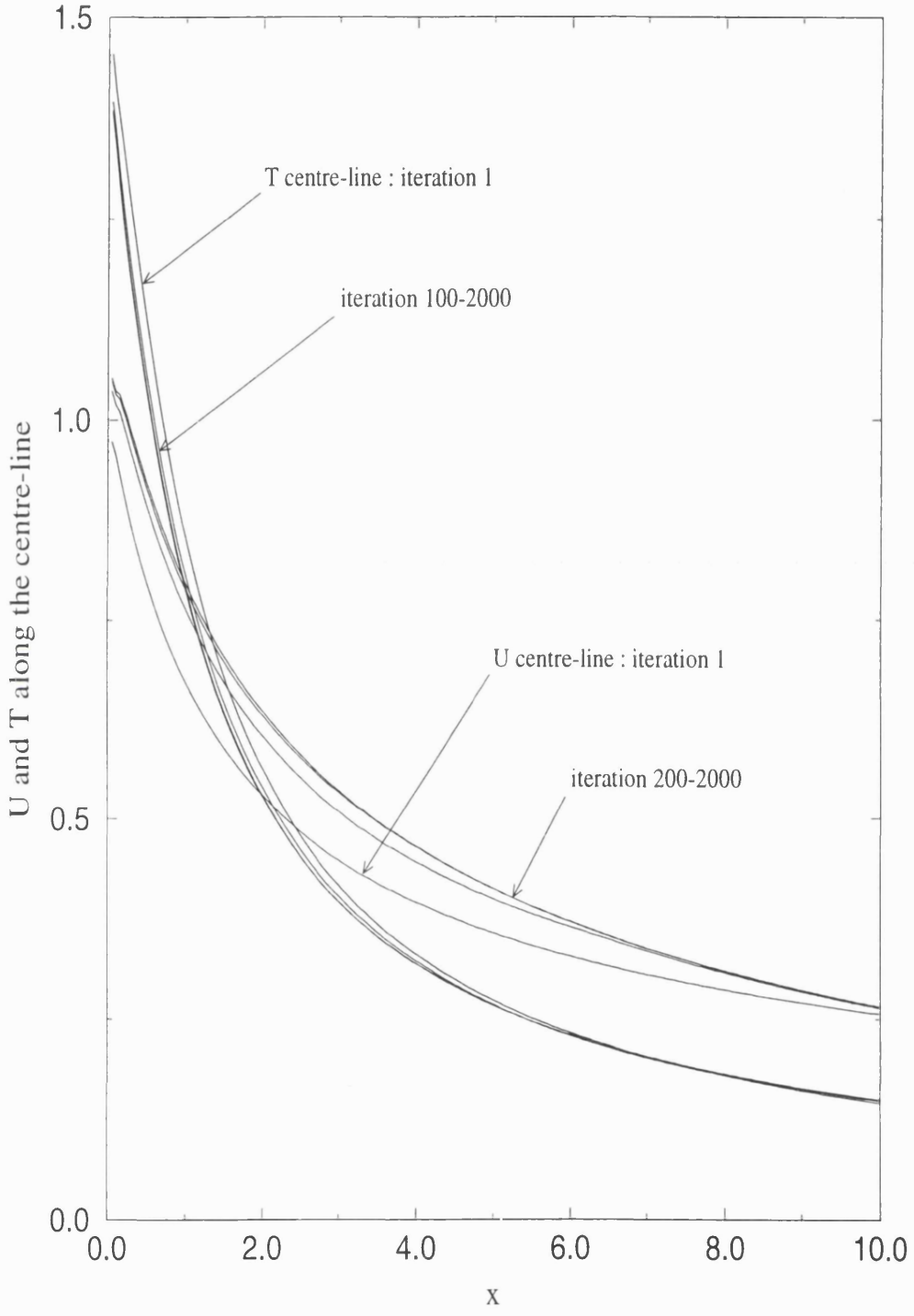

Figure 7.6: $p = 5.0$, $T_w|_{x=0} = 1.25$, $T_w|_{x=10} = 0.25$, $\Delta x = 0.05$.

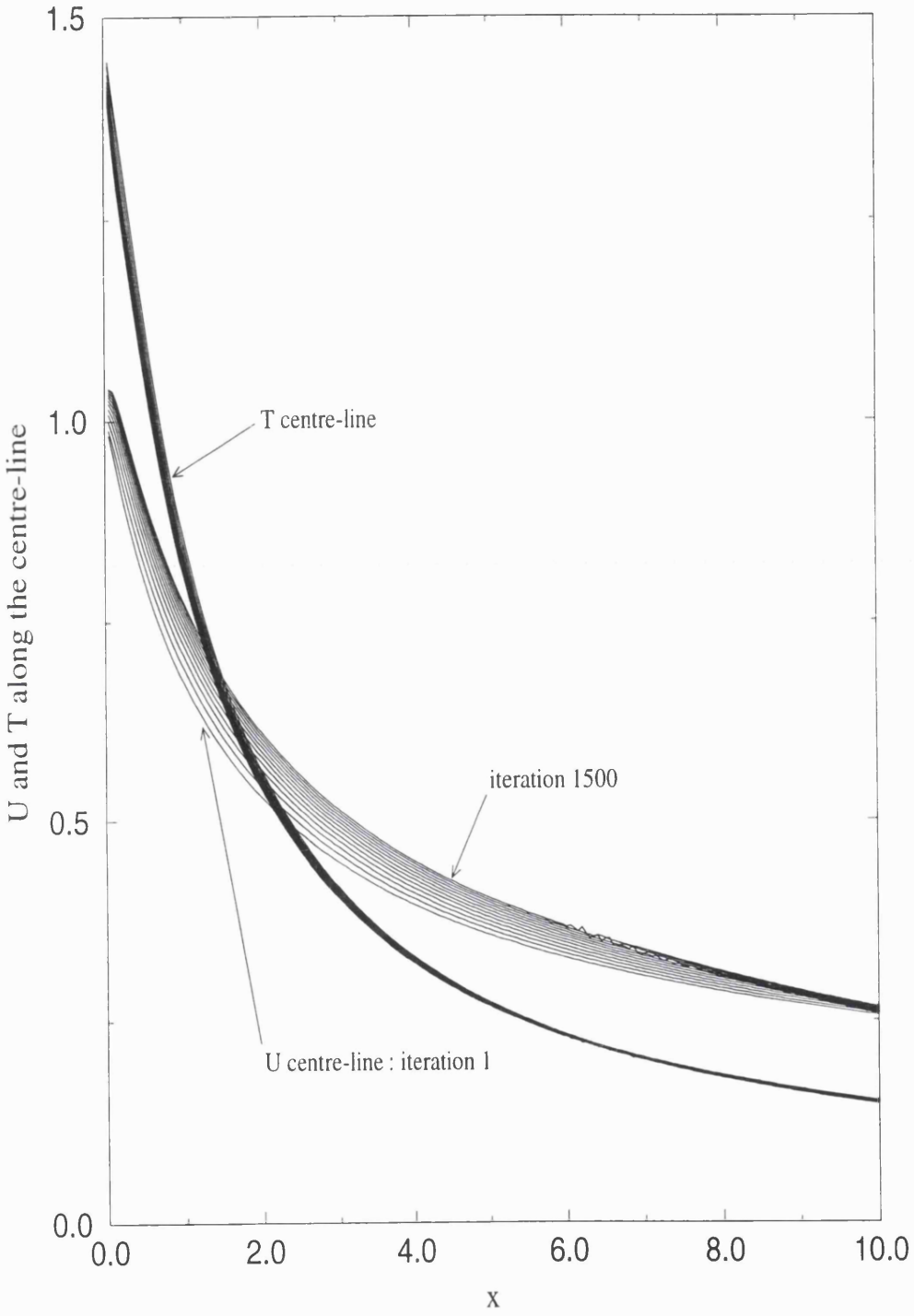

Figure 7.7: $p = 5.0$, $T_w|_{x=0} = 1.25$, $T_w|_{x=10} = 0.25$, $\Delta x = 0.005$.

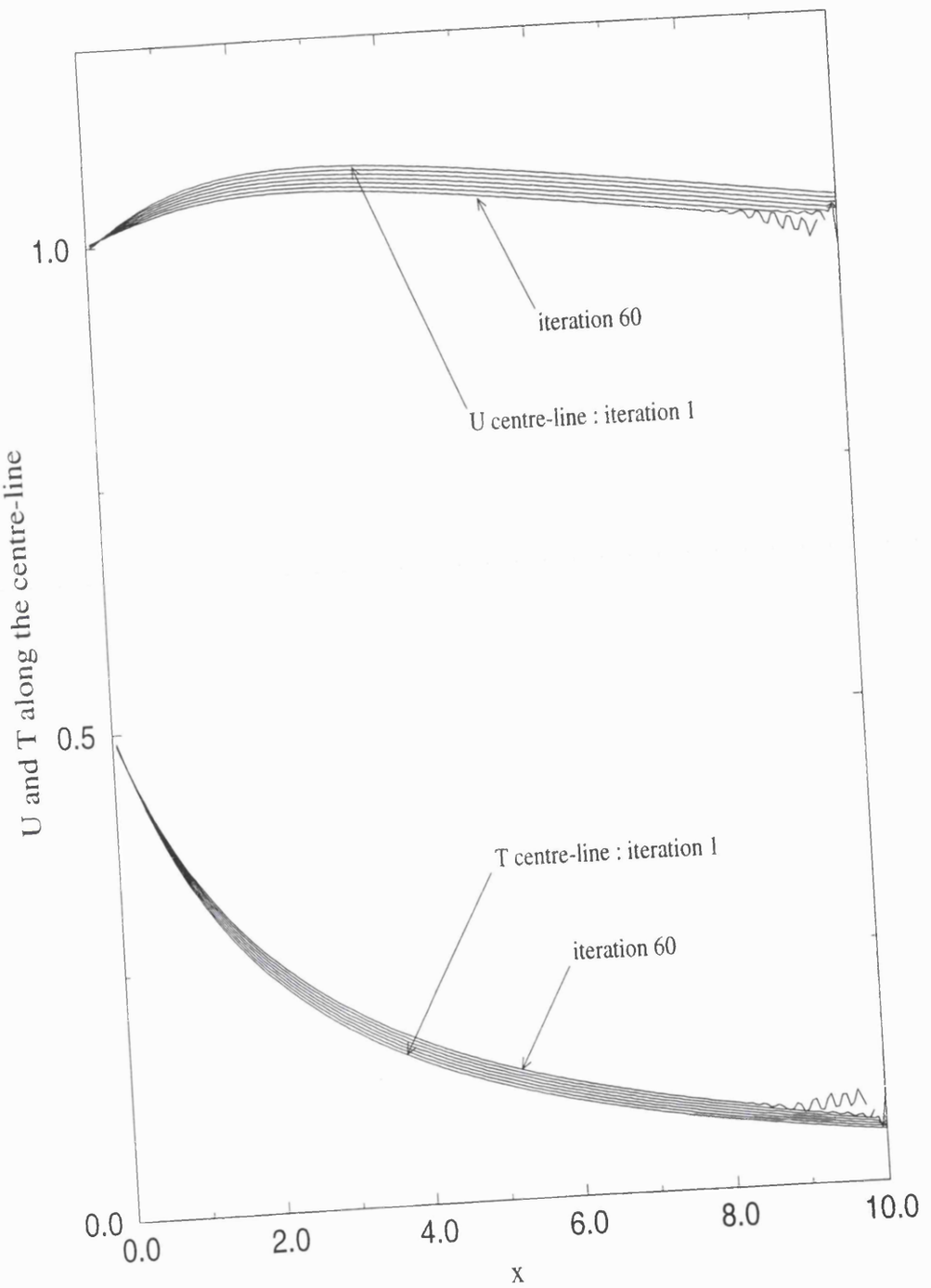

Figure 7.8: $p = 5.0$, $T_w = 0.25$ (constant), $\Delta x = 0.005$.

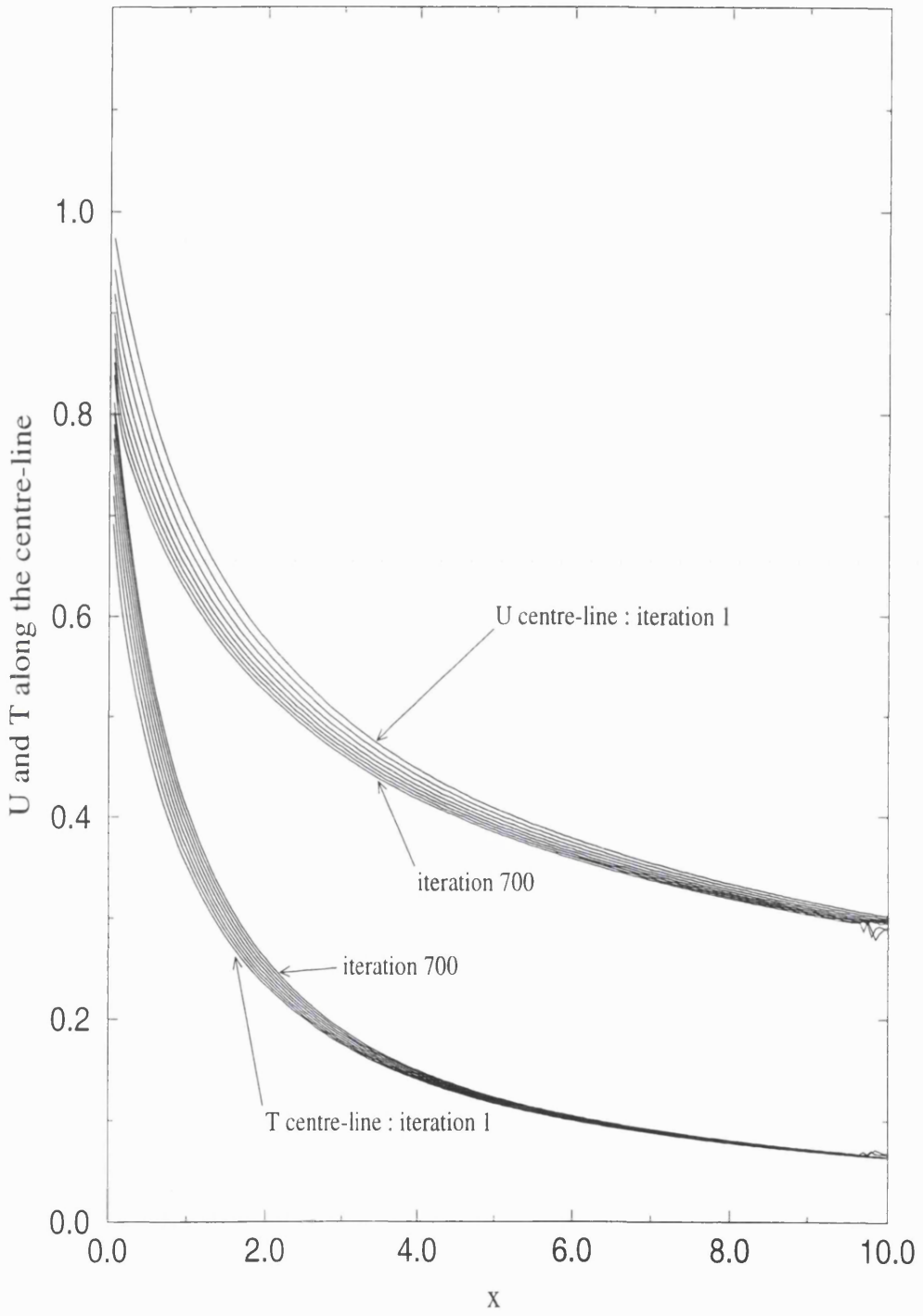

Figure 7.9: $p = 1.0$, $T_w|_{x=0} = 0.5$, $T_w|_{x=10} = 0.25$, $\Delta x = 0.005$.

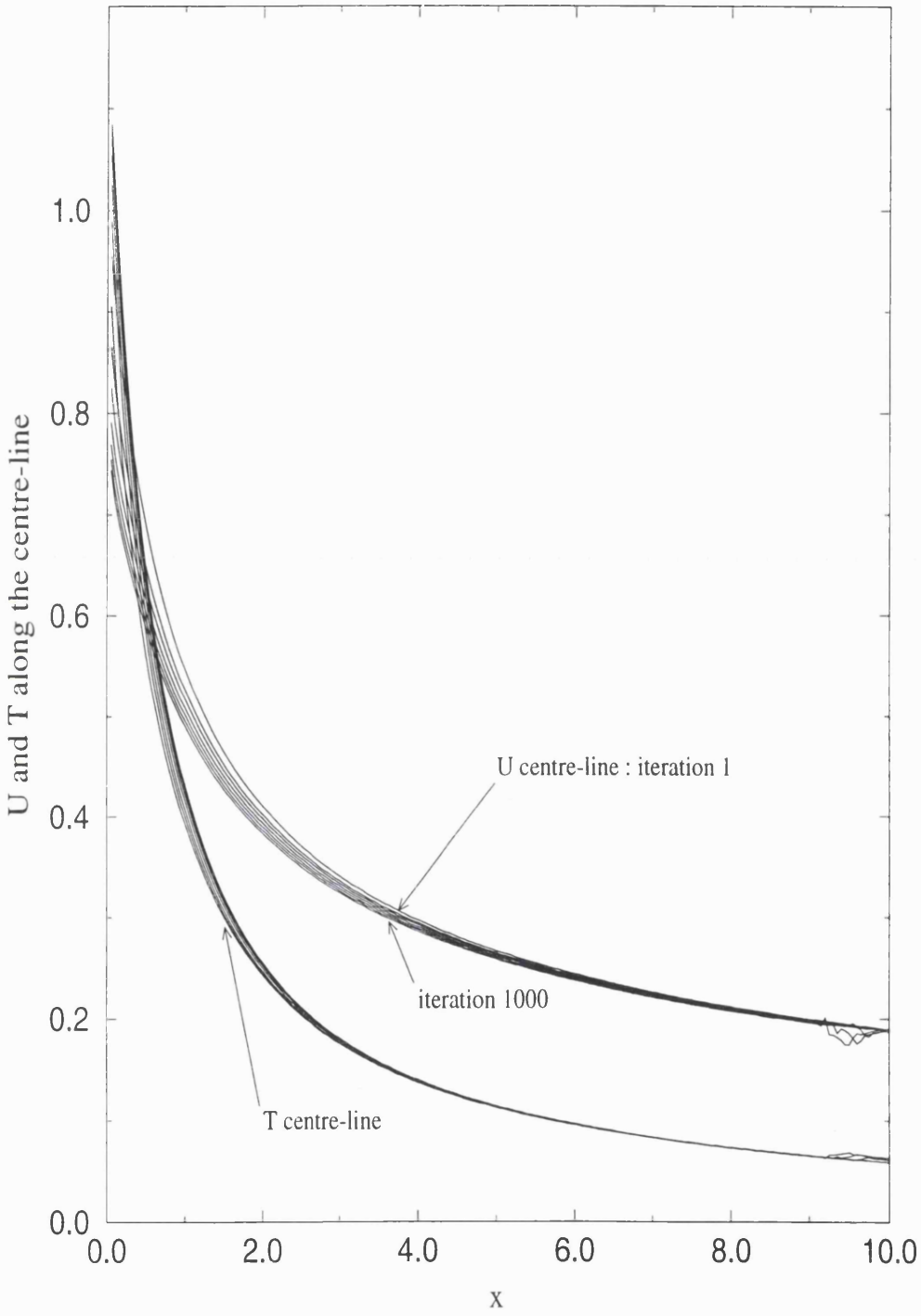

Figure 7.10: $p = 1.0$, $T_w|_{x=0} = 0.75$, $T_w|_{x=10} = 0.25$, $\Delta x = 0.005$.

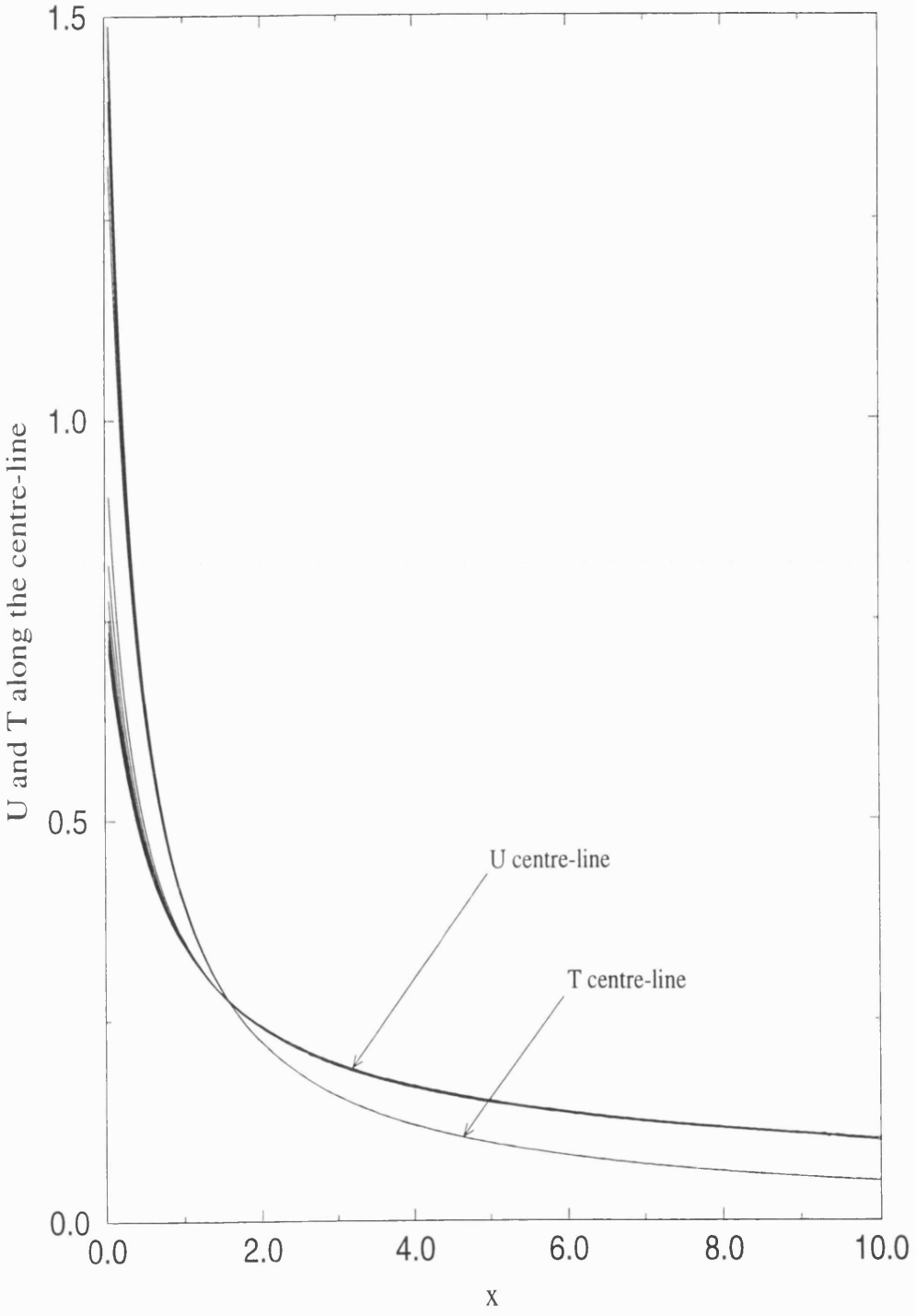

Figure 7.11: $p = 1.0$, $T_w|_{x=0} = 1.25$, $T_w|_{x=10} = 0.25$, $\Delta x = 0.005$.

Figures in chapter 7

Figures 7.1-7.3 : the computational results for the velocity u and the temperature T at the centre-line are plotted against x, for every 100 iterations, with the initial wall temperature $T_w|_{x=0} = 0.75$, the downstream wall temperature $T_w|_{x=10} = 0.5$ and the initial pressure $p_{x=0} = 5.0$. The grid sizes are taken to be $\Delta x = 0.1$ for Fig 7.1, $\Delta x = 0.05$ for Fig 7.2, $\Delta x = 0.005$ for Fig 7.3.

Figures 7.4-7.5 : similar configurations but with the initial wall temperature $T_w|_{x=0}$ $= 0.5$ and the downstream wall temperature $T_w|_{x=10} = 0.25$. The grid sizes are taken to be $\Delta x = 0.05$ for Fig 7.4, $\Delta x = 0.005$ for Fig 7.5.

Figures 7.6-7.7 : similar configurations but with the initial wall temperature $T_w|_{x=0}$ $= 1.25$ and the downstream wall temperature $T_w|_{x=10} = 0.25$. The grid sizes are taken to be $\Delta x = 0.05$ for Fig 7.6, $\Delta x = 0.005$ for Fig 7.7.

Fig 7.8 : also similar configurations but with a constant wall temperature $T_w = 0.25$ throughout x. The grid sizes are taken to be $\Delta x = 0.005$.

Figures 7.9-7.11 : showing u and T with the initial pressure $p_{x=0} = 1.0$. The initial wall temperatures are taken to be $T_w|_{x=0} = 0.5$ for Fig 7.9, $T_w|_{x=0} = 0.75$ for Fig 7.10 and $T_w|_{x=0} = 1.25$ for Fig 7.11, but the final ones are $T_w|_{x=10} = 0.25$ for all three cases.

Chapter 8

Final Comments

The present study has been concerned mostly with upstream influence in hypersonic planar flow through a nozzle. Hypersonic flow has the special and important feature of prolonged upstream influence, in the presence of viscous forces, as upstream influence in a compressible boundary layer increases with increasing Mach number. Non-uniqueness is associated with eigenvalues and corresponding eigenfuctions in an expansion in powers of the distance from a reference point. One of the objectives in this thesis has been to allow for the presence of upstream influence in the internal flow system, which is accompanied by local non-uniqueness of the solutions. The eigenfunction above is due essentially to the interaction of viscous and inviscid layers, and is analogous to the eigenfunction in hypersonic external flow. This non-uniqueness of the solution has been a particular focus in the analysis.

The eigenvalue problem has been discussed in the context of a composite approach. A single composite system of equations has been derived to cover the four separate flow regions of the nozzle, cf. Brown *et al.* (1991), and the system is still a subset of the Navier-Stokes system. The boundary layer equations as a composite system are shown in section 3.1 to be consistent with all the main governing equations throughout the entire domain of the nozzle. Then similarity solutions are deduced, when the nozzle shape is taken to be in the form of a power of the coordinate x, which are related to the Illingworth-Stewartson transformation. Numerical treatment of the similarity solutions in section 4.2 shows the existence of branches in the solutions themselves, which indicate one (perhaps surprising) form of non-uniqueness possible in the local flow.

Another form of non-uniqueness in the flow, due to upstream influence within the composite partial-differential system, is examined analytically and through a numerical method by means of eigenvalues in the flow solution (chapter 5). The equations of the perturbation terms associated with upstream influence are derived with certain

boundary conditions, from substitution into the composite system. The computational results suggest that there are positive eigenvalues α associated with the local expansion. The analytical predictions there agree well with the numerical results.

The presence of upstream influence was also shown by analysis of a pressure equation in chapter 6, for a limiting case. Analytically, an ordinary differential equation was derived for the pressure $p(x)$, in which two boundary conditions were required to determine the pressure profile through the nozzle. The numerical results confirm that the pressure profiles are determined by fixed pressures downstream and upstream. Both analytical and numerical cases verify the presence of upstream influence in the flow system. The results also confirm the existence of concise exact solutions for nozzle-wall pressure when the effective Chapman constant is large.

In a preliminary attempt at solving the composite partial-differential system, a semi-implicit computational method was introduced based on finite-differencing, with the pressure gradient forward-differenced, and on multiple sweeping (chapter 7). The method performs quite well in some cases. The results show, however, that the method, as applied so far at least, is not always sufficiently stable to incorporate all the strong upstream influence present. In order to handle the underlying ellipticity of the present partial-differential problem, this method is perhaps required to be improved. Faster stable methods are described by Brotherton-Ratcliffe (1986) for example, including methods originating from earlier research by R.T. Davis and by J.E. Carter. Further work is called for also on an improved or alternative treatment of the downstream boundary condition, for instance of a similarity or limit form as studied earlier in the present thesis.

Bibliography

Abramowitz, M. and Stegun, I.A. 1964 *Handbook of Mathematical Functions*, National Bureau of Standards, Washington.

Anderson, J.D. 1982 *Modern Compressible Flow: With Historical Perspective*, McGraw-Hill.

Anderson, J.D. 1989 *Hypersonic and High Temperature Gas Dynamics*, McGraw-Hill.

Anderson, J.D. 1991 *Fundamentals of Aerodynamics*, McGraw-Hill.

Anderson, J.D. 1995 *Computational fluid dynamics - The Basics with Applications*, McGraw-Hill.

Blackaby, N.D. 1991 *On Viscous, Inviscid and Centrifugal Instability Mechanisms in Compressible Boundary Layers, including Non-linear Vortex/Wave Interaction and the Effects of Large Mach Number on Transition*, Ph.D. thesis, University of London.

Blottner, F.G. 1962 Computation of the Compressible Laminar Boundary-Layer Flow including Displacement Thickness Interaction using Finite-Difference Methods, Ph.D. thesis, Stanford University, U.S.A.

Bowles, R.I. 1990 *Applications of Nonlinear Viscous-Inviscid Interactions in Liquid Layer Flows and Transonic Boundary Layer Transition*, Ph.D. thesis, University of London.

Bowles, R.I. and Smith, F.T. 1993 On Boundary-Layer Transition in Transonic Flow. *Journal of Engineering Mathematics* **27**, 309-342.

Brotherton-Ratcliffe, R.V. 1986 *Boundary-Layer Effects in Liquid Layer Flows*, Ph.D. thesis, University of London, U.K.

Brown, S.N., Cheng, H.K. and Lee, C.J. 1990 Inviscid-Viscous Interaction on Triple-Deck Scales in a Hypersonic Flow with Strong Wall Cooling. *Journal of Fluid Mechnics* **220**, 309-337.

Brown, S.N., Khorrami, A.F., Neish, A. and Smith, F.T. 1991 On Hypersonic Boundary-Layer Interactions and Transition. *Philosophical Transactions of the Royal Society of London* A **335**, 139-152.

Brown, S.N. and Stewartson, K. 1975 A Non-uniqueness of the Hypersonic Boundary Layer. *Quarterly Journal of Mechanics and Applied Mathematics* **28**, 75-90.

Brown, S.N., Stewartson, K. and Williams, P.G. 1975 Hypersonic Self-Induced Separation. *Physics of Fluids* **18**, 633-639.

Carter, J.E. 1979 A New Boundary Layer Inviscid Iteration Technique for Separated Flows. *AIAA Paper* 79-1450.

Cassel, K.W., Ruban, A.I. and Walker, J.D.A. 1995 An Instability in Supersonic Boundary-Layer Flow over a Compression Ramp. *Journal of Fluid Mechanics* **300**, 265-285.

Cebeci, T. and Bradshaw, P. 1977 *Momentum Transfer in Boundary Layers*, McGraw-Hill.

Chapman, D.R. and Rubesin, M.W. 1949 Temperature and Velocity Profiles in the Compressible Laminar Boundary Layer with Arbitrary Distribution of Surface Temperature. *Journal of the Aeronautical Sciences* **16**, 547-565.

Cohen, C.B. 1954 Similar Solutions of Compressible Laminar Boundary Layer Equations. *Journal of the Aeronautical Sciences* **21**, 281-282.

Cowley, S.J. and Hall, P. 1990 On the Instability of Hypersonic Flow past a Wedge. *Journal of Fluid Mechanics* **214**, 17-42.

Davis, R.T. 1970 Numerical Solution of the Hypersonic Viscous Shock-Layer Equations. *AIAA Journal* **8**, 843-851.

Davis, R.T. 1984 A Procedure for Solving the Compressible Interacting Boundary-Layer Equations for Subsonic and Supersonic Flows. *AIAA Paper* 84-1614.

Davis, R.T. and Werle, M.J. 1982 Progress on Interacting Boundary-Layer Computations at High Reynolds Numbers. *Numerical and Physical Aspects of Aerodynamic Flows*, Springer-Verlag.

Dorodnitsyn, A.A. 1942 Laminar Boundary Layer in a Compressible Gas. *Prikladnaya Matematika i Mekhanika* **6**, Pt.6.

Dusa, D.J. and Younghans, J.L. 1998 Nozzles and Diffusers. *The Handbook of Fluid Dynamics*, CRC Press.

Giordano, D., Marraffa, L., Russo, G. 1991 Simoun and Scirocco Wind Tunnel Nozzle Viscous Flow Study. *Aerothermodynamics for Space Vehicles.* ESA SP-318, 197-207.

Hall, P. 1990 Görtler Vortices in Growing Boundary-Layers - the Leading-Edge Receptivity Problem, Linear Growth and the Nonlinear Breakdown Stage. *Mathematika* **37** 151-189.

Hall, P. and Fu, Y. 1992 Nonlinear Develpment and Secondary Instability of Large-Amplitude Görtler Vortices in Hypersonic Boundary Layers. *European Journal of Mechanics* B **11**, 465-510.

Hall, P. and Smith, F.T. 1989 Nonlinear Tollmien-Schlichting Vortex Interaction in Boundary-Layers. *European Journal of Mechanics* B **8**, 179-205.

Hall, P. and Smith, F.T. 1989 On Strongly Nonlinear Vortex/Wave Interactions in Boundary-Layer Transition. *ICASE Report* 89-82.

Hall, P. and Smith, F.T. 1991 On Strongly Nonlinear Vortex/Wave Interactions in Boundary-Layer Transition. *Journal of Fluid Mechanics* **227**, 641-666.

Hausenblas, H. 1950 Die nichtisotherme Laminare Strömung einer zähen Flüssigkeit durch enge Spalte und Kapillarröhren. *Ingenieur-Archiv* **18**, 151-166.

Hayes, W.D. and Probstein, R.F. 1959 *Hypersonic Flow Theory*, Academic Press.

Howarth, L. 1948 Concerning the Effect of Compressibility on Laminar Boundary Layers and Separation. *Proceedings of the Royal Society of London* A **194**, 16-42.

Illingworth, C.R. 1949 Steady Flow in the Laminar Boundary Layer of a Gas. *Proceedings of the Royal Society of London* A **199**, 533-558.

Jones, E. 1981 An Asymptotic Outer Solution Applied to the Keller Box Method. *Journal of Computational Physics* **40**, 411-429.

Keller, H.B. 1978 Numerical Methods in Boundary-Layer Theory. *Annual Review of Fluid Mechanics* **10**, 417-433.

Kendall, J.M. 1975 Wind Tunnel Experiments relating to Supersonic and Hypersonic Boundary-Layer Transition. *AIAA Journal* **13**, 290-299.

Khorrami, A.F. 1991 *Hypersonic Aerodynamics on Flat Plates and Thin Airfoils*, D.Phil. thesis, University of Oxford.

Khorrami, A.F. and Smith, F.T. 1994 Hypersonic Aerodynamics on Thin Bodies with Interaction and Upstream Influence. *Journal of Fluid Mechanics* **277**, 85-108.

Korte, J.J. 1992 A CFD-based Aerodynamic Design Procedure for Hypersonic Wind-Tunnel Nozzles. *70th AGARD Fluid Dynamics Panel Symposium "Theoretical and Experimental Methods in Hypersonic Flows"*, Torino.

Korte, J.J., Kumar, A., Singh, D.J. and Grossman, G. 1992 Least-Squares/Parabolized Navier-Stokes Procedure for Optimising Hypersonic Wind-Tunnel Nozzles. *Journal of Propulsion and Power* **8**, 1057-1063.

Li, T.Y., and Nagamatsu, H.T. 1953 Similar Solutions of Compressible Boundary Layer Equations. *Journal of the Aeronautical Sciences* **20**, 653-655.

Li, T.Y., and Nagamatsu, H.T. 1955 Similar Solutions of Compressible Boundary Layer Equations. *Journal of the Aeronautical Sciences* **22**, 607-616.

Liepmann, H.W and Roshko, A. 1957 *Elements of Gasdynamics*, John Wiley.

Liepmann, H.W and Puckett, A.E. 1947 *Introduction to Aerodynamics of a Compressible Fluid*, John Wiley.

Lighthill, M.J. 1953a On Boundary Layers and Upstream Influence. I. A Comparison between Subsonic and Supersonic Flows. *Proceedings of the Royal Society of London* **217**, 344-357.

Lighthill, M.J. 1953b On Boundary Layers and Upstream Influence. II. Supersonic Flows without Separation. *Proceedings of the Royal Society of London* **217**, 478-507.

Lukasiewicz, J. 1973 *Experimental Methods of Hypersonics*, Dekker Inc., New York.

Lysenko, V.I. and Maslov, A.A. 1984 The Effect of Cooling on Supersonic Boundary-Layer Stability. *Journal of Fluid Mechanics* **147**, 39-52.

Mack, L.M. 1984 Boundary Layer Linear Stability Theory. *AGARD Report* 709.

Malik, M.R. 1987 Prediction and Control of Transition in Hypersonic Boundary Layers. *AIAA Paper* 87-1414.

Malik, M.R. and Hall, P. 1989 The Growth of Görtler Vortices in Compressible Boundary-Layers. *Journal of Engineering Mathematics* **23**, 239-251.

Meyer, T. 1908 *Über Zweidimensionale Bewegungsvorgänge in einem Gas, das mit Überschallgeschwindigkeit Stromt*, Doktorarbeit, Universität Göttingen.

Moretti, G. and Abbett, M. 1966 A Time-Dependent Computational Method for Blunt-Body Flows. *AIAA Journal* **4**, 2136-2141.

Mulard, V., and Moules, G. 1991 Numerical Simulation of Non-Equilibrium Viscous Flows in Hypersonic Nozzles. *Aerothermodynamics for Space Vehicles.* ESA SP-318, 359-364.

Muylaert, J., Voiron, T., Sagnier, P., Lourme, D., Papirnyk, O., Hannemann, K., Bütefisch, K. and Koppenwallner, G. 1991 Review of the European Hypersonic Wind Tunnel Performance and Simulation Requirements. *Aerothermodynamics for Space Vehicles.* ESA SP-318, 559-574.

Neiland, V.Ya. 1969 Theory of Laminar Boundary Layer Separation in Supersonic Flow. *Izvestiya Akademii Nauk SSSR Mekhanika Zhidkosti i Gaza* **4** (4) 53-57.

Neiland, V.Ya. 1970 Upstream Propagation of Perturbations in Hypersonic Boundary Layer Interactions. *Izvestiya Akademii Nauk SSSR Mekhanika Zhidkosti i Gaza* **5** (4) 40-49.

Neiland, V.Ya. 1973 Boundary-Layer Separation on a Cooled Body and Interaction with a Hypersonic Flow. *Izvestiya Akademii Nauk SSSR Mekhanika Zhidkosti i Gaza* **8**, (6) 99-109.

Owczarek, J.A. 1964 *Fundamentals of Gas Dynamics*, International Textbook.

Patankar, S.V., and Spalding, D.B. 1972 A Calculation Procedure for Heat, Mass and Momentum Transfer in Three-Dimensional Parabolic Flows. *Internatinal Journal of Heat Mass Transfer* **15**, 1787-1806.

Pope, A. and Goin, K.L. 1965 *High-Speed Wind Tunnel Testing*, John Wiley.

Prandtl, L. 1904 Über Flüssigkeitsbewegung bei sehr Kleiner Reibung. *Proceedings of International Congress of Mathematicians, Heidelberg*, 484-491.

Rizzetta, D.P., Burggraf, O.R. and Jenson, R. 1978 Triple-Deck Solutions for Viscous Supersonic and Hypersonic Flow past Corners. *Journal of Fluid Mechanics* **89**, 535-552.

Roache, P.J. 1976 *Computational Fluid Dynamics*, Hermosa Publishers, Albuquerque.

Ruban, A.I. and Timoshin, S.N. 1986 On Upstream Influence in the Boundary Layer on the Walls of a Planar Channel. *Izvestiya Akademii Nauk SSSR Mekhanika Zhidkosti i Gaza* **21** (2) 74-79.

Schlichting, H. 1979 *Grenzschicht-Theorie*, G. Braun, Karlsruhe.

Seddougui, S.O., Bowles, R.I. and Smith, F.T. 1991 Surface-Cooling Effects on Compressible-Boundary-Layer Instability and on Upstream Influence. *European Journal of Mechanics* B **10**, 117-145.

Smith, F.T. 1982 On the High Reynolds-Number Theory of Laminar Flows. *IMA Journal of Applied Mathematics* **28**, 207-281.

Smith, F.T. 1989 On the First-Mode Instability in Subsonic, Supersonic or Hypersonic Boundary Layers. *Journal of Fluid Mechanics* **198**, 127-153.

Smith, F.T. and Brown, S.N. 1990 The Inviscid Instability of a Blasius Boundary-Layer at Large Values of the Mach Number. *Journal of Fluid Mechanics* **219**, 499-518.

Smith, F.T. and Gajjar, J.S.B. 1983 On Hypersonic Self-Induced Separation, Hydraulic Jumps and Boundary Layers with Algebraic Growth. *Mathematika* **30**, 77-93.

Smith, F.T. and Khorrami, A.F. 1991 The Interactive Breakdown in Supersonic Ramp-Flow. *Journal of Fluid Mechanics* **224**, 197-215.

Stetson, K.F. 1987 On Predicting Hypersonic Boundary Layer Transition. AFWAL-TM-84-160-FIMG, Flight Dynamics Laboratory, Air Force Wright Aeronautical Laboratories, Wright-Patterson Air Force Base, Ohio, March 1987.

Stewartson, K. 1949 Correlated Compressible and Imcompressible Boundary Layers. *Proceedings of the Royal Society of London* A **200**, 84-100.

Stewartson, K. 1964 *The Theory of Laminar Boundary Layers in Compressible Fluids*, Oxford University Press.

Stewartson, K. and Williams, P.G. 1969 Self-induced separation. *Proceedings of the Royal Society of London* A **312**, 181-206.

Timoshin, S.N. and Smith, F.T. 1995 Singularities Encountered in 3-Dimensional Boundary-Layers under an Adverse or Favourable Pressure-Gradient. *Philosophical Transactions of the Royal Society of London* A **352**, 45-87.

Townend, L.H. 1999 Hypersonic Aircraft - Lifting Re-entry and Launch. *Philosophical Transactions of the Royal Society of London* A (In the press)

Van Driest, E.R. and Blume, C.B. 1962 Boundary Layer Transition at Supersonic Speeds. *Journal of Aero/Space Sciences* **29**, 909-916.

Van Dyke, M. 1954 Applications of Hypersonic Small-Disturbance Theory. *Journal of the Aeronautical Sciences* **21**, 179-186.

Van Dyke, M. 1964 *Perturbation Methods in Fluid Mechanics*, Academic Press.

Werle, M.J., Dwoyer, D.L. and Hankey, W.L. 1973 Initial Profile for the Hypersonic-Shock / Boundary-Layer Interaction Problem. *AIAA Journal* **11**, 525.

White, F.M. 1991 *Viscous Fluid Flow*, McGraw-Hill.